THE EFFECT OF SIMULATED ORTHOSTATIC HYPOTENSION ON CARDIAC FUNCTION IN EXPERIMENTAL SPINAL CORD INJURY

by

BRIAN HAYES

BKin, The University of British Columbia, 2016

A THESIS SUBMITTED IN PARTIAL FULFILLMENT OF

THE REQUIREMENTS FOR THE DEGREE OF

MASTER OF SCIENCE

in

THE FACULTY OF GRADUATE AND POSTDOCTORAL STUDIES

(Kinesiology)

THE UNIVERSITY OF BRITISH COLUMBIA

(Vancouver)

July 2019

The following individuals certify that they have read, and recommend to the Faculty of Graduate and Postdoctoral Studies for acceptance, a thesis entitled:

The effect of simulated orthostatic hypotension on cardiac function in experimental spinal cord injury

submitted by Brian Hayes in partial fulfillment of the requirements for

the degree of Master of Science

in Kinesiology

Examining Committee:

Christopher R West, Department of Cellular and Physiology Sciences, Southern Medical Program, UBC
Supervisor

Aaron A Phillips, Department of Cellular and Physiological Sciences, University of Calgary
Supervisory Committee Member

David J Granville, Department of Pathology and Laboratory Medicine, UBC
Supervisory Committee Member

Abstract

High thoracic and cervical spinal cord injuries (SCI) are detrimental to autonomic function, increasing cardiovascular disease prevalence and impairing cardiac, cerebrovascular and arterial function. Complete SCI to the third thoracic segment (T3) or higher is known to be detrimental to the structure and intrinsic function of the left ventricle (LV). In addition, injuries to T6 or higher are known to impair the cortically-derived cardiovascular response to postural change, causing episodes of low systemic blood pressure known as orthostatic hypotension (OH) up to 28 times each day. While these frequent episodes of OH following SCI are associated with impairments in cerebrovascular function and an increased risk of coronary artery disease, it is not clear whether there is a direct relationship between OH and cardiac dysfunction following SCI. The purpose of this thesis was, therefore, to examine the impact of regular bouts of OH on cardiac function following SCI. To do so, we developed a preclinical model of OH simulation using lower body negative pressure (LBNP) in a rodent model of experimental SCI. The impact of either sham injury, T3 transection alone or T3 transection with 8 weeks of daily simulated OH on cardiac structure and function was assessed *in vivo* using pressure-volume catheterization and echocardiography, and *ex vivo* via histological analysis of myocardial tissue. We found that daily simulation of OH caused an uncoupling of the ventricular-arterial interaction following SCI, indicating a decrease in the efficiency and adaptability of the cardiovascular system that was driven by decreased LV contractile function. Additionally, we found evidence of atrophy and remodeling of cardiomyocytes following SCI and an increase in myocardial collagen following OH simulation in SCI animals. Together, the findings of this thesis imply that frequent occurrence of OH following T3 SCI may accelerate the onset of cardiac dysfunction that follows SCI and subsequently increase the risk of cardiovascular disease. Future clinical investigations are needed to understand whether these differences translate to the bedside, and apply more direct measures of ventricular mechanics and arterial function to provide context to our PV data and drive the development of informed treatment protocols.

Lay Summary

Before this study, we knew that the heart changes after spinal cord injury, but we did not know what caused these changes. One potential explanation is that when people with spinal cord injury transfer from their bed to their wheelchair, or from the wheelchair to a standing frame, gravity pulls blood away from the heart and brain down into their abdomen and legs. To explore whether gravity pulling blood away from the heart can change the structure and function of the heart, we created a method to simulate the effect of gravity on blood pressure in rats with spinal cord injuries. After 9 weeks, we found that simulated blood pressure reductions made decreased the heart's efficiency, likely increasing the risk of cardiovascular disease and early death. This is the first study to show that blood pressure instability can decrease cardiac efficiency after spinal cord injury.

Preface

All data contained in this thesis were collected by Brian Hayes and the West Lab at the International Collaboration On Repair Discoveries (CORD) UBC. All animal protocols were reviewed and conducted under UBC Animal Care Committee guidelines (A18-0344) and adhered to the guidelines issued by the Canadian Council for Animal Care. No portions of this thesis are presently published.

I was the lead investigator on this project and was primarily responsible for the study design and implementation, as well as the analysis of the resulting data. All works were conducted by members of the West lab; animal spinal surgeries were conducted by the Erin Erskine, outcome catheterization surgeries were conducted by Dr. Malihe-Sedat Poormasjedi-Meibod, and animal care and histological works were performed by me and supported by Mary Fossey.

Dr. Christopher R West was the supervisory author for this project and was closely involved in the conceptualization, design and collection of the data, and additionally provided thesis revisions.

Table of Contents

List of Tables

List of Figures

List of Abbreviations

ABR: Arterial baroreflex

AD: Autonomic Dysreflexia

ANS: Autonomic nervous system

AP: Action potential

ATP: Adenosine tri-phosphate

AV: Atrioventricular

CN: Cranial Nerve

CNS: Central nervous system

CO: Cardiac output

CT: Connective tissue

CVD: Cardiovascular Disease

CVS: Cardiovascular System

DBP: Diastolic Blood Pressure

Ea: Arterial elastance

ECM: Extra-cellular matrix

EDHF: Endothelium derived hyperpolarizing factor

EDV: End diastolic volume

EDVPR: End diastolic pressure volume relationship

Ees: End systolic elastance

EF: Ejection fraction

EPR: Exercise pressor reflex

ESPVR: End systolic pressure volume relationship

ESV: End systolic volume

HFpEF: Heart failure with preserved ejection fraction

HFrEF: Heart failure with reduced ejection fraction

HR: Heart rate

IVSd: Interventricular septum thickness at end of diastole

LBNP: Lower body negative pressure

LOI: Level of injury

LV: Left Ventricle

LVIDd: Left ventricle internal diameter at end of diastole

LVPWd: Left ventricular posterior wall thickness at end of diastole

MAP: Mean Arterial Pressure

NO: Nitric Oxide

NTS: Nucleus tractus-solitarii

OH: Orthostatic Hypotension

PBS: Phosphate buffered saline

Pmax: Maximal pressure during cardiac cycle

PNS: Peripheral nervous system

PSNS: Parasympathetic nervous system

RAAS: Renin-angiotensin-aldosterone system

RVLM: Rostral ventrolateral medulla

SA: Sinoatrial

SBP: Systolic Blood Pressure

SCI: Spinal Cord Injuries

SERCA: Sarcoplasmic reticulum calcium transport ATPase

SNS: Sympathetic nervous system

SV: Stroke volume

SW: Stroke work

UPS: ubiquitin proteasome system

VAC: Ventricular arterial coupling

VSI: Ventricular stiffness index

Acknowledgements

I would like to start by offering my deepest thanks to the entirety of the West Lab, as well as the greater academic community at ICORD. It has been a privilege to work, learn and grow in such a unique scientific setting that fostered such cooperation and peer-support in the pursuit of scientific excellence.

I would particularly like to thank May Fossey, Dr. Malihe-Meibod Poormasjedi-Sedat and Erin Erskine of the West Lab for their amazing work, passion and dedication to high-quality science. This project would not have been possible without their significant efforts, abilities and support.

I thank Dr. Dave Granville for the valuable insight and support he has provided at ICORD, and for offering unique equipment and training from his own lab which was crucial in the collection and analysis of data for this thesis.

I thank Dr. Aaron Phillips for his mentorship and trust in sharing his ideas, insight and designs to create a truly unique and impactful thesis project. I also thank Dr Phillips for providing the opportunity and encouragement to expand my research experience beyond ICORD and Canada.

And, of course, I would like to thank my supervisor Dr Christopher West for 2+ years of incredible research experience and fantastic mentorship. The balance you struck between providing support and encouraging independent problem solving has caused my professional skillset and academic self-confidence to grow exponentially. Thank you for being open to my somewhat-ambitious timelines and supporting my research-abroad experience despite the complications that arose. I know that the development of my ability to interpret and appreciate research that took place throughout my MSc will be invaluable in my career moving forwards, and for this I am grateful.

Dedication

I would like to dedicate this thesis to my family, who have been incredibly supportive throughout my six years of study. I do so, however, with an emphasis on two particular individuals; First to my dad for his invaluable support, encouragement and enthusiasm at every step of my graduate school experience. Secondly to my grandfather who, despite no longer being present, taught me to love science and lifelong learning regardless of challenges or barriers along the way.

Chapter 1 – Introduction

1.1 Introduction to the Cardiovascular System:

The cardiovascular system, composed of the heart and an extensive network of blood vessels, is a closed system that circulates blood throughout the body. This allows for the delivery of oxygen and metabolites to tissues for the production of energy, and the transportation of carbon dioxide and waste to our lungs, kidneys and liver. Blood is also a key figure in the regulation of bodily pH and temperature, the transportation of hormones and drugs, and the regulation of the osmotic pressure throughout the body[1]. At the center of this system, the four-chambered heart acts (in a simplistic sense) as a pump, propelling blood into the two different circuits of the cardiovascular system: the pulmonary circulation that circulates blood to the lungs, and the systemic circulation that circulates blood to the rest of the body. These circuits are composed of a series of vessels, which in turn can be divided into three categories: the arterial system carries blood away from the heart, the capillary system allows nutrient exchange between the blood and the lungs or bodily tissues to occur, and the venous system returns blood back to the heart[1]. The four chambers of the heart can be divided into a right and left atrium, which accept blood from the systemic and pulmonary circulation respectively, as well as the right and left ventricles, which expel blood into the pulmonary and systemic circulations respectively. In other words, the two atria accept blood from veins and the two ventricles expel blood from the heart. Furthermore, the right side of the heart handles deoxygenated blood, while the left side handles oxygenated blood. To provide a more functional summary of the circulatory system, it is also pertinent to consider the trajectory of blood as it flows through the system.

1.1.2. Trajectory of Blood Flow

Deoxygenated blood returns to the heart from the systemic circulation via the inferior and superior vena cava, entering the right atrium of the heart and moving through the right ventricle into the

pulmonary artery. From this point the pulmonary artery branches and carries the blood to one of the two lungs, where carbon dioxide and waste metabolites are released into the alveoli for expulsion while oxygen is absorbed back into the blood. This newly oxygenated blood then travels through the pulmonary veins back into the left atrium of the heart, from where it moves into the left ventricle and is pumped out into the aorta. Now in the systemic circulation, the aorta transports blood to a series of smaller arteries, which branch into progressively smaller sub-parts known as arterioles to deliver oxygen to each corner of the body. By the time the blood reaches a site for gas and nutrient exchange, such as a muscle or organ, the arterioles have divided extensively into the microscopic capillaries. Blood moves extremely slowly through these vessels, the walls of which are only a single cell thick, making these capillaries the primary site for nutrient and gas exchange. Upon exiting the capillary beds, the now deoxygenated blood is gathered into venules, which guide the blood back towards the heart. As the venules get closer to the heart, they gradually combine to form larger veins, then culminate into the superior and inferior vena cava, which return the blood to the right atria to start the process all over again. Refer to ***figure 1.1*** to supplement this breakdown of blood flow throughout the cardiovascular system[2].

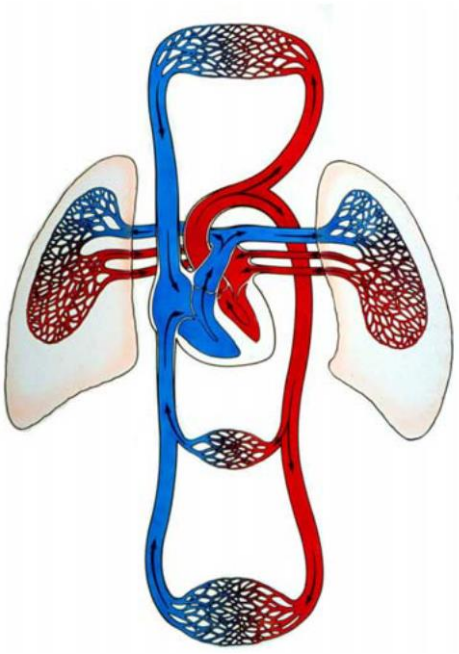

Figure 1.1. *Conceptual summary of the trajectory of blood flow throughout the circulatory system. Blue blood indicates deoxygenated blood, whereas red blood indicates oxygenated. Reproduced from Burkhoff et al, 2011* [2].

The final important detail about the composition of the cardiovascular system, which is highly influential on the structure and function of the heart, is the different pressures that exist throughout the system. The systemic circulation experiences much greater pressures than the pulmonary system, largely because it moves more blood over a much greater distance. This pressure is greatest as the blood is being expelled from the heart through the arteries and is significantly lower in the veins that return blood to the heart. Put quantitatively, the pressure in the systemic circulation usually modulates between 120 and 80mmHg in the arteries, and has decreased to as low as 10-13mmHg by the time it returns to the heart via the inferior/superior vena cava[3]. In contrast, the pulmonary circulation usually modulates between 15-20mmHg in the pulmonary artery, decreasing to 5-10mmHg by the time it returns to the heart via the pulmonary veins[3].

1.2 Cardiac Anatomy

1.2.1 Anatomical Orientation

Located in a compartment of the thorax known as the middle mediastinum, the heart resides between the two lungs (tucked slightly into the left lung). The diaphragm and the great vessels provide the inferior and superior borders, while the sternum and the esophagus make up the anterior and posterior borders respectively. As shown in ***Figure 1.2,*** the heart assumes an oblique orientation in the thorax, with two thirds of its structure extending to the left of the anatomical midline. The apex, or point, of the heart is composed of the left ventricle, and sits just above the diaphragm in the fifth intercostal space. The base of the heart, the most superior and posterior surface of the heart made up of mostly the left atria, reaches up to just below the level of the third rib[1,3].

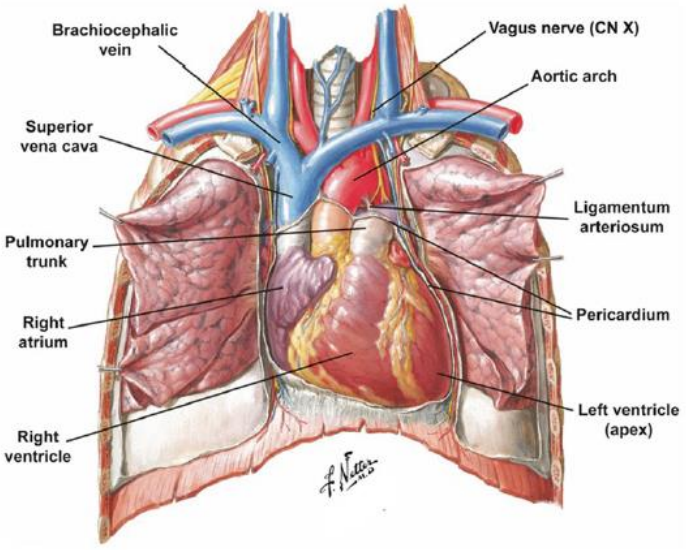

Figure 1.2. *Illustrated dissection of the mediastinum retrieved from Netter[4], with lungs reflected to reveal location and orientation of the heart with respect to other thoracic structures*

It is worth noting that the heart does not follow conventional anatomical orientation, which is largely accredited to early investigations on the heart being done after the organ was removed from the body and dissected. Therefore, the “base” of the heart is the most superior portion, whereas the “apex” is the most inferior portion. Likewise, the right and left chambers (atria and ventricles) are not labelled in

reference to standard anatomical orientation. The right ventricle forms the anterior surface of the heart, whereas the right atria forms the right border, the left atria and the left ventricle form the posterior surface, and the left ventricle alone forms the left border[3].

1.2.2 Pericardium

Nestled into the cardiac notch of the left lung, the heart is surrounded by a structure known as the pericardium. As displayed in ***Figure 1.3***, the relationship between the heart and the pericardium is akin to pressing your fist (the heart), into a balloon (the pericardium), and the balloon engulfing your fist in a two-layered sheath with space in between[1,3]. This pericardial sheath has two layers; an inner visceral portion called the *epicardium*, which covers the entire surface of the heart and base of the great vessels, and an outer layer called the *fibrous pericardium*, which attaches superiorly to the base of the great vessels and inferiorly to the diaphragm. Between these two layers is a fluid-filled cavity known as the *pericardial cavity*, which can accumulate excess fluids and provide excessive pressure on the heart (i.e., pericardial constraint) in the case of pathological conditions[3].

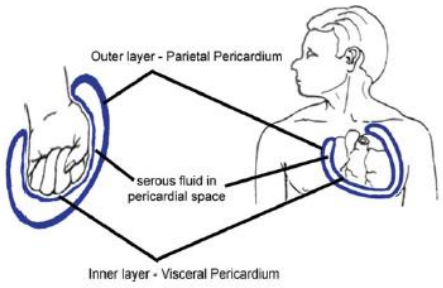

Figure 1.3. *Conceptual illustration of the physical relationship between the heart and the pericardium retrieved from Iaizzo et al. 2008*

1.2.3 Cardiac Structure

The heart itself, as previously mentioned, can be divided into four chambers: two atria and two ventrcles[1,3]. In addition to being divided by function, these chambers are also divided by two types of physical structures: septum and valves. On the exterior of the heart, landmarks called *sulci* can also be used to distinguish the trajectory of important vessels. For example, the *coronary sulcus* marks the boundary between the atria and ventricles, while the *posterior* and *anterior interventricular sulci* outline the separation between the two ventricles.

There are four major valves in the heart which, due to their uni-directional nature, function mainly to ensure that blood flows in one continuous direction through the heart without "backing up", or "regurgitating" into previous chambers. Two of these valves are *atrioventricular* valves, separating each atrium from their respective ventricle. The three-leaflet tricuspid valve separates the right atrium from the right ventricle, preventing blood from flowing from the right ventricle back into the right atrium. The two-leaflet bicuspid (or mitral) valve separates the left atria and left ventricle, preventing blood from flowing back from the left ventricle into the left atria[1]. The other two valves are termed *semilunar* valves due to the shape of their valve leaflets, and function to separate the ventricles from the great vessels. The Aortic valve separates the left ventricle from the aorta, while the Pulmonary valve separates the right ventricle from the pulmonary trunk[1,3]. In conclusion, it should be noted that there are no valves separating the atria from their respective conducting vessels (the vena cava or the pulmonary vein). This becomes important for pathological and physiological adaptations later in this review. Refer to ***figure 1.4*** for a visual of the four major heart valves during diastole (A) and systole (B)

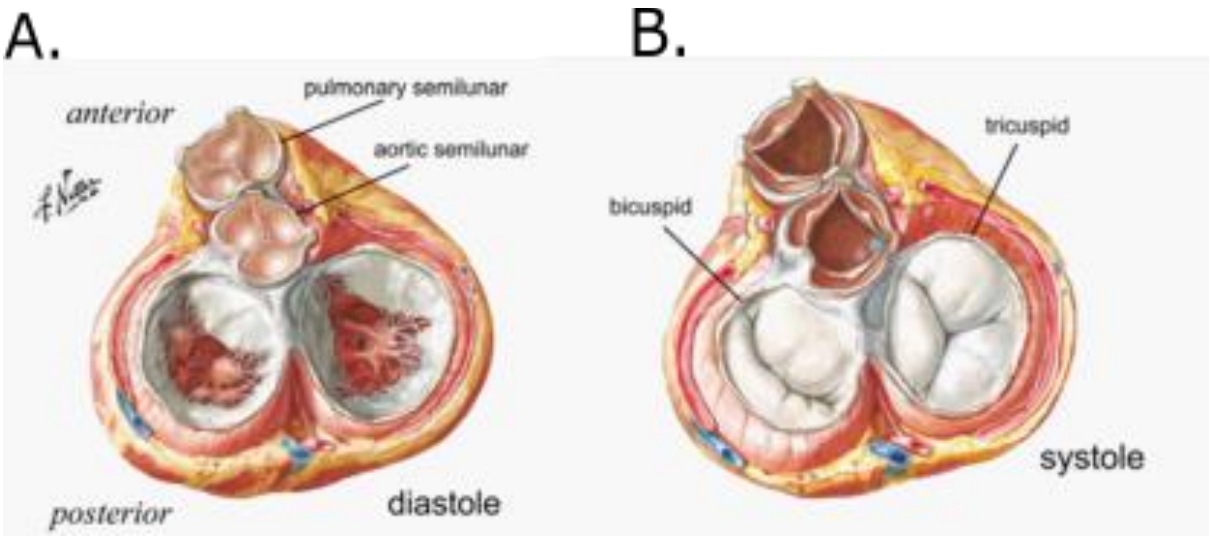

Figure 1.4. *Cross-sectional image of the heart in the transverse plane, showing all four heart valves during diastole (A) and systole (B). Reproduced from Netter, 2014.*

The two sides of the heart (left and right) can be divided by two different septa; the interatrial septum and the interventricular septum[1,3,5]. The interatrial septum is the thinner of the two, functioning to separate the right and left atria. The interventricular septum, alternatively, separates the two ventricles and is significantly thicker than the interatrial septum. The reason for this size difference is two-fold: the interventricular septum acts as a conduit for many important nerve pathways crucial to cardiac contraction, and the pressure difference between the ventricles is much greater than that between the atria[1,3].

This idea of pressure difference between chambers is an important one to appreciate for this literature review. The heart, like most other parts of our body, is constantly recycling and remodeling its tissues to ensure that all cardiac tissue is healthy and functioning, but also to continually match the heart's functional capacity to the systemic demand of the body[1]. This is best reflected in the thickness of the walls of each respective chamber of the heart. The right atrium, the thinnest of the four chambers, has an internal pressure that fluctuates between 1-8mmHg throughout the cardiac cycle. The left atrium experiences slightly higher pressures, from 1-10mmHg, making its walls slightly thicker than those of the right atrium. The right ventricle can have internal pressures as low as 1-8mmHg during filling, and 15-30mmHg during contraction, making its walls somewhat thicker than those of the atria. But it is the left ventricle which demonstrates this principle most significantly, experiencing internal pressures of 2-12mmHg during filling and 100-140mmHg during contraction. This leads to the left ventricle having by-far the thickest walls of the four chambers of the heart, reflecting not only the larger pressure difference but also the crucial role of this chamber in pushing blood throughout the entire systemic circulation[3].

1.2.4 Coronary Circulation

Like any other muscle in the body, the heart itself requires a constant supply of nutrient-rich blood to drive its continuous action. Branching from the aorta immediately after its emergence from the left ventricle, the right and left coronary arteries supply blood to the myocardium during the relaxation phase

of the heart. The left coronary artery branches to form Left Anterior Descending branch, travelling along the anterior interventricular sulcus to supply both ventricles with blood, and the Circumflex branch, which lies in the coronary sulcus and supplies blood to the left atrium and ventricle[1,6]. The right coronary artery supplies small branches to the right atrium before splitting into two different arteries; the Posterior Interventricular Branch, which runs in the posterior interventricular sulcus and supplies both ventricles with blood, and the Marginal Branch, which runs down the right border of the heart to supply the right ventricle with blood[1,6].

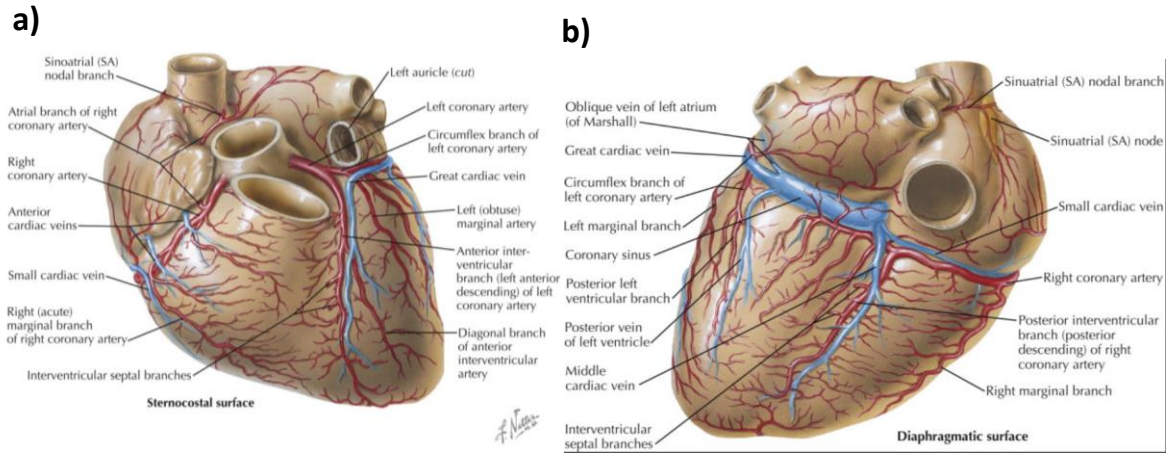

Figure 1.5. *Retrieved from Netter (2014)[7], this illustration depicts the major vessels of coronary circulation, from the anterior view (panel a) and the Posterior view (panel b).*

Deoxygenated blood must also be drained from the myocardium and returned to the right ventricle, a role which is performed by the cardiac veins. Most of the deoxygenated blood is gathered by cardiac veins in the Coronary Sinus, which sits in the coronary sulcus on the posterior aspect of the heart and empties into the right atrium. There are four principal tributary veins, three of which direct deoxygenated blood into this Coronary Sinus. The Great Cardiac Vein lies in the anterior interventricular sulcus and drains the region supplied by the left coronary artery. The Middle Cardiac Vein lies in the posterior interventricular sulcus and drains the regions supplied by the posterior interventricular artery. The Small Cardiac Vein lies in the coronary sulcus and drains the two atria. Finally, the Anterior Cardiac

Veins drain the right ventricle, but empty directly into the right atrium. See ***figure 1.5*** for an anatomical overview of the cardiac circulation.

1.3: Cardiac Physiology

The tissue of the heart can be broken down into the fibrous skeleton, which acts as a cardiac scaffold, and the myocardial tissue, which is responsible for the contractile capacity function of the heart.

1.3.1. Fibrous Skeleton of the Heart

As implied by the name, the fibrous skeleton of the heart is composed almost entirely of dense connective tissue, providing structure and stability for the contracting cardiac tissue and supporting the integrity of the heart valves[1,4,8]. The fibrous skeleton can be conceptualized into three parts; the *annuli fibrosis* which encircles the four heart valves, the *trigonum fibrosum* which form two triangular sheets running between the valves, and lastly the *septum membranaceum* which lies between the two ventricles[4,8]. While the fibrous skeleton is important to keep in mind due to its role in providing the scaffold for the myocardium, the remainder of this review will focus on chamber function and myocardial structure.

1.3.2 Myocardial Physiology

The heart musculature is generally composed of three layers of tissue, similar to the structure of arteries. The internal layer is called the *endocardium*, which lines the inside of the cardiac chambers. The *epicardium* is the outer layer, which has two layers of its own, a deeper fatty connective tissue layer and a thin fibrous exterior that is continuous with the pericardium[4]. Finally, the *myocardium* is the middle layer, and is the thickest of the three due to its role as the contractile layer of the heart, a relationship shown in ***figure 1.6***. The myocardium consists largely of bundles of cardiomyocytes, which are interlaced with richly vascularized connective tissue into spiraling shapes that wind up the heart from the apex to the base[4]. Within this largest layer, the extracellular matrix (ECM) is composed of a complexly woven

series of fibers and proteins commonly referred to as connective tissue (CT), which together provide structural support for the cardiomyocytes and assist in the extracellular signaling and regulation. Three variants of collagen (I, III, V) reside in abundance in the ECM, which together with glycoproteins, proteoglycans and elastin provide a structural foundation capable of maintaining tensile strength and myofibrillar organization[9,10].

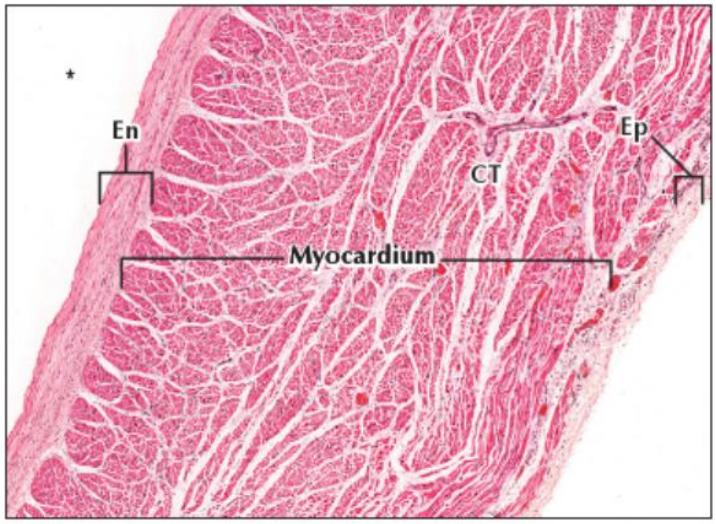

Figure 1.6. *Retrieved from Netter's Essential Histology, 2008[4], this cross-section of the LV freewall demonstrates how the myocardium is by far the largest of the three layers of cardiac tissue, compared to the endocardium (En) and the epicardium (Ep). The white spaces within the myocardium represent the ECM, which is occupied by a variety connective tissues (CT).*

1.3.3 LV Fiber Orientation and Twist Mechanics

While examination of the heart from a cross-sectional perspective (as in *figure 6*) can make it difficult to detect, the fiber orientation of the myocardium does not run parallel or perpendicular to the long axis of the heart. Instead, the fibers wind diagonally from the apex towards the base of the heart[11,12], as can be seen in panel A and E of ***figure 1.7***. In addition, the angle at which myocardial fibers are

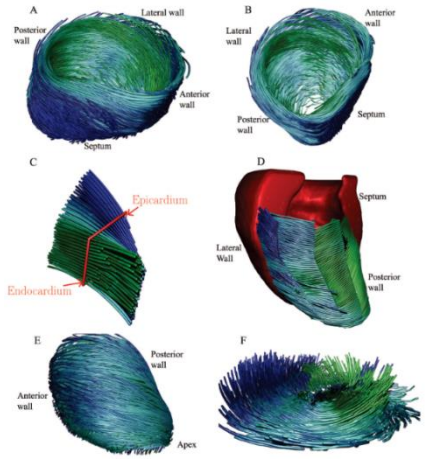

Figure 1.7. *Retrieved from Rohmer et al. 2005, MRI-derived visualization of LV fiber orientation, with green representing endocardial fibers and blue epicardial.*

oriented differs throughout the myocardial layer. Panel D of ***figure 1.7*** demonstrates how the deeper fibers of the myocardium adjacent to the endocardium (in green) wrap around the heart in a counterclockwise manner, while the more superficial fibers adjacent to the epicardium (in blue) conversely wrap around the heart in a clockwise direction. The transition between these two orientations occurs smoothly throughout the myocardium, as seen in panel C of ***figure 7***. This fiber orientation is important from a functional perspective, as it allows the heart to contract in a twisting manner, with the apex rotating clockwise and the base counterclockwise during systole[12], as demonstrated in ***figure 1.8***.

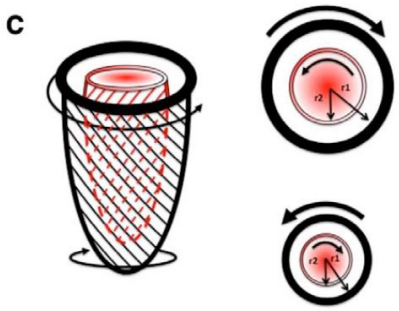

Figure 1.8. *Retrieved from Omar et al. 2015, conceptual illustrations of the epicardium (black) rotating the base of the heart counterclockwise and the apex clockwise, contrary to the weaker pull of the endocardium (red). This results in the heart exhibiting a twisting motion throughout the contractile cycle.*

This transitions the LV from the traditional concept of a squeezing pump, to a dynamically twisting chamber that "wrings" blood out during its twisting contraction in systole, and creates additional suction by untwisting during diastole to increase passive filling[12–14].

1.3.4. Cardiomyocytes

The roughly cylindrical contractile cells of the heart are known as cardiomyocytes. Due to their contractile function, the internal volume of these cells is largely composed of contractile subunits of proteins known as sarcomeres. These sarcomeres are organized into columns of myofibrillar protein, which in turn are woven into a lattice that occupies the majority of the volume inside each cardiomyocyte. Sarcomeres are made of three categories of proteins; contractile proteins, regulatory proteins and structural proteins. The two contractile proteins of note are myosin thick filaments, and actin thin filaments. These are present at a ratio of roughly 1 myosin: 2 actin, with the actin anchored to the z-discs at either end of the sarcomere, and the myosin sitting in the middle of the sarcomere anchored to proteins along the M-line. These thick and thin filaments are situated overlapping each other, with the degree of

overlap dependent on the contractile state of the tissue[1,4]. The relationship between these two proteins will be explored later in this review. The main regulatory proteins of the sarcomere are faciliatory proteins known as troponin and tropomyosin. These two proteins are woven around the actin thin filaments and play crucial roles in promoting/inhibiting the contractile action of the sarcomeres[1,3]. Lastly, there are approximately a dozen proteins that are key to the structural integrity of the sarcomere. Of particular note are; Titin, which is capable of adjusting the resting tension of the sarcomere, α-actinin which forms the core of the z-discs, myomesin which forms the core of the M-line and Nebulin which supports the integrity of the thin filaments[1].

Cardiomyocytes are also joined together in a somewhat interlaced fashion, bound end-to-end by proteins known as *Intercalcated Disks*. These disks are formed by strong associations between membrane-bound proteins and the cellular membrane of adjacent cardiomyocytes. The crucial proteins to these disks are desmin, N-cadheren, connexin, vinculin, beta-catenin, desmoplakin-1, desmocollin-2 and plankoglobin-2[3]. Within these intercalated discs are small passages that allow for rapid propagation of action potentials through the myocardial tissue, which are known as gap junctions [4].

The sarcolemma, or cell membrane of the cardiomyocytes, sends projections known as *T-tubules* down into the cardiomyocyte, which intersperse between myofilaments and play a crucial role in stimulating the contraction of sarcomeres. This function is aided by the *Sarcoplasmic Reticulum*, which can be thought of as a network/web of storage tubes for calcium that are draped over the myofilaments. Together, the T-tubules and sarcoplasmic reticulum release and sequester the calcium that drives cardiomyocyte activity, making the operation of these organelles crucial to cardiomyocyte function. Of particular importance for this purpose are the Sarcoplasmic Reticulum Calcium ATPase (SERCA) and sodium-calcium exchange proteins of the sarcoplasmic reticulum, parvalbumin buffering proteins and the ryanodine receptors of the T-tubules[1,15].

While cardiomyocytes are the functional units of the myocardial tissue of the heart and take up roughly 80-90% of the myocardial volume, cardiomyocytes only make up 30-50% of the number of cells in the myocardium[16]. The majority of the other 50-70% are cardiac fibroblasts, which are crucial in maintaining a healthy balance of structure and elasticity within the myocardial tissue, but which have also been linked to pathological myocardial fibrosis in response to regulatory dysfunctions[16,17].

1.4: Cardiac Innervation

1.4.1 Intrinsic control: Autorhythmic cardiac electrophysiology

Approximately 1% of cardiac muscle fibers are specialized to be self-excitable, capable of consistently generating action potentials without any neural influence from outside of the heart[1,4]. These fibers, termed *Autorhythmic Fibers*, are closely grouped in a region of the right atrium known as the *Sino-Atrial (SA) node*. Their naturally leaky cell membranes cause them to constantly generate action potentials (APs) at an intrinsically set rate of ~100 beats per minutes, an action which can continue even after the heart is removed from the body. These APs utilize the gap junctions between cardiomyocytes to propagate out across both atria, culminating back to the *Atrioventricular (AV) Node* where the signal is typically slowed due to structural differences in the cells of the AV node itself. The AP then travels down the *Atrioventricular Bundle*, also called the Bundle of His, dividing into the right and left bundles to travel through the interventricular septum to the apex of the heart. From there, the signal travels back up the ventricular free walls in the *Purkinje fibers*[1]. See ***Figure 1.9*** for a visualization of the trajectory of these signals.

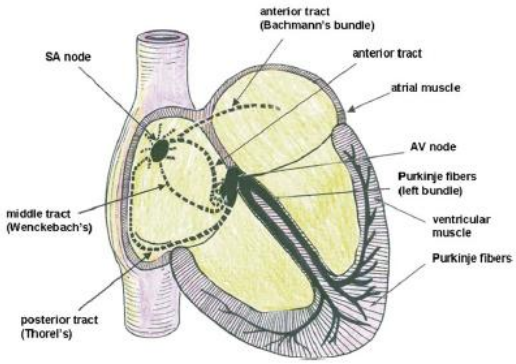

Figure 1.9. *An outline of the autorhythmic cardiac conduction system, with AP trajectory outlined in green. Retrieved from Iaizzo et al, 2015*

1.4.2 Extrinsic Control: Anatomy of the Autonomic Nervous System

The nervous system can be divided either structurally into the central nervous system (CNS) and peripheral nervous system (PNS), or functionally in the somatic nervous system and the autonomic nervous system (ANS). In terms of the structural divisions, the CNS incorporates the brain and the spinal cord, whereas the PNS involves all peripheral nerves. The functional divisions on the other hand, particularly the ANS, are crucial to the topic of spinal cord injury and cardiovascular function. The somatic nervous system is responsible for the conscious experience of sensory information and control over bodily movements, which is classically divided into sensory and motor portions respectively[1]. These sensory and motor capacities provide us with the ability to experience and interact with our environment, whether through reading and writing a test or training for a marathon, and therefore can indirectly influence long-term cardiovascular health. However, it is the ANS regulating our automatic bodily functions without our conscious awareness which is most directly involved in the health and function of our cardiovascular system. To understand this concept, we must examine the ANS in its two functional divisions; the sympathetic nervous system (SNS) and the parasympathetic nervous system (PSNS).

Sympathetic Nervous System

Put simply, the SNS is responsible for moving the body into states of increased excitement. This is commonly explained as the SNS stimulating the "fight or flight" response, preparing the body for quick, urgent movement and fast responses to environmental stimuli.

Anatomically, the SNS originates largely in two regions of the brainstem; the Nucleus Tractus Solitarii (NTS) and the Rostral Ventrolateral Medulla (RVLM). The NTS receives a constant battery of sensory afferent information from chemoreceptors, baroreceptors, mechanoreceptors, and metaboreceptors which it processes and sends onto the RVLM[18]. From the RVLM, efferent sympathetic pathways project down the spinal cord and synapse in the lateral horn of grey matter with the cell bodies of pre-ganglionic sympathetic neurons. Between segments T1-L2, these myelinated preganglionic neurons

exit the spinal cord via the ventral horn, bundling together briefly with the dorsal root to form the spinal nerve before finally branching off into the White Ramus Communicans via the anterior rami of the spinal nerve[18,19]. The preganglionic neuron is then directed to either the *Sympathetic Trunk* or the *Prevertebral Ganglia*. The sympathetic trunk is a chain of paravertebral ganglia that run along either side of the spinal column from the base of the skull to the coccyx[1]. The prevertebral ganglia on the other hand are sympathetic ganglia that sit anterior to the spinal column, closer to the visceral organs that they influence[1,20].

Striving to understand the exact trajectory of each post-ganglionic neuron as it travels from ganglia to target organ moves beyond the scope of this review. For our purpose, understand that the "chain" nature of the sympathetic trunk in particular allows for information from different spinal segments to be sent both rostrally and caudally, making comprehension of sympathetic innervation much more difficult than the myotome organization of somatic motor innervation[1,18]. Due to this nature, it can be said that all spinal nerves from T1-L2 are involved in the sympathetic regulation of the cardiovascular system, though the exact contributions of each nerve are still debated. This concept is summarized below in ***Figure 1.10*****.**

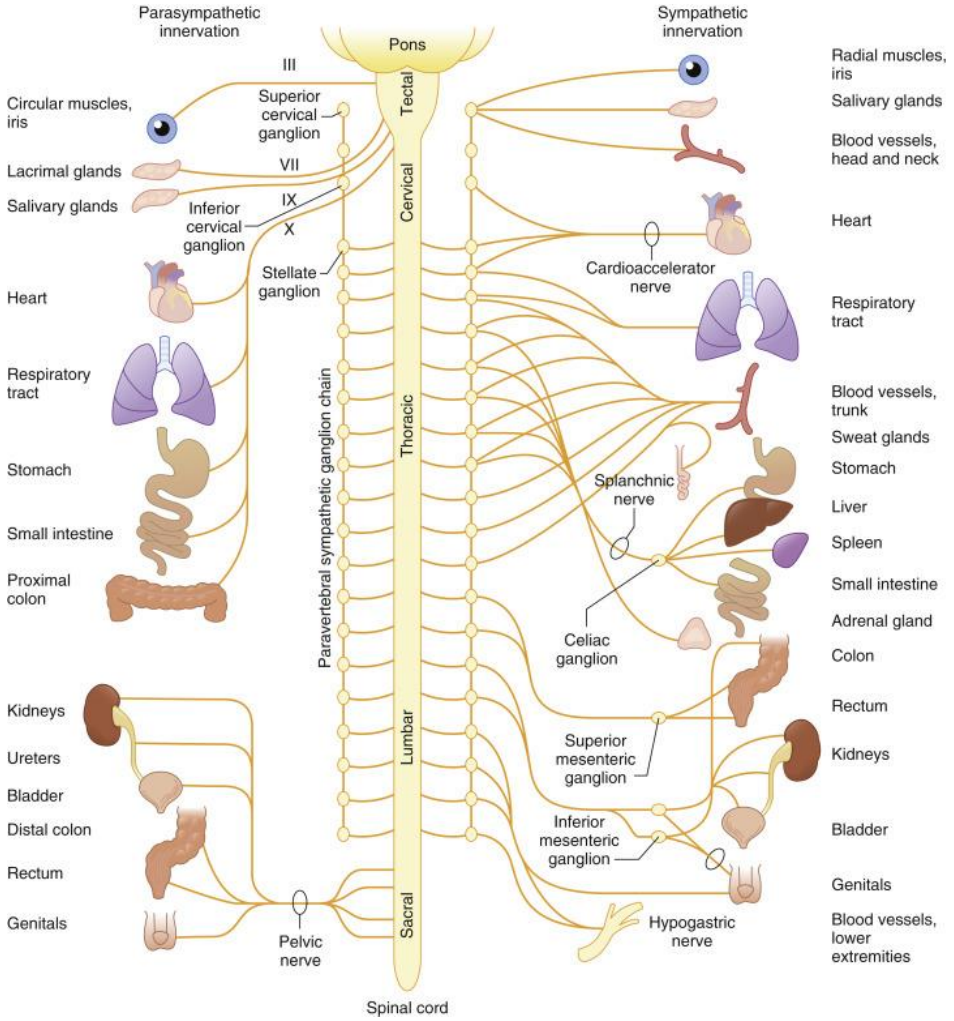

Figure 1.10. *Conceptual map of the basic organization of the sympathetic (right) and parasympathetic (left) nervous systems in relation to major organs and tissues of the body. Retrieved from Conti et al 2014*[7]*.*

Parasympathetic Nervous System

The parasympathetic nervous system (PSNS) is responsible for generally instilling a state of "rest and recovery" in the body[1]. Where the SNS prepares the body for sprinting and excited motion, the PSNS promotes digestion, relaxation of tensed tissues and slows the delivery of blood flow.

Named because it anatomically brackets the sympathetic nervous system both rostrally and caudally (para = beside), the PSNS originates from four cranial nuclei and three sacral spinal segments (see ***Figure 1.10)***. Of these different divisions of the PSNS, mainly neurons from the vagus nerve (cranial nerve X), originating in the nucleus ambiguous of the medulla and projecting to the viscera outside of the spinal

cord, have any significant influence on the cardiovascular system[1,20]. Additionally, the glossopharangeal nerve (cranial nerve IX) contributes specifically to cardiovascular reflex pathways[21].

1.4.4 Extrinsic Control: Autonomic control of the Cardiovascular System

The cardiovascular system receives sympathetic innervation from all spinal segments T1-L2 (see ***figure 1.10*** *and* ***figure 1.12***). Sympathetic preganglionic neurons projecting from spinal segments T1-T5 synapse onto the cell bodies of their postganglionic counterparts in seven different ganglia of the sympathetic trunk using acetylcholine as a neurotransmitter. From the three cervical ganglia and the upper four thoracic ganglia of the sympathetic trunk, these postganglionic neurons then project to the cardiac muscle of all four chambers of the heart, as well as specifically to the AV and SA nodes[1,22,23] (see ***Figure 1.11***). This projection is not symmetrical, as post-ganglionic fibers from the left stellate ganglia innervate the majority of the LV, while the right stellate ganglia mostly innervates the right side of the heart.[23] Upon synapsing with cardiac tissue, these sympathetic post-ganglionic neurons emit norepinephrine to act on β1 and β2 adrenergic receptors, increasing heart rate and conduction velocity at the SA and AV nodes, and increasing contractility and conduction velocity in the atria and ventricles[22].

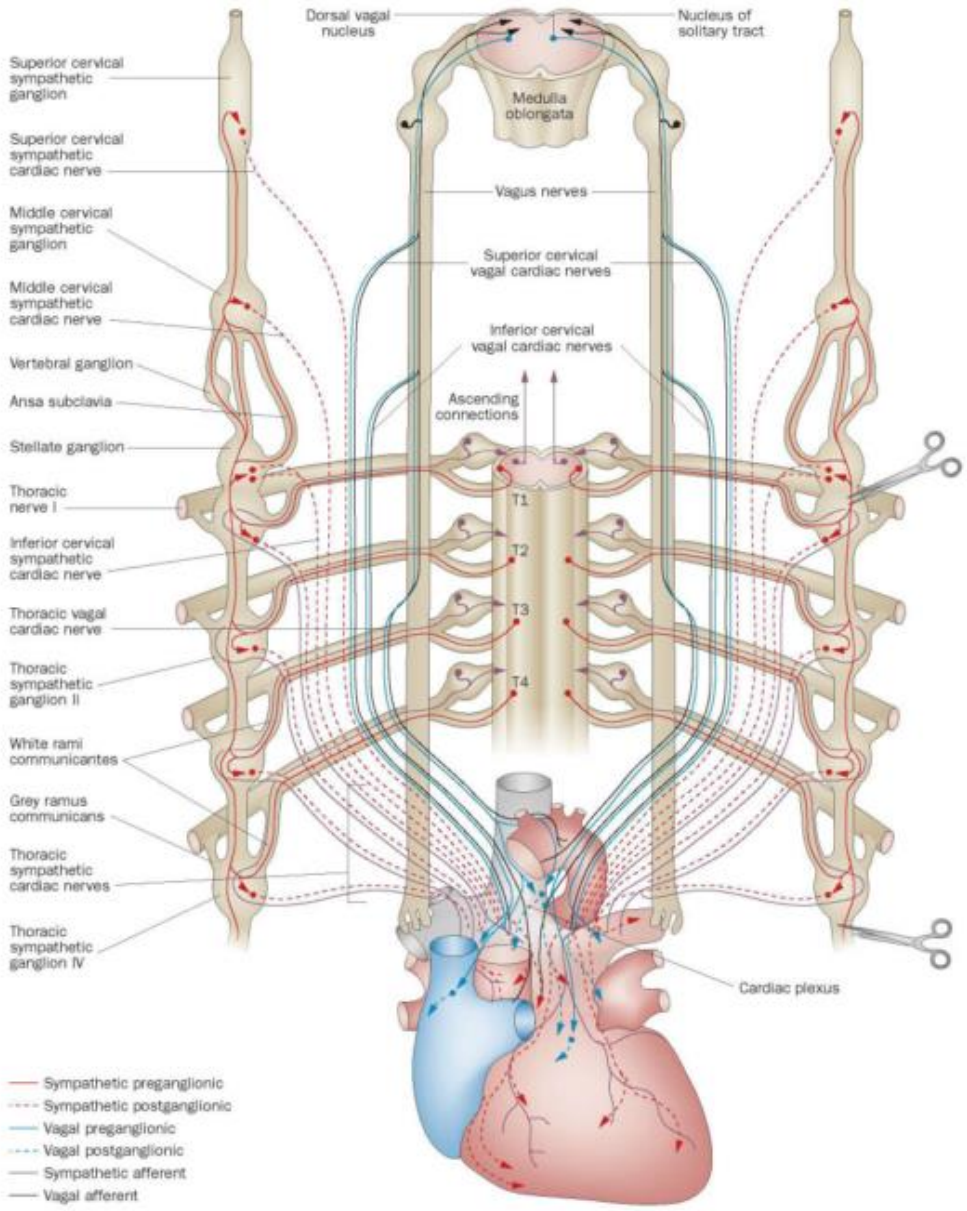

Figure 1.11. *Retrieved from Schwartz. 2014, this conceptual illustration provides a visual summary of the sympathetic and parasympathetic innervation of the heart itself. Note in particular how the left stellate ganglia has more direct input to the left ventricle than the right stellate ganglia*[23]*. This could be considered significant in the discussion of unilateral/asymmetrical SCI.*

The sympathetic preganglionic neurons arising from spinal segments T5-L2 synapse with postganglionic neurons lower on the Celiac, Superior Mesenteric and Inferior Mesenteric ganglia of the sympathetic trunk, also using acetylcholine as a neurotransmitter (see ***figure 1.12***). The postganglionic neurons then project to the abdominal viscera and lower limbs via the greater, lesser, least and lumbar splanchnic nerves, synapsing onto the tunica media of major arteries and veins of those regions[4]. In the vasculature, norepinephrine will largely act on α1 adrenergic receptors to stimulate vasoconstriction, though in selective regions this same norepinephrine can act on β2 adrenergic receptors to stimulate vasodilation (skeletal muscles, coronary arteries, abdominal viscera)[1]. A notable exception to this tidy orientation of pre/postganglionic neurons is the SNS's interaction with the adrenal medulla. As the adrenal medulla develops embryologically in tandem with the SNS, the medulla has the capacity to act as a modified ganglia, receiving preganglionic neurons directly from the spinal cord to trigger the rapid release of catecholamines[1,20].

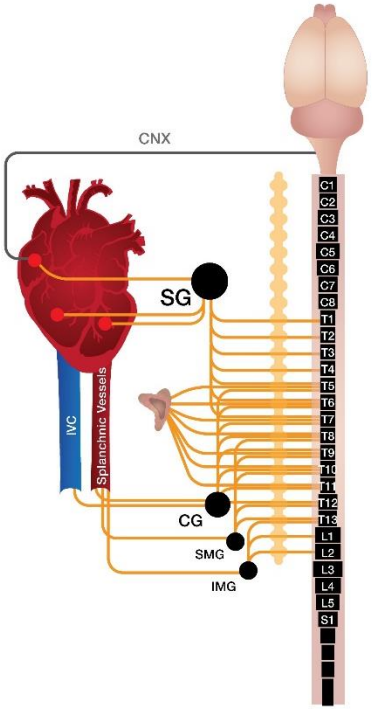

Figure 1.12. *Conceptual illustration of the autonomic innervation of the heart and peripheral vasculature, retrieved with alternations from Squair et al. 2017*

The parasympathetic preganglionic neurons, travelling mostly in the bilateral Vagus nerves (CN X), project from the cranium towards the heart, using acetylcholine to synapse with postganglionic neurons in either the inferior vagal ganglia or the cardiac plexus, which is situated at the base of the heart. The short parasympathetic postganglionic neurons then project to the AV and SA nodes, as well as the atria (see ***Figure 11***). Using acetylcholine as a neurotransmitter to act on M2 muscarinic receptors, these parasympathetic postganglionic neurons can then reduce the heart rate at the SA node, decrease conduction velocity at the AV node and decrease contractility at the atria[22]. In the context of the rest of

the cardiovascular system, the parasympathetic nervous system has a limited influence, capable of causing vasoconstriction of coronary arteries, vasodilation of salivary, gastric and intestinal arteries for the release of hormones, and mild vasodilation in skeletal muscles to promote blood flow[1]. There is also a minor contribution from the glossopharangeal nerve (CN IX) to the carotid bodies, which regulate baroreflex function[1].

In summary, sympathetic projections from T1-T5 are capable of increasing heart rate and contractility, while those from T6-L2 are capable of stimulating vasoconstriction in the viscera and lower limbs. The parasympathetic contribution to cardiovascular function is mainly from the vagus nerve (CN X), capable of slowing heart rate, reducing atrial contractility (see ***Figure 9***), stimulating the secretion of select glandular hormones, and increasing blood flow to select skeletal muscles.

1.5: Vascular Physiology

Physiologically, blood vessels are subdivided into three separate categories: arteries, veins and capillaries. Arteries are efferent vessels that operate under high pressure conditions. As such, those close to the heart are highly elastic in nature to allow for consistent blood flow despite pulsatile pressure from the heart, and those in large vascular beds near major organs are highly muscular to allow for quick and precise control over blood flow distribution[4]. Arteries are composed of three layers of tissue; the internal-most tunica intima is made largely of elastin and collagen fibres along with the endothelium on the luminal surface, the middle Tunica Media is composed largely of smooth muscle cells and elastin, and the outer-most Tunica Adventitia is composed of loosely organized

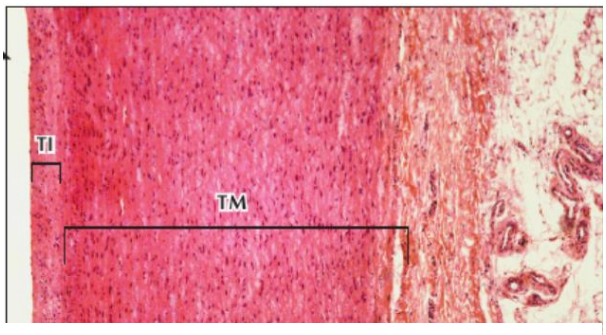

Figure 1.13. *A cross-sectional view of the wall of the aortic arch through a light microscope, demonstrating the three layers of arterial structure: Tunica Intima (TI), Tunica Media (TM) and Tunica Adventitia (TA). Retrieved from Ovalle 2008*

longitudinal collagen fibres, fibroblasts and small nutritive blood vessels[1,4]. Large elastic arteries such as the aorta have a greater prevalence of elastin in their two inner-most layers, while muscular arteries can have a relatively larger tunica media due to greater prevalence of smooth muscle cells[4].

Veins are afferent vessels which operate in a significantly lower pressure environment, leading to them having much thinner walls than their arterial counterparts. Veins are composed of the same three layers, but the characteristics of each differs greatly from those in the arteries. The Intima is composed of one thin layer of endothelial cells anchored to the media by a small layer of sub-endothelial connective tissue. The media is not well developed, in larger veins such as the vena cava it is composed of a layer of circularly arranged smooth muscle cells and in smaller veins and venules often may exist as a single layer of smooth muscle cells. The Adventitia is the thickest layer, composed primarily of longitudinally arranged collagen fibres[4]. One characteristic that is unique to the venous system are a series of semilunar valves in small and medium sized conducting veins, which help counter the force of gravity pulling blood caudally and working in tandem with the contraction of skeletal muscles to return blood to the heart[1,4].

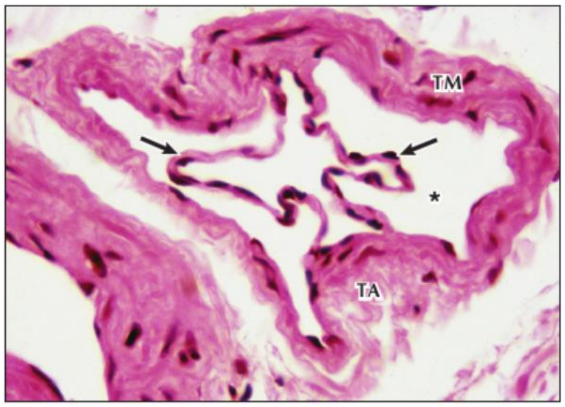

Figure 1.14. *A cross-sectional view of a small vein, with arrows indicating the two leaflets of a valve projecting into the lumen. Retrieved from Ovalle, 2008.*

Capillaries, finally, are the smallest type of vasculature which are situated between the arterial and venous system. They make up approximately 90% of the vasculature in the body and their walls are composed of a single layer of endothelial cells. Capillaries have an extremely large cumulative cross-sectional area, but the lumen of individual vessels is barely large enough for a red blood cell to flow through (5-10µm) at a very slow rate[4]. These

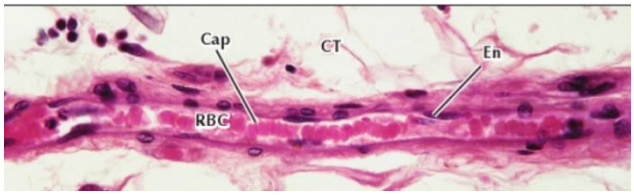

Figure 1.15. *A longitudinal section of a capillary, with the endothelium (En) and circulating red blood cells (RBC) clearly visible.*

factors make capillaries ideal sites for gas and fluid exchange between circulating blood and bodily tissue[1,4,24].

1.6: The Cardiac Cycle

1.6.1 Breaking down the Cardiac Cycle

The cardiac cycle, a series of events that lead to the heart ejecting blood into pulmonary and systemic circulations, can be broken down into two major phases; systole and diastole. Systole is the contractile phase of the cycle, in which the heart tissue utilizes both stored potential energy and actively generated mechanical energy to eject blood from the heart. Diastole is the relaxation portion of the cardiac cycle, in which the myocardium releases tension and the heart expands to refill with blood before the next systole begins[1]. While the cardiac cycle can be broken into these two distinct phases, not all chambers contract simultaneously during systole, or relax simultaneously during diastole. To better understand this, it is worth reviewing the trajectory of the intrinsic electrical signal that stimulates contraction[1,2], with additional consideration to ***Figure 16a***, which outlines the changes in pressure and volume experienced by the left atrium and ventricle, and the aorta at different time-points of the cardiac cycle. Furthermore, cardiac function can also be evaluated by plotting the changes in pressure vs volume throughout the cardiac cycle, as seen in ***Figure 16b.*** This concept will be discussed further in the methods section.

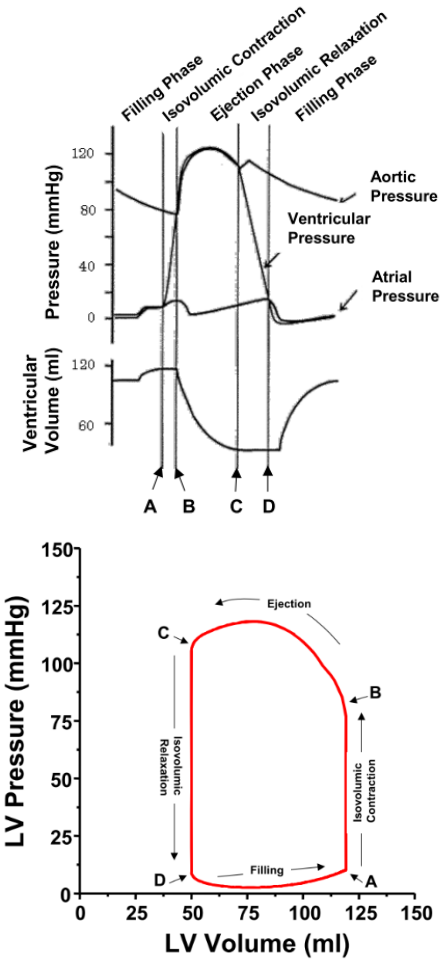

Figure 1.16. *A) Pressure and Volume traces in different chambers of the heart throughout the cardiac cycle. B) A typical resting pressure-volume loop. Reproduced from Burkhoff, 2011.*

Systole is triggered by the aforementioned autorhythmic fibers of the SA node, whose APs travel around the atria to the AV node, where they are briefly delayed. Due to this delay, the two atria contract well before the ventricles, causing the atrial pressure to exceed the ventricular pressure. This early atrial contraction loads the ventricles well in excess of passive diastolic filling. The AP then travels down the interventricular septum, rounding the apex of the heart and travelling up the walls of the ventricles back towards the base of the heart. This trajectory causes the ventricles to pump upwards, squeezing from the apex towards the base in a twisting motion to increase the pressure towards the aortic and pulmonary valves. Once the pressure inside the ventricles exceeds that in the respective artery (aorta for left ventricle, pulmonary for right), the valves open and blood is ejected from the heart and into circulation[1,2].

Diastole begins when enough blood has been pumped out of the maximally contracted ventricles that the pressure inside the ventricles drops below that of the aorta and pulmonary trunk. As the AP passes and the myocardium is no longer excited to contract, the ventricles start to relax. The aortic and pulmonary valves then close and the ventricles relax isovolumically, while the atria continue to passively refill from the pulmonary and systemic circulation (this began while the ventricles were still ejecting blood from the heart during systole). As the ventricles relax enough for their pressure to equal that in the atria, the tricuspid and bicuspid valves open again, and blood fills all four chambers again[2–4].

1.6.3: Excitation-Contraction Coupling:

Previous sections examined how the heart contracts anatomically, but what physiological processes allow this contraction to happen? Why and how does the myocardium contract?

The key players driving contraction of the myocardium are calcium ions (Ca^{2+}). As the previously outlined action potential generated at the SA node reaches a cardiomyocyte, it depolarizes the sarcolemma, creating an AP that expands across the sarcolemma and down into the cardiomyocyte via the transverse-tubules[1,15]. This depolarization of the sarcolemma activates L-type calcium receptor channels, which open to allow a small amount of Ca^{2+} to flux into the cytoplasm from the sarcoplasmic

reticulum. This small quantity of calcium functions mainly to activate the intracellular aspect of Ryanodine receptors, which then open to allow a much larger quantity of Ca^{2+} ions to flux into the cytoplasm[15]. This large quantity of calcium binds to the calcium receptors on troponin, changing the shape of regulatory proteins, as well as that of their associated tropomyosin[1]. This results in tropomyosin shifting to uncover the myosin binding sites on the actin thin filaments. The myosin head of the thick filament is now free to bind to the actin thin filament, adhering to specific binding sites, then cocking to wind the thin filament adjacent to the thick filament. ATP is then required to break the chemical bond between the myosin head and the actin, breaking the ATP into ADP and Pi and resetting the myosin head to begin the cycle all over again[1]. This happens countless times within each sarcomere, driving the shortening of the sarcomeres and thereby contraction of the muscle tissue. [1]

1.6.4: Calcium handling throughout the Contractile Cycle

Calcium plays a crucial role in regulating the intensity and duration of muscle contraction. At rest, calcium is present in very small quantities inside the cytosol of the cardiomyocytes but is present in much greater concentrations just outside the sarcolemma in the extracellular space[25]. As previously mentioned, the large calcium flux that triggers the ECC occurs in two stages. Typically, the depolarization of the sarcolemma causes slower voltage-gated Ca^{2+} channels to open, allowing calcium to leak into the cytosol of the cardiomyocyte. This leaking calcium interacts further with ryanodine receptors in the sarcolemma, which then open to allow huge amounts of calcium to influx into the cytosol[15,25].

An important point that is often overlooked is how the calcium is sequestered back out of the cell after the AP passes. This is done passively by sodium/calcium exchangers (which do assist slightly with the reverse action of letting calcium flow into the cytosol), and actively by proteins such as the *sarcoplasmic reticulum calcium transport ATPase (SERCA)*[15]. An additional protein called *Parvalbumin* is also capable of buffering the Ca^{2+} ions, to provide more immediate release from the contractile filaments while re-uptake is occurring. This sequestration is vital to allow the tropomyosin to move back into place inhibiting the

myosin heads from binding actin, thereby preventing further ECC coupling and allowing the sarcomere to relax back to its resting state[15].

1.7: Neurohumoral Control of Circulation

1.7.1: General interaction of ANS and CVS:

At rest, on average 7% of the body's blood volume resides in cardiac structures, 9% resides in the pulmonary circulation, and the remainder can be found in the systemic circulation. Dividing this systemic distribution further, roughly 13% of the body's blood resides in systemic arteries and arterioles, 7% in the capillaries, and the remaining 64% in the systemic veins and venules[1]. Therefore, while close regulation of the body's arteries may be important for directing oxygen delivery and reflex modulation, the control over the distribution of the body's blood volume, which is important when considering cardiac loading, occurs through modulation of the venous system[1].

Blood flow can also change drastically depending on the metabolic demands being placed on the body, such as during states of rest vs. rigorous exercise. The first notable difference in this comparison is that cardiac blood flow will increase up to five times during exercise compared to when at rest, pumping out over 25L/minute of blood in the average person. During both states the heart will receive roughly 4% of the CO, but due to the increase in CO this maintained percentage results in a 5-fold increase in cardiac circulation as well. The rest of the organs and viscera actually receive a smaller proportion of blood during exercise, with the one exception of course being the skeletal muscle. At rest skeletal muscle receives roughly 20% of the CO, but during vigorous exercise this jumps as high as 80-85%, meaning that the heart sends up to 21L/min of blood to skeletal muscle during exercise[24].

But how does this distribution get altered, and how can the heart suddenly pump out five-times more blood? The answer to these question lies partly in the autonomic nervous system (***Figure 1.10***). Tonic autonomic tone is always present, with both the sympathetic and parasympathetic nervous systems acting on all possible tissues continuously[1,20,21,26,27]. The modulation of their affects occurs by shifts in the intensity of their activity. For example, regions that require more blood experience a withdrawal of the tonic tone from postganglionic sympathetic neurons, diminishing sympathetic input to allow vasodilation and increased blood flow to their associated tissues. Conversely, increased sympathetic stimulus triggers vasoconstriction of major conducting vessels, which in combination with skeletal muscle pumps, increase the amount of blood returning to the heart[1,20]. Lastly, local tissue perfusion is largely controlled by the contraction and dilation of precapillary sphincters (see ***Figure 1.17***), the latter of which is activated by *increased* sympathetic tone. Conversely, withdrawal of sympathetic tone will cause the precapillary sphincters to constrict and reduce blood flow to the associated capillary bed[6,28].

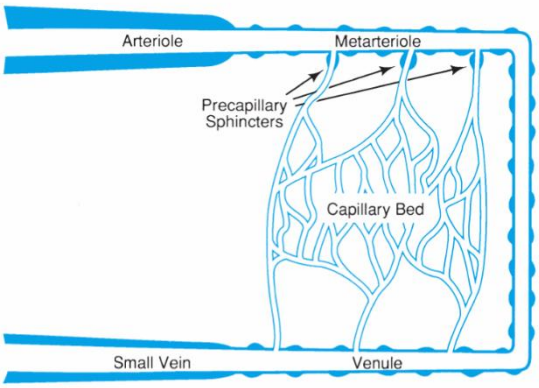

Figure 1.17. *Illustration of the microcirculation, which includes the metarterioles, precapillary sphincters, capillaries and venules. Retrieved from Johnson et al. 2009*

In terms of cardiac function, cardiac output can be influenced by two major factors, heart rate and the stroke volume. At rest the average individual will have a heart rate between 60-70 beats/minute (bpm)[24]. This is lower than the previously mentioned intrinsic heart rate from the autorhythmic fibers of the SA node (which depolarized at roughly 100bpm). The reason for this difference is the tonic input from the Vagus nerve of the parasympathetic nervous system, which slows the depolarization at the SA while at rest[1,24]. Recent works have suggested that, similar to vascular control, this maintenance of HR is always overseen by a balance of sympathetic and parasympathetic input, with changes in HR being modulated by alterations in the balance of input from the SNS and PSNS[27]. For example, as an individual begins to

exercise, parasympathetic outflow from the Vagus nerve decreases, while sympathetic outflow from spinal segments T1-T5 increase the rate of depolarization at the SA and AV nodes, increasing the heart rate to as high as 200bpm in young adults[1,24,27]. From a neurological activity perspective, this increase in HR from resting to maximal during exercise is characterized by a resting PSNS:SNS balance of 4:1, to an active PSNS:SNS balance of 1:4[27] (***figure 1.18)***. Simultaneously, sympathetic outflow from those same spinal segments stimulate the ventricles to contract harder and faster, increasing stroke volume. When combined with the increase preload provided by the greater venous return during exercise (due to the Frank-Starling Law[29]), stroke volume can increase from 60-70mL/beat at rest to 120-140mL/beat in a moderately fit individual[24].

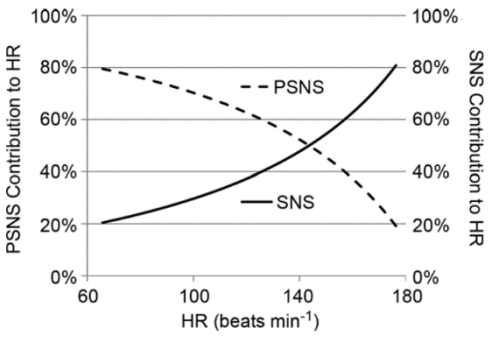

Figure 1.18. *Depiction of the change in PSNS:SNS balance from resting HR to maximal HR. Retrieved from White et al. 2014*

1.7.2: Neural Control of Cardiovascular Function During Movement

In a tidy description of cardiovascular response to movement and exercise, Dr Peter Raven describes arterial blood pressure and heart rate as being inherently dependent on three factors; central command (CC), the arterial baroreflex (ABR) and the exercise pressor reflex (EPR)[21,24]. These three pathways respond to efferent signals by altering the balance of parasympathetic and sympathetic outflow.

CC refers to signals, similar to those which simultaneously stimulate movement, sent from the motor cortex to the brainstem to elicit a withdrawal of parasympathetic activity and an increase in sympathetic drive. The magnitude of this change is directly proportional to the magnitude of the elicited skeletal muscle movement, in that larger movements elicit a more drastic shift in autonomic balance.[24] The EPR is stimulated by local chemical and mechanical changes within exercising skeletal muscle, which afferently feeds back to the brainstem to shift the autonomic balance in favor of sympathetic activity. The magnitude of this response is also proportional to the magnitude of the effort and/or movement. Finally,

the ABR is a two-part reflex pathway capable of tightly regulating cardiac and vascular function to maintain blood pressure homeostasis during postural change. The first branch of the reflex responds to high pressure stimuli and arises from stretch receptors located mostly in the carotid arteries and aortic arch, while the second branch responds to low pressure stimuli and arises from cardiopulmonary stretch receptors in the heart and lungs[30,31]. The afferent signals from these two branches travel through cranial nerves IX and X to the brainstem to allow for beat-by-beat reflexive control of cardiac and arterial function. For an example of reflex function, decreases in arterial pressure lead to decreases in cardiopulmonary receptor stretch, stimulating a near-immediate increase in sympathetic activity and decrease in parasympathetic activity which is maintained on a negative-feedback basis until arterial pressure returns to a resting value. Increases in arterial pressure elicit the opposite response to decrease blood pressure back to the resting range[24,31]. The ABR is particularly important in the maintenance of adequate cardiovascular function and tissue perfusion in response to postural change and centrifugal/gravitational force.

These three pathways are very powerful in their capacity to elicit quick system changes to demands such as exercise and play key roles in the renowned “fight or flight” response. However, circumstances exist in which more long-term, or more localized responses to stimuli are required.

1.7.3: Influence of Hormones & Neuropeptides on the Cardiovascular System

Hormones and neuropeptides provide a less instantaneous, though longer-lasting effect on the cardiovascular system. The neuropeptides epinephrine and norepinephrine can elicit physiological changes by interacting with vascular β_2 and α-receptors, as well as cardiac β_1-receptors to influence vasomotor tone and cardiac function. These catecholamines can be released by the adrenal glands to circulate in the blood.[20] Interactions with β_1-receptors in the heart elicit both a chronotropic and inotropic effect[20], while epinephrine stimulates vasodilation via β_2 receptor activity and norepinephrine elicits vasoconstriction via α-receptors activity.

Blood volume can also be transiently increased by the presence of the mineralocorticoid Aldosterone, regulated through a pathway known as the *Renin-Angiotensin-Aldosterone System (RAAS)*. When the kidneys sense a reduction in systemic blood pressure, they release the hormone renin, which, through activation of Angiotensinogen I/II stimulates the release of aldosterone from the adrenal cortex. Aldosterone increases the reabsorption of Na^+ at the kidney's, creating an osmotic gradient that leads to additional water absorption, increasing overall blood volume[1]. This hormone therefore provides a mechanism of control over blood volume, and indirectly over systemic pressure. However, an emerging body of literature has posed questions as to the long-term effects of elevated levels of circulating aldosterone[32,33]. Mild elevations of aldosterone have been reported in patients suffering from hypertension, and have been found to induce oxidative stress, hypertrophic remodeling, inflammation, fibrosis and possibly endothelial dysfunction in both systemic vasculature and the heart itself independently from the loading effects[32–35]. This can be taken as an indicator that hormones such as aldosterone are a capable tool for transiently regulating blood volume and pressure, but which may have negative long-term consequences if relied upon too heavily.

1.7.4: Local Factors Influencing Blood Flow

In addition to the systemic regulators of cardiovascular function, there are also factors which are locally produced and released to stimulate changes which are either more specific or beyond the scope of those described previously. A potent example of this is the stimulus for vasodilation. While most of the vasoconstriction is performed by the sympathetic nervous system, the parasympathetic nervous system doesn't directly influence the vasculature, besides one or two exceptions around the heart. Instead, vasodilation is largely controlled by local factors, which are produced and released by the blood vessels themselves in response to circulating neurohumoral factors and/or mechanical stress from blood flow[1]. In particular, three specific factors have a strong vasodilatory influence; Nitric Oxide (NO), Prostacyclins and Endothelium-Derived Hyperpolarizing Factor (EDHF)[36].

Perhaps the most widely studied of the three is NO. Circulating factors such as bradykinin and shear stress cause an increase in intracellular Ca^{2+} in the vascular endothelium, activating nitric oxide synthase to produce NO, which acts as a paracrine hormone to stimulate dilation of nearby vessels[36]. Prostacyclin is an unsaturated fatty-acid produced in the vascular endothelium in response to circulating acetylcholine which, like NO, stimulates vasodilation and prevents platelet aggregation in nearby vasculature[37,38]. Lastly, EDHFs are a class of uncharacterized factors which respond to circulating bradykinin and mechanical stress by eliciting K^+ channels in the membrane of the vascular smooth muscle to open, hyperpolarizing the sarcolemma of the cell. This decrease in resting membrane potential diminishes action potentials, thereby causing a relaxation of the vascular smooth muscle and dilation of the vessel[36,39,40].

These vasodilators are capable of eliciting changes in local vascular diameter in response to an increase in the rate of blood flow, in an action known as *flow mediated vasodilation.* This is the inference that as flow-rate inside the vessels increases, the aforementioned local factors respond to cause dilation and reduce the resistance to flow to reduce shear stress on the vessel walls[36]. Many vascular diseases, such as atherosclerosis and hypertension, are associated with a reduction in the production and release of NO in response to typical stimulus[36]

Working in counteraction to the dilators are a variety of local vasoconstrictors, the two most potent being Endothelin-1 and Thromboxanes. Endothelin-1 is produced by the vascular endothelial cells in response to free radicals or signals molecules such as endothelin, epinephrine and angiotensin-II. Endothelin-1 stimulates the vascular smooth muscle to contract, thereby eliciting vasoconstriction[36,41]. Thromboxanes are a type of prostaglandin which has been proposed to act in direct opposition to prostacyclin, with larger concentrations of thromboxanes leading to local vasoconstriction[42].

1.8: Influence of External Stresses on Cardiac Function

1.8.1: The Frank Starling Law and Assessing Cardiac Function

In the late nineteenth and early twentieth centuries, Otto Frank and Earnest Starling applied the novel concept of a force-length relationship discovered in skeletal muscle, namely that the force-generating capacity of a tissue was inherently dependent on its starting length, to cardiac muscle[43,44]. This manifested in what is currently referred to as the Frank-Starling Law of the heart, which states that the stroke volume of the heart increases in response to additional blood volume loaded into the ventricles during diastole[29] (demonstrated in ***Figure 1.19)***. This law implies that the ability of the heart to eject blood into systemic and pulmonary circulation is dependent not only on the function of the heart itself, but also on the amount of blood made available to the heart through venous return.

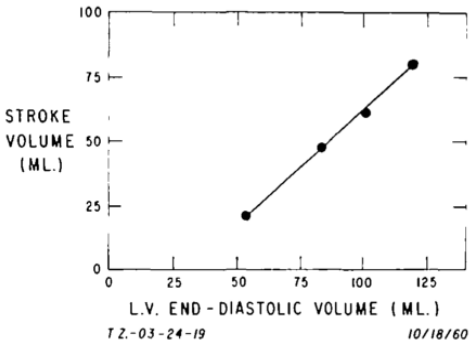

Figure 1.19. *Relationship between left ventricular end-diastolic pressure and stroke volume, demonstrating the Frank-Starling Law of the heart. Reproduced from Braunwald & Ross, 1964*

This understanding provides an additional perspective from which to assess cardiac function. As previously discussed, cardiac function can be analyzed by dividing the cardiac cycle into the functional phases of systole (contraction) and diastole (relaxation). However, the behaviour of the heart in each of these actions is reliant not only on the intrinsic capacity of the heart itself, but also on the functional capacity of the other portions of the cardiovascular system. This is an important concept to grasp, as it allows for the exploration of cardiac function by an additional division: load dependent or load independent function. Load dependent measures of cardiac function are influenced by either the heart's intrinsic function, or by changes elsewhere in the cardiovascular system that influences cardiac loading. In contrast, load-independent measures are influenced by the function of the heart alone. The Frank-

Starling Law is a perfect example of how loading conditions can influence cardiac performance, wherein increasing cardiac preload leads to a direct and proportional increase in stroke volume (***figure 1.19***). Therefore, while load-dependent measures such as stroke volume indicate how the heart is performing, these indices do no provide insight into whether the function of the heart itself is altered, or whether performance changes are driven by a different part of the cardiovascular system. For example, a reduction in stroke volume could be due to either a decrease in the intrinsic ability of the LV to contract or a reduction in preload on the heart.

Initial investigations into the load-independent function of the LV stretch back over four decades, when the boundaries of cardiac functional understanding were being pushed by groups performing invasive preclinical studies on mongrel dogs[45,46]. The Suga group established calculations of both load dependent and load independent cardiac function based on pressure and volume data collected from within the left ventricle itself. The pressure and volume data necessary for these calculations is best collected by inserting a pressure-volume catheter into the LV to directly measure real-time changes to LV pressure and volume[47]. However, as this technique carries many innate risks, clinical models have estimated LV end-diastolic pressure using a Swann-Ganz catheter to measure pulmonary capillary wedge pressure from the right side of the heart[48–50]. As even this technique is highly invasive, carries health-risks for subjects and requires significant training and expertise, load-independent assessments of cardiac function of this nature are rare in clinical trials, and aren't even truly "common" in preclinical works.

This discrepancy between load-dependent and load-independent measures is crucial to understand for this review, as most clinical assessments of cardiac function are load-dependent in nature. Techniques such as echocardiography and hemodynamic monitoring are widely used for diagnostic cardiac assessment because they are relatively inexpensive and non-invasive. However, this has resulted in most investigations, particularly in populations with SCI who do not tolerate invasive procedures well, being based on load-dependent measures which do not allow for the development of mechanistic

understanding to the observed physiological symptoms. Studies which include load-independent methods of assessing cardiac function (many of which are preclinical in nature), hold the capacity to provide this mechanistic insight to load-dependent clinical findings, and therefore play a key role in our understanding of the influence of SCI on cardiac function. These concepts will become more important in later sections of this review.

1.8.2: Ventricular-Arterial Coupling

Expanding on the concept of the inter-dependence of segments of the cardiovascular system, a hot topic of recent cardiac research has been the quantification of the *efficiency* of the cardiovascular system by examining the interaction of different segments/compartments. Of particular relevance to this review is the concept of Ventricular-Arterial Coupling (VAC), which quantifies the interaction of the LV with the arterial system to characterize the efficiency at which blood is pumped into the systemic circulation[2,51]. Calculated as a ratio of the arterial elastance and LV contractility (Ea/Ees), this index quantifies cardiac efficiency by contrasting the change in total pressure-volume area (PVA) and the mechanical stroke work (area inside the PV loop), as demonstrated in ***figure 1.20***. Since the PVA represents the sum of the potential energy of the LV and the mechanical work exerted to eject blood, a change in the PVA that does not change the size of the PV loop (thus, not changing mechanical work) represents an increase in the potential energy of the system, thus a decrease in cardiac efficiency. This will be explored in further detail in section 1.10.2. Clinical investigations

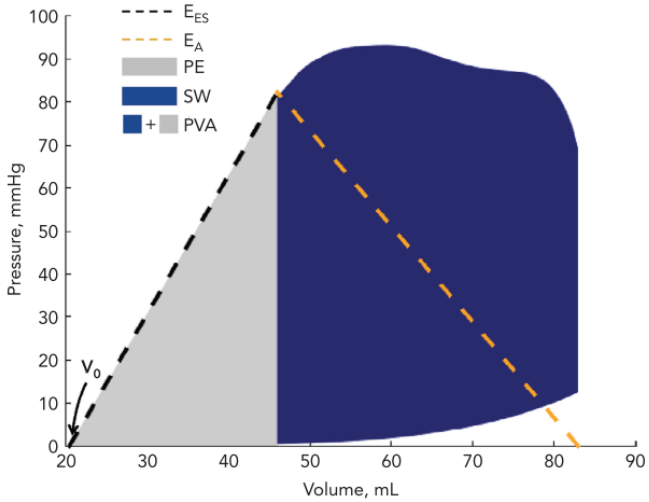

Figure 1.20 *Depiction of a pressure-volume loop and the end-systolic pressure-volume relationship in black. The blue shading represents LV stroke work, while the grey area represents the potential energy invested to drive the cardiac contraction. Together, the grey and blue regions represent the pressure-volume area, or the total energy expended in one cardiac cycle.*

have established that cardiac stroke volume is maximized when the ratio is near 1 but the efficiency of the interaction is greatest when the ratio is near 0.5[52]. As this ratio is dependent on measures of both arterial and LV function, it allows for the examination of how changes to cardiac and/or vascular function influence systemic function. Pathological conditions such as chronic hypertension and heart failure have been found to disrupt this coupling, pushing the ratio far outside of the healthy range to decrease cardiovascular efficiency, thereby increasing the energy required to maintain adequate circulation and making individuals more sensitive to altered loading conditions[2,51,53–55].

1.8.3: Cardiovascular Adjustments to Postural Change

The cardiovascular system undergoes constant tuning and adjustment to maintain consistent tissue perfusion as our body moves dynamically in the environment. This can be conceptualized through the regulation of systemic blood pressure, which in turn is dependent on three factors. 1) the pressure from the heart, 2) the pressure from the passive and active properties of the vasculature, and 3) the hydrostatic pressure of the cardiovascular system[56]. This last factor is particularly important to note, as it represents the influence of gravitational forces on the distribution of blood throughout our bodies. In general, the effect of hydrostatic pressure on systemic perfusion is greatest while standing and at a minimum when supine or prone. As posture changes to a more vertical position, such as moving from supine to sitting, the hydrostatic pressure on the system increases and pulls blood away from higher tissues such as the brain, effectively lowering central blood pressure, as demonstrated in **figure 1.21**. The other two factors influencing tissue perfusion; pressure from the heart and vasculature, must adjust to offset this change in hydrostatic pressure, thus maintaining consistent systemic blood pressure and perfusion[56].

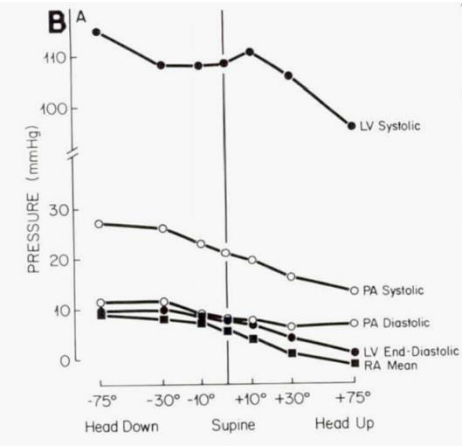

Figure 1.21. *Central blood pressure response to graded postural tilt in humans, from head down to head up. Retrieved from Blomqvist et al. 1991*

In considering how the body actually accomplishes this re-balance, previous investigations have led to the conclusion that the immediate response to changes in postural stress is a dramatic redistribution of systemic venous volume, with secondary increases in ventricular filling and stroke volume seen soon afterwards[56]. This very quick response is thought to be largely regulated by vasoconstriction of large veins by the sympathetic nervous system, a reaction that is believed to be triggered at least in part by the previously described arterial baroreflex[21,30,56]. In fact, cardiovascular adjustments within the first 2-3 seconds following postural change are thought to be almost exclusively mediated by the sympathetic nervous system[56–58], making this reflexive adjustment highly vulnerable to conditions that interrupt sympathetic function.

1.9: Impact of spinal cord injury on neural control of the CVS

1.9.1: What is a Spinal Cord Injury

Spinal cord injuries (SCI) affect over 2.5 million people worldwide, nearly 86 000 of whom currently reside in Canada[59,60]. The serious and prolonged health complications that follow SCI challenge public healthcare systems and are detrimental to a patient's quality of life. While it is common to consider the loss of motor function as the most debilitating chronic issue following SCI, the loss of automatic regulatory function throughout the body causes far-reaching deteriorations in cardiovascular, renal, digestive and sexual function[61]. In fact, in a survey evaluating the rehabilitative priorities of individuals with chronic SCI, it was found that only the restoration of hand function (for those who had partially/fully lost it due to SCI) ranked higher than the restoration of proper autonomic control[62]. This autonomic dysfunction following SCI is distinctly different in the acute and chronic phases of injury recovery, which has led to the understanding that studies must address both windows of time to inform the development of effective treatments[58]. However, for the remainder of this thesis we will focus on the effect of chronic SCI on autonomic function, specifically in the cardiovascular system.

1.9.2: How does SCI relate to the CVS

The cardiovascular system is strongly impacted by this loss of autonomic control. Depending on the level of injury, SCI acutely causes severe hypotension and bradycardia, and diminished orthostatic tolerance[57]. This level-dependent relationship is due to the anatomical relationship between the sympathetic nervous system and the cardiovascular system, as outlined in ***Figure 1.21***. In the case of complete SCI, injuries below the second lumbar segment (L2) leave the sympathetic nervous system, and therefore the cardiovascular system, under complete descending control from the brain (***Figure 1.22A****)*. An injury to the fifth thoracic segment or higher, however, will remove descending sympathetic control over the vasculature of the splanchnic region and the lower limbs. This inhibits the ability of the brain to mobilize the majority of the venous blood volume that sits in reserve in the gut and lower limbs but leaves the upper limb vasculature and heart under sympathetic control *(**Figure 1.22B**)*. Finally, injuries to the first thoracic vertebrae (T1) or higher will completely remove descending control over the sympathetic nervous system, leaving the brain largely incapable of modulating blood flow and hemodynamic reflexes[63] *(**Figure 1.22C**)*.

An important distinction to make at this point is that SCI results in the *removal* of the brain's control over the sympathetic nervous system, not the *denervation* of the actual SNS. This is a crucial concept, as removal of descending control implies that the brain can no longer control the sympathetic circuitry below the level of injury, but that same circuitry is still capable of operating in response to sub-cortical reflexive input. In the case of sympathetic denervation, these reflexes would also disappear, and no sympathetic activity of any type would be possible. While most of these implications span beyond the scope of this review, it is worth noting that due to SCI leaving reflexes below the LOI intact, stimulation of these reflexes can lead to exaggerated, uncontrolled responses. A textbook example of this is in the condition known as Autonomic Dysreflexia (AD), in which triggered reflexes can lead to extreme bouts of hypertension, with systolic BP exceeding 300mmHg[64].

Our understanding about the chronic effects of SCI on the cardiovascular system indicates both that SCI is highly detrimental for long-term health, and that much more research is needed into this field. This is best reflected in the fact that mortality rates from cardiovascular disease (CVD) are over 3x greater in the SCI population compared to the able-bodied population[65]. Even though this makes it clear that understanding and treating cardiovascular decrements following SCI is important, we must first reflect on what research has been done thus far on the topic before looking ahead.

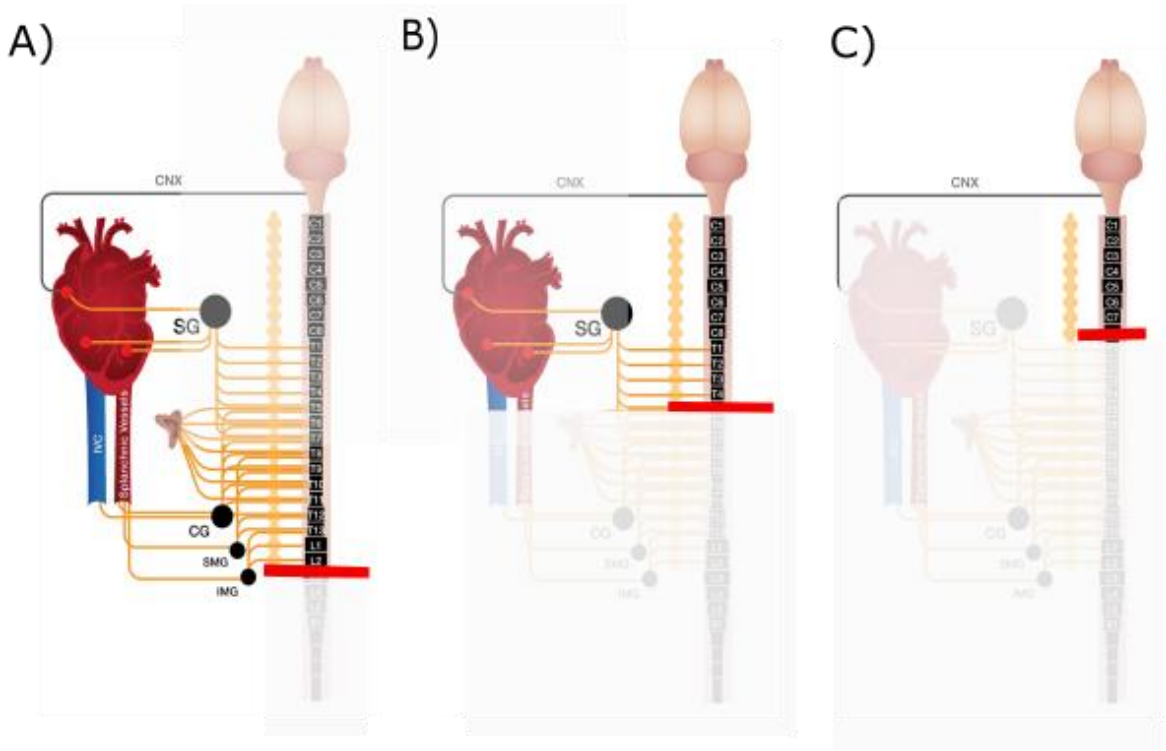

Figure 1.22. *Influence of level of SCI on descending sympathetic control over the cardiovascular system. A) Injury to the L3 segment or below does not remove any direct SNS control over the CVS. B) Injury to the T5 segment removes descending control over SNS input to splanchnic and lower limb vasculature but leaves control over the heart intact C) Injury to the T1 segment or higher removes all descending sympathetic control over the entire cardiovascular system.*

1.10: Long-term effects of spinal cord injury on the Cardiovascular System

1.10.1: Impact on Global Cardiovascular Health

Much of the early work on the impact of SCI on the cardiovascular system examined global measures of cardiovascular function, indicating that SCI patients chronically experience bradycardia and hypotension, as well as a reduction in stroke volume and cardiac output, which all increase in severity in more rostrally-located injuries[57,66]. These findings can be explained through various reported symptoms of SCI such as chronically reduced blood volume[57,66], reduced physical activity[67], altered neurohumoral control[68–70], chronic decreases to preload and afterload[63,71], the loss of descending sympathetic control[64] and changes to the intrinsic structure of the heart itself[72–74]. While the aforementioned factors all certainly influence cardiac function after SCI and are worth investigating, the current techniques, equipment and expertise of our lab make the pursuit of the question of altered descending sympathetic control, loading conditions and cardiac structure pertinent targets for this thesis.

More recent works investigating vascular health following SCI have found strong evidence of vascular dysfunction below the level of injury, particularly in the form of reduced conduit artery diameter and blood flow, increased shear rate and leg vascular resistance, increased arterial stiffness and adrenoceptor hyper-responsiveness[57,75–78].

But based on these previous works, what do we really know about the heart itself?

1.10.2: Impact of SCI on Cardiac Dimensions and Volumes

In investigating the impact of chronic SCI on cardiac dimensions and volumes, significant decreases in the cavity size and mass of the heart have been consistently observed in both clinical and preclinical works[66,67,79–85]. The severity of this decrement is directly related to the level of SCI, with patients suffering from high thoracic and cervical SCI (who would like have impaired descending sympathetic cardiovascular control) consistently displaying this decreased cardiac mass and LV size[66,67,79].

In addition to the anatomical changes, previous clinical and preclinical investigations have also indicated a reduction in the functional volume-derived indices of the LV following the same high thoracic and cervical injuries. In particular, end diastolic volume (EDV) and left ventricular intrinsic diameter at the end of diastole (LVIDd) are consistently reduced following high thoracic or cervical SCI[72,80–82]. End systolic volume (ESV) and left ventricular internal diameter at the end of systole (LVIDs) on the other hand have only been found to be significantly different in select preclinical trials[72,80].

But how do these observed changes translate to heart's contractile and relaxation capacities?

1.10.3: Impact of SCI on Systolic Function

The systolic action of the left ventricle, or the ability of the heart to expel blood out into systemic circulation, is a crucial function for the circulatory capacity of the cardiovascular system. To appreciate what is currently known, as well as to identify what questions remain unanswered, the influence of SCI on systolic LV function will be explored from first a load-dependent, then load-independent perspective.

Load-Dependent

Investigations of both clinical and preclinical nature have led to the understanding that the load-dependent systolic function of the LV is reduced following SCI to both the high thoracic region and cervical spinal segments[63,66,72,79–82,84,86]. Clinical assessments were based on echocardiographic and hemodynamic analyses, while preclinical analyses applied the same measures in combination with *ex vivo* working heart models or direct measurement of pressure and volume within the LV via pressure-volume catheterization. Together this battery of techniques has led to consistently reported reductions in: cardiac output ((CO) volume of blood expelled from the LV in one minute), dP/dT_{max} (maximum rate of LV pressure increase, taken as an index of maximal rate of LV contraction), stroke work ((SW), mechanical work done by the LV during contraction), and LV pressure at the end of systole (Pes). Based on these findings, it can be said that individuals with high thoracic or cervical SCI frequently experience a decrease in LV systolic function. Interestingly though, ejection fraction (the percent of blood ejected from the LV during systole (EF)) a key

variable for clinical assessment of systolic function, is consistently reported as being unchanged following SCI. This is largely assumed to be due to the significant decrease in LV dimensions and blood volume[87]. However, as these findings are based on load-dependent measures, the observed decrements in systolic function could be due to intrinsic changes to the LV, vascular function, or reduction in systemic blood volume. To further investigate the cause of this reduced systolic function, a review of our current knowledge on load-independent systolic function following SCI is necessary.

Load Independent

To date, only a small number of studies have applied Suga's calculations[45,46,88] to LV pressure and volume data to examine load-independent LV function following SCI. Our lab is one of the few groups currently doing so, recently assessing both the load dependent and load independent function of the LV using *in vivo* rodent models[72,81,82]. By using a conductance catheter to examine the changes to the pressure and volume inside the LV in response to preload reductions from inferior vena cava (IVC) occlusions, we have been able to assess multiple aspects of load-independent systolic function. Based on calculations of end-systolic elastance ((Ees), intrinsic contractile capacity of the LV) and preload recruitable stroke work ((PRSW) the capacity for the LV to perform work based on the amount of preload it receives), these works demonstrated a significant reduction in the *in vivo* intrinsic contractile capacity of the LV following high thoracic SCI[72,81,82], independent from loading conditions.

Ventricular-Arterial Coupling

In addition to understanding how SCI affects different segments of the cardiovascular system individually, determining how SCI impacts the *interaction* between these different organs is equally crucial. As previously described, ventricular-arterial coupling (VAC) quantifies the efficiency of the interaction between the heart and the arterial system during systole[2]. While the application of this concept to study cardiovascular health has been gaining traction recently in efforts to understand various pathologies of heart failure in able-bodied individuals, it has only been applied directly in one study of SCI.

In a preclinical model of SCI, the VAC ratio was significantly increased following chronic high thoracic SCI, implying that SCI disrupts cardiovascular efficiency. Should this finding be replicable in additional studies, this would indicate that SCI causes even greater cardiovascular dysfunction than we currently appreciate. Current measures of predicting CVD and mortality rely largely on measures of individual segments of the cardiovascular system, such as cardiac imaging or pulse-wave velocity calculations. However, there is evidence to suggest that VAC is a stronger predictor of CVD than assessment of LV function alone, as displayed in a longitudinal analysis by Ky et al. (2013) where a decreased VAC ratio was a predictive measure of all cause prognosis of systolic heart failure, but assessment of LV contractility alone was not (see ***Figure 1.23***)[89].

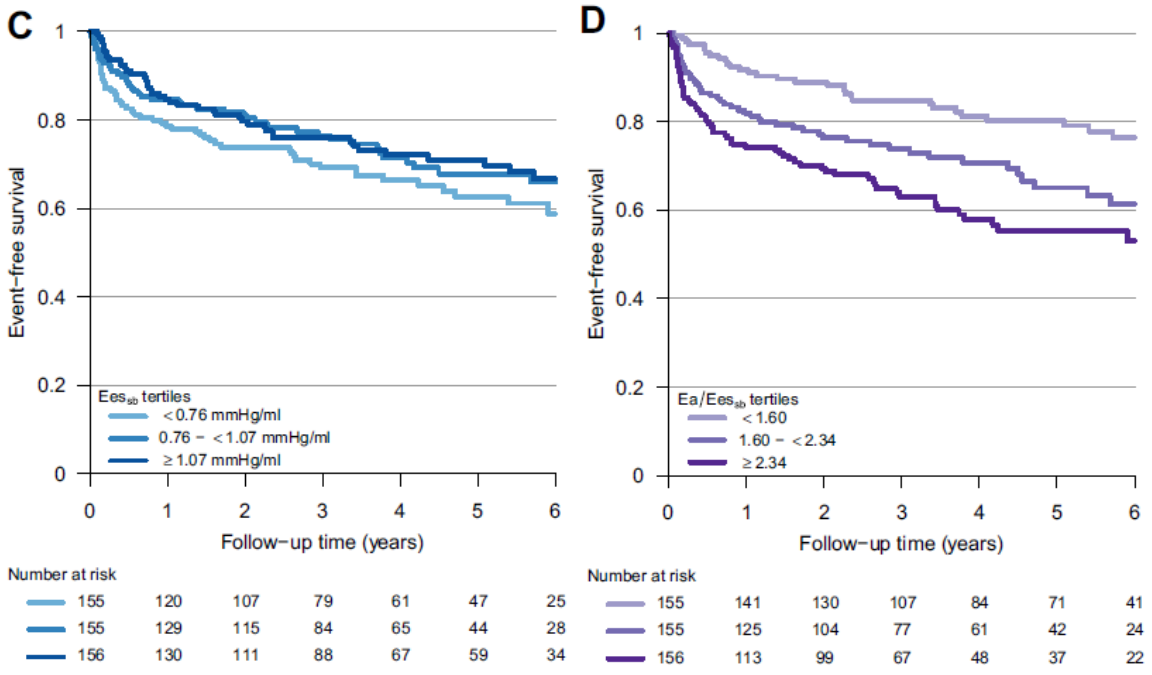

Figure 1.23. *Estimates of all-cause deaths, cardiac transplant and ventricular assist device insertion divided up into echocardiography-derived tertiles of C) End systolic elastance and D) Ventricular-arterial coupling. Note the significant association high-tertile patients and decreased survival in VAC but not Ees. Retrieved from Ky et al. 2013*[89]

In the non-SCI literature, interpretation of this VAC ratio has largely been categorized under two pathologies of heart failure; heart failure with preserved ejection fraction (HFpEF) and heart failure with

reduced ejection fraction (HFrEF)[54,55]. In ***figure 1.24,*** Chirinos et al (2013)[90] provided a tidy visualization of the relationship between resting PV loop dimensions, LV contractility and arterial afterload at rest in a healthy scenario (**a)** and in two cases of HFrEF, which represent HF due to a decrease in LV contractility (**b**) or an increase in arterial afterload (**c).** In both cases of HFrEF, VAC is doubled, thus indicating a decrease in cardiac efficiency. This is interesting to note, as preclinical studies of SCI have reported both a decrease in LV contractility and an increase in arterial elastance (an index of arterial afterload). However, ejection fraction is typically preserved in individuals with chronic SCI due to concomitant reductions in heart size[87]. SCI therefore does not fit the profile of HFrEF. Conversely, HFpEF is reported in individuals who have both increased LV systolic and arterial elastance[91], which also is not in tune with the cardiac pathology following chronic SCI. These cases of HFpEF are not often accompanied by a change in VAC, due to both the numerator (Ea) and denominator of the ratio (Ees) being increased. SCI, therefore, presents a unique pathology that does not fit either criteria of HFrEF or HFpEF, in which LV contractility (Ees) is decreased and arterial elastance (Ea) is increased with no accompanying change in EF. Despite there being only one previous study on VAC following SCI, the fact that the VAC can be calculated as a ratio between LV afterload and contractility (Ea/Ees) allows us to postulate how the SCI may affect VAC from a physiological stand-point.

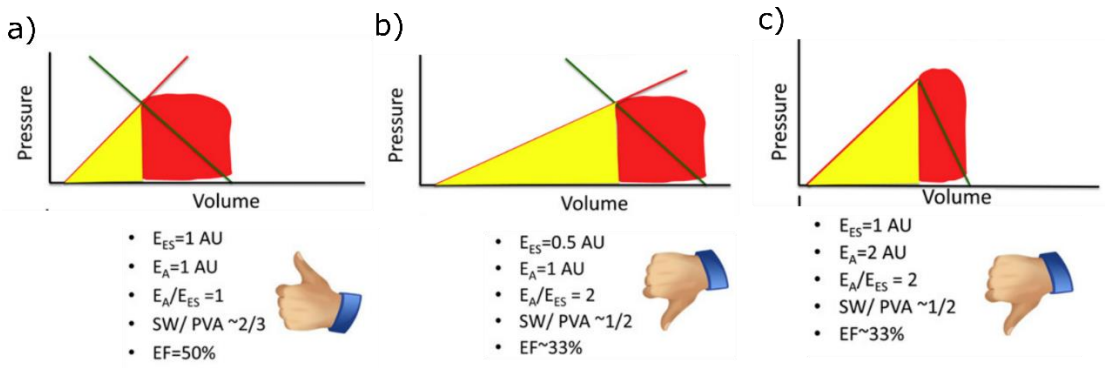

Figure 1.24. *Visualization of the interaction of End Systolic Elastance (red line) and Arterial Elastance (green line) with a resting PV loop in theoretical cases of* ***a)*** *healthy cardiovascular function,* ***b)*** *HFrEF with decreased LV contractility or* ***c)*** *HFrEF with increased arterial elastance. The red-shaded region represents the mechanical work done by the LV during systole, whereas the yellow region represents the potential energy invested by the LV to overcome afterload and begin ejecting blood into the systemic circulation. Note how the increase in require potential energy, and therefore decrease in efficiency, in both cases of heart failure (b & c). Reproduced with alterations from Chirinos et al, 2013*[90]*.*

High thoracic and cervical SCI is known to cause not only a decrease in vasomotor tone and endothelial function, but also an increase in central arterial stiffness[76]. This amplified stiffness increases the velocity of aortic pulse-wave reflections, causing the reflected waves to arrive back at the heart during late systole instead of early diastole, disrupting coronary perfusion and increasing myocardial workload[55]. Together these changes make the arterial system less pliable and adaptable to changes in blood volume, which translates to an increase in ventricular afterload. In an able-bodied individual these effects could be mitigated through compensatory increase in LV contractility. However, as previously discussed, SCI causes a reduction in LV contractility. Quantitatively combining this increased afterload and decreased LV contractility would lead to the VAC ratio being increased following high thoracic or cervical SCI. Such increases have been previously reported in patients suffering from heart failure with reduced ejection fraction (HRrEF), and were associated with decreases in systemic tissue perfusion and increased myocardial workload[51,54,55,90].

The VAC ratio, therefore, provides insight into the integrated function of the arterial system and the LV, allowing for further understanding of not only the function of individual organs but the capacity

of the entire cardiovascular system to adapt to different physiological stresses. The only study to examine VAC following SCI demonstrated a potentially pathological increase in the ratio, which is supported by examination of data from other studies of LV contractility and afterload[82]. This suggests that SCI may reduce the efficiency of the interaction of the LV and arterial system, reducing the functional reserve of the entire cardiovascular system. Performing additional assessments of VAC following SCI would provide greater certainty as to the impact of SCI on the cardiovascular system as a whole and allow us to elucidate whether this change in VAC ratio is due to alterations in function of the LV and/or the arterial system.

1.10.4: Impact of SCI on LV diastolic function

Adequate diastolic function, or the capacity of the heart to relax and refill between beats, is equally as crucial as systolic function in determining the ability of the human heart to circulate blood in response to varied metabolic demand. To appreciate what is already known, and what questions remain unanswered pertaining to diastolic function following SCI, it is necessary to discuss the impact of SCI on both the load dependent and load-independent diastolic function of the LV.

Load-Dependent

Until recently, load-dependent analyses of diastolic function after SCI had identified no significant changes[80–82,84,92], however a systematic review our lab published this year identified a shift in recent literature[87]. Echocardiographic assessments examining early (E) and late (A) mitral filling[82,84,92], as well as doppler tissue imaging of the mitral valve(e')[84] had previously demonstrated a trend for reduced diastolic function, but not to any degree of significance. However, three independent studies have recently indicated decreases in mitral filling in chronic SCI patients[93,94]. This lack of clear consensus in likely due to the load-dependent nature echocardiographic indices, and the varied sample sized leading to a lack of power for these specific indices. In addition, it has been previously suggested that this lack of noted change in diastolic function based on echocardiographic analysis could be due to a concomitant decrease

in the LA volume[84], which would inhibit the detection of diastolic dysfunction based on standard calculations[95].

Additionally, our lab recently performed preclinical investigations into the influence of SCI on diastolic function using both an *ex vivo* working heart model and an *in vivo* direct assessment of intrinsic pressure and volume from within the LV using pressure-volume catheterization. The findings largely supported previous echocardiographic data that SCI does not influence diastolic function[80–82]. However, each of the time constant of LV pressure decay (tau), the maximal rate of relaxation ($-dP/dT_{min}$) and pressure at the end of diastole (Ped) were significantly reduced in different studies, which could be interpreted as an indicator of impaired LV relaxation[72,80,81]. Therefore, there is mixed evidence for diastolic dysfunction following SCI based on load-dependent indices of LV function, so SCI *may* influence diastolic function. However, as with the previous discussion of systolic function, these load-dependent analyses do not allow us to determine conclusively whether a decrement in intrinsic LV diastolic function is taking place. Therefore, load-independent indices of LV function must also be examined to determine the influence of SCI on the diastolic function of the LV itself, independent from the rest of the cardiovascular system.

Load Independent

Investigations into the load-independent diastolic function of the LV following SCI are extremely limited, consisting to our knowledge of only three previous works executed by our lab. Utilization of LV pressure-volume catheterization and preload reductions via IVC occlusion to examine the end diastolic pressure-volume relationship (EDPVR) *in vivo* in a rodent model indicated that high thoracic SCI causes no significant change in intrinsic diastolic function compared to SHAM injuries[72,81,82]. However, the EDPVR measurements relied upon IVC occlusions to alter cardiac loading, a technique which poses two specific limitations: 1) It only allows for the study of LV pressure and volume in response to reduced preload, NOT in response to increased preload, such as would occur during exercise, and 2) it is a highly transient

manipulation, not allowing for the examination of changes to resting function at different states of preload. Therefore, developing a novel investigative technique to address these two limitations would provide a more complete, clinically relevant understanding of the intrinsic changes to LV function following SCI, and assist in resolving the current conflict in load-independent findings. As no such technique has been applied to our knowledge in the field of SCI, it is therefore pertinent to look to other related fields of cardiovascular function.

In the able-bodied population, clinical investigations into the influence of factors such as age and altered chronic loading (via physical activity to increase loading and bed-rest or spaceflight to decrease loading) have used a combination of Lower Body Negative Pressure (LBNP) and injection of precise volumes of saline to manipulate preload for the purpose of load-independent analysis of diastolic function. LBNP involves sealing the lower limbs in an air-tight chamber and vacuuming air out to create a negative pressure space inside the chamber. This functions to hold more blood in the subject's legs, thus reducing the amount returning to the heart and providing a highly controlled and sustained manner of decreasing cardiac preload[96]. Clinical application of this LBNP and Saline injection methodology in an able-bodied population by Dr. Levine's lab at the University of Texas has thus far demonstrated a clear decrement in load-independent LV compliance with natural aging, which is only inhibited by chronic high levels of physical activity[97,98]. These findings translate well, albeit indirectly, to the field of SCI, as SCI has widely been regarded as a model for early aging due to the increased chronic stress the condition places on cardiovascular and metabolic systems in particular[99]. In addition, it is widely acknowledged that levels of physical activity are drastically lower in the chronic SCI population[67]. Therefore, not only do these works from the able-bodied population present a more robust method of studying diastolic function via LBNP and saline injection, the findings of decreased compliance with aging and a lack of physical activity, both of which are observed in cases of chronic SCI, imply that LV compliance may be decreased by SCI as well.

Therefore, in summary, high thoracic and cervical SCI have consistently been shown to cause significant reductions in both load-dependent and load-independent systolic function of the LV. The case of diastolic function is not so clear, with most findings implying that while changes in load-dependent filling may occur, load-independent diastolic function is unchanged following the same injuries. However, there are clear limitations to the techniques used in both the preclinical and clinical studies that established this current understanding. In examining additional fields of cardiovascular research outside of SCI, alternative methods exist which hold the potential to provide more direct and externally valid study of both systolic and diastolic function following SCI.

1.10.5: Changes to Myocardial Structure after SCI

Up until this point, this review has focused on the functional capacity of the LV following SCI, but chronic functional changes are often accompanied by underlying structural changes as well. Recent work by our lab demonstrated for the first time that high thoracic SCI causes not only atrophy of the whole heart, but also of the cardiomyocytes themselves. This was reported through reduced myocyte length, z-disc width and the number of sarcomeres per cardiomyocyte (see ***Figure 1.25***)[72,73,81]. Further investigation revealed that ECM degradation factors muscle metalloprotease 9 (MMP9) and the inhibitor TIMP1 were upregulated following the high thoracic SCI, an observation which has previously been implicated in a variety of cardiac pathophysiological conditions[81,100]. Additional investigations on cardiac physiology following SCI have revealed increased centrally-activated cardiac inflammation[101], increased collagen deposition and upregulation of TGF-β, SMAD3/6 and PDGFB[80]. Together, these findings imply a dysfunction in the growth-mediating pathways of cardiac tissue, thereby decreasing the available contractile mechanisms, while simultaneously indicating a shift towards greater deposition of fibrotic materials such as collagen. Whether these cellular changes are consequences of previously described functional changes, or themselves are the factors driving those changes has yet to be examined conclusively. In addition, our lab recently demonstrated that these structural changes are accompanied

by decreased levels of circulating catecholamines and increased plasma angiotensin II, providing the first clear connection between changes to circulating growth factors and cardiac atrophy following SCI[72]. To our knowledge, this select handful of papers represents the current knowledge about the pathophysiological implications of SCI on the heart. Altogether, this paints a worrying picture for cardiac pathology following SCI and leaves many questions unanswered about the exact mechanisms behind this remodeling, and the direct implications they have on cardiac function.

Molecular Factors of Atrophy

To further investigate what may be occurring, and to provide direction for further research, we will now shift our attention to other related fields of literature on cardiac remodeling. Cardiac atrophy, often referred to as a significant decrease in cardiac mass[102], has been noted across the literature in three different setting; periods of weightlessness (such as spaceflight), prolonged bed rest and chronic SCI[102–105]. All mechanistic studies of myocardial atrophy have found the ubiquitin-proteasome system (UPS) to be highly upregulated, implying that atrophy is at least in-part an active process, using UPS to catalyze the degradation of muscle proteins[102]. Clinical unloading studies have observed significant reductions in LV mass and LV free wall thickness, suggesting a structural adaptation to chronic unloading[103,106]. Investigations comparing the cardiac structure and function of astronauts before and after spaceflight have implied similar reductions in LV mass and function following periods of prolonged weightlessness in space[105,107]. In addition to UPS, the autophagy pathway is often discussed in literature as the other highly influential pathway in protein degradation and atrophy[108]. Excessive upregulation of autophagy has been closely related to the development of cardiovascular

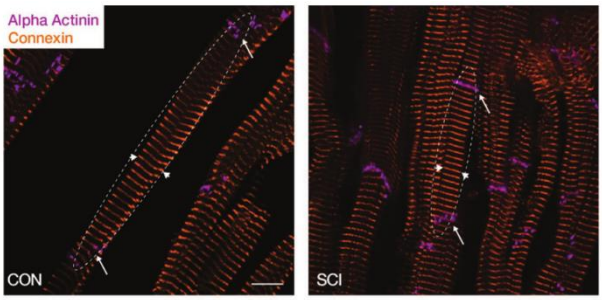

Figure 1.25. *Immunohistochemical stain of cardiomyocytes following T3 SCI (right) or SHAM surgery (left). Analysis of these data provided evidence of a decrease in length and width of cardiomyocytes in the SCI group. Retrieved from Squair et al, 2017[47].*

disease in general, with more direct works implying that this upregulation of autophagy can be either detrimental or supportive of cardiac function depending on its timing[108]. Our lab recently conducted the first investigation into the activity of UPS and autophagy in cardiac tissue following high thoracic SCI, and found an increase in key factors of both pathways[72]. It therefore appears that these pathways are responsible, at least in part, for the structural changes to the myocardium following SCI, but further work is needed to confirm these findings and investigate the temporal nature.

Cardiac Fibrosis

Cardiac fibrosis, or the excessive production of ECM in the myocardium[16], has been directly associated with increased mechanical stiffness of the myocardium. This increased stiffness is believed to lead initially to diastolic dysfunction, then further systolic dysfunction and heart failure[17]. The cause of dysregulation of these fibrotic pathways is debated, and has been noted to differ depending on the pathological stimulus, but it is clear that interactions between an array of growth factors and micro-RNAs are at the core of these observed changes[16]. Various members of the transforming growth factor beta family (TGFβ), matrix metalloproteases (MMPs), connective tissue growth factor (CTGF) and miRNAs 21, 29, 101, 1 and 133 are just a few who have been directly tied to this pathological cardiac remodeling[16,17,93,109]. What is clear from the literature is that excessive deposition of ECM components in atrophic remodeling, particularly collagen 1, can cause myofibrillar disarray and significant tissue stiffening[110]. Unfortunately, there are conflicting findings in the literature about increased collagen deposition following SCI. The majority of studies have demonstrated a significant increase in interfibrillar collagen deposition following high thoracic SCI[80,111,112], but similar models of SCI and cardiac denervation have conversely found no clear change in interfibrillar collagen content[73,113]. This lack of consensus is likely due, in part, to the discrepancy in measurement techniques, with studies relying on either semi-quantitative analysis[80] or software-based assessment[73,111,114] with different software packages. There is, therefore, no clear consensus as to whether SCI causes an increase in interfibrillar collagen. In addition to

collagen deposition, recent works outside of SCI have suggested that changes in the passive stiffness of the myocardium could also be due to changes in the phosphorylation state of titin proteins within the sarcomeres[15,115,116]. A series of protein kinases have been identified as capable of phosphorylating titin molecules, thereby reducing their passive stiffness[115]. However, changes to titin phosphorylation states following SCI have yet to be investigated.

The fibrotic remodeling following high-level SCI influences the passive capacities of the myocardium, similar to an elastic band losing its elastic properties and no longer stretching as easily. However, the other piece to myocardial relaxation is the active component, which is largely mediated by calcium sequestration capacity of the cardiomyocytes[115]. As previously discussed, calcium release is largely modulated by L-type calcium channels and ryanodine receptors, while the re-sequestration is performed by sodium-calcium exchangers (NCX) and sarcoplasmic reticulum calcium ATPase (SERCA) proteins gathering Ca^{2+} back into the SR. Previous research in models of cardiac overloading demonstrated that this active relaxation was upregulated in response to increased afterload, while passive components simultaneously became much stiffer. The author interpreted this to mean that the active relaxation proteins were being upregulated to offset the increased stiffness from these passive components, almost in a "balancing" factor[115]. Whether this occurs in an unloaded heart has yet to be investigated.

In summary, limited investigations into the effects of SCI on myocardial structure after SCI have been performed. Thus far, atrophic remodeling and mixed evidence of cardiac fibrosis have been observed, and a handful of signaling factors and miRNAs associated with these changes. However, it remains unclear what the exact impact of chronic SCI is on the passive and active contributors to myocardial stiffness.

1.11: Impact of SCI on the Ability to Tolerate Orthostatic Stress

Orthostatic stress, as first discussed in section 1.6.2, is a reference to an increase in the force of gravity pulling blood caudally due to a postural change to a more upright position[56]. The compensatory physiological responses that counteract this stress, namely vasoconstriction and increase heart rate and contractility, have a rapid and effective onset thanks to the baroreflex. However, as the sympathetic responses of this reflex travel efferently through the spinal cord, the consequences of SCI disrupting this reflex pathway must be explored.

An inability to tolerate orthostatic stress following SCI is demonstrated by the high prevalence of Orthostatic Hypotension (OH) in this population. OH is a clinically diagnosed condition characterized by "a severe drop in systemic blood pressure when moving to a more upright posture which is often accompanied by presyncopal symptoms"[57]. The criteria for this condition are decreases in blood pressure of >20mmHg systole or >10mmHg diastole during postural change[117]. Over 50% of individuals living with chronic cervical SCI experience OH regularly[117], while those with injuries to T6 and above also experience OH to a lesser, albeit still significant degree[57]. Furthermore, a recent study involving 24-hour blood pressure monitoring in individuals with SCI showed that those with cervical SCI experience up to 28 episodes of OH in a single day[118]. This prevalence of OH following high level SCI has been largely attributed to the loss of sympathetically-mediated vasoconstriction of systemic vasculature (particularly the venous beds)[57,85,119]. However, studies in which this vascular function was normalized by pharmacologically stimulating vasoconstriction found that orthostatic hypotension still occurred, albeit to a lesser degree[119]. This indicates that in addition to loss of vasomotor tone, the removal of control over cardiac inotropy and chronotropy also contributes to OH.

In addition to the unpleasant symptoms of syncope, there is evidence to suggest that frequent bouts of hypotension can cause and/or accelerate pathologies elsewhere in the cardiovascular system. While this field of research is still in its infancy, the presence of OH has been correlated with increased

risk of stroke, hypertension and coronary heart disease[120–122]. Further investigations into cognitive and cerebrovascular function have associated chronic OH in SCI with a myriad of mood disorders, cerebrovascular remodeling and general cognitive decline, making it a major limiting factor in a patient's progression through rehabilitation[119,123]. However, the effect of chronic OH on other organs following SCI, such as the heart, have yet to be investigated.

As previously discussed, it is widely recognized that cardiac function declines following SCI, but it is unclear whether, as with cerebrovascular function, this decline is due in part to repeated bouts of OH post-SCI. While no research has directly addressed this knowledge gap, there is sufficient evidence to suspect a connection between chronic OH and cardiac dysfunction following SCI. For example, individuals with SCI have increased reliance on RAAS to maintain blood pressure homeostasis, as demonstrated by elevated plasma renin concentrations both at rest and during stress[124–126]. Increases in the activity of select RAAS byproducts, namely aldosterone and angiotensin II, is known to either elicit the development of new pathological changes or amplify pre-existing dysfunction in both the arterial system and the heart itself[32–34]. Among these pathological adaptations are central arterial stiffening and myocardial atrophy, both of which have been previously reported following SCI[57,63,76,81,87] and are associated with decreased cardiac reserve, reduced cardiac contractility and increased cardiovascular disease risk[25,54,127]. Furthermore, work on ventricular-vascular coupling has implied that a combination of compliant arteries and large LV contractile reserve allows healthy individuals to maintain constant coronary and systemic perfusion in response to reductions in central blood volume, such as during OH. However, as arterial stiffness increases and LV contractile function decreases following SCI[72,76,81], it is likely that individuals with SCI are less capable of maintaining adequate coronary perfusion during bouts of OH.

In summary, OH is known to occur frequently following high thoracic and cervical SCI, and the cardiovascular system's compensatory response to OH without the baroreflex (namely, increased RAAS activity) has been shown to chronically damage both vascular and cardiac health. When combined with

the reduced capacity to maintain coronary and tissue perfusion during OH, there is ample evidence to imply that the chronic occurrence of OH following SCI contributes to the increased rate of cardiac disease in the SCI population. However, to our knowledge no studies have examined the impact of chronic OH on cardiac function in individuals with high level SCI.

Chapter 2 - Methods

2.1: Purpose and Overview

2.1.1: Study purpose

We conducted a cross-sectional preclinical experiment to further our understanding of the influence of OH and high thoracic SCI and on the intrinsic function and structure of the left ventricle (LV), during both systole and diastole. A custom-made rodent LBNP chamber was used to safely and concisely manipulate cardiac preload to A) simulate OH on a daily basis and B) allow for the evaluation of LV function across different loading conditions. Echocardiography was performed at the start of the study and repeated at the study endpoint along with pressure-volume catheterization to provide a detailed, multifaceted *in vivo* analysis of LV function. Complimentary histological assays were then performed to assess the histological and physiological changes to cardiac tissue following SCI and regular simulation of the physiological response to OH.

2.1.2: Study Aim

This study was designed to answer the question: Does OH exacerbate the LV structural remodelling and functional decline caused by high thoracic SCI?

2.1.3: Hypothesis

It was hypothesized that: 1) Repeated bouts of acute orthostatic stress would further exacerbate LV dysfunction following SCI. This was based on evidence that SCI uncouples the sympathetic arm of the baroreflex, and the baroreflex response is the principle physiological response to acute orthostatic stress. 2) Both cardiomyocyte atrophy and an increase in the deposition of intrafibrillar collagen would occur following SCI, with the deposition of collagen being further increased in the T3 OH group. This was based on assumed increased activity of the RAAS system following SCI that would be further increased with the addition of simulated OH, the products of which have been associated with myocardial atrophy and fibrosis.

2.1.4: Study animals and timeline

The subjects of this study were 29 male Wistar rats, a breed used previously in our lab and others to perform mechanistic investigations into the deleterious effect of spinal cord injury (SCI) on the cardiovascular system[47,80,81,114,128–130].

Study Groups:

Group size was set based on previous preclinical investigations in our lab, wherein 7 animals in each group were be sufficient to detect group differences at 80% power at an alpha level of 0.05 for echocardiographic indices, while both histological and PV indices are more robust and have typically allowed us to detect group differences with as little as 5 animals per group[72,81,82]. However, due to the variability of our echocardiographic measures, the use of new catheterization technology and the invasive nature of the surgical procedures, one animal was initially added to the SHAM group and three-four animals to each SCI group to adequate power for all measures at study termination.

Group 1: Dorsal durotomy, no daily OH (SHAM), n = 8

Group 2: Spinal transection at 3rd Thoracic Vertebrae, no daily OH (T3 SCI), n = 11

Group 3: Spinal transection at 3rd Thoracic Vertebrae, daily simulated OH (T3 SCI OH), n = 10

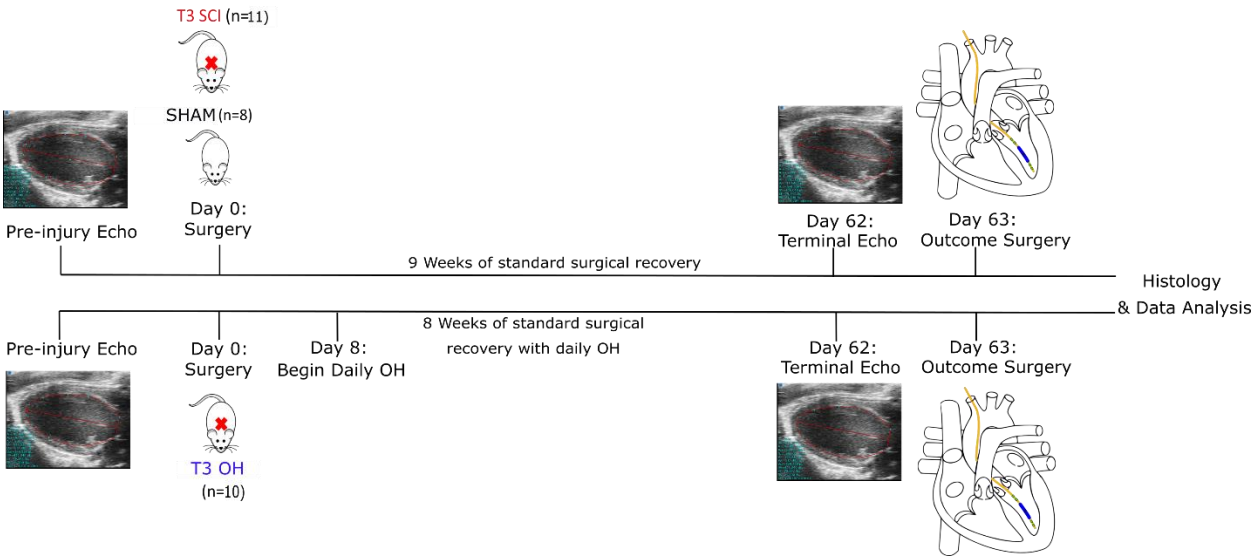

Figure 2.1: *Timeline of the laboratory portion of the study, from pre-injury assessment to tissue collection.*

2.1.5: Group Details

Groups 1 and 2 (SHAM & T3 SCI) allowed for a comparison of the impact of high thoracic spinal cord injury alone on the function of the left ventricle. Specifically, this model presented an opportunity to examine a case of nearly complete removal of descending control over the sympathetic nervous system. This is an externally valid model, as it leaves the reflex pathways below the level of injury intact which are commonly associated with pathological dysregulation of cardiovascular function. The T3 OH group underwent daily simulated bouts of orthostatic stress each day beginning 8 days after spinal surgery, continuing until the termination of the study after 9 weeks. Simulated OH was started at this time due to a general lack of data around the occurrence of OH in the acute phase of clinical SCI, as well as to avoid placing excessive stress on the surgical site immediately following the injury. Comparing groups 2 and 3 (T3 SCI & T3 OH) provided an indicator of the impact of adding simulated OH on LV structure and function following T3 SCI. Lastly, comparisons of SHAM and T3 OH provided an index of the differences in LV structure and function caused by the combination of high thoracic SCI and repetitive OH stress compared to able-bodied animals.

2.1.6: General Animal Housing and Enrichment:

All animal-related procedures were performed in accordance with guidelines from the Canadian Council for Animal Care and approved by the University of British Columbia Animal Care Committee (ACC).

Animals were housed in the ICORD Vivarium at the Blusson Spinal Cord Center, which is a temperature and light controlled facility operated on a 12-hour light-dark cycle. This cycle was offset from outdoor conditions with lights coming on at 9pm, to ensure that daily measurements did not disturb the rats' sleep cycles. There were 2-4 rats housed per cage to ensure social enrichment but avoid overcrowding. Cages contained red polycarbon housing/huts, as these are perceived by the rats as being opaque but are transparent to the human eye, therefore acting as ideal observable hiding places for the rats. In addition to standard rat food, animals received sliced fruit, cereal and sunflower seeds, particularly during the first week after surgery.

2.2: Spinal Surgery

2.2.1: Pre-operative care

Animals were housed at the ICORD Vivarium for 5 days prior to the beginning of the study, to ensure adaptation to the new environment before any further stress was added by injections, husbandry or surgical procedures. Beginning three days before surgery, animals received Enrofloxacin (Baytril), a broad-spectrum antibiotic used to prevent infection following invasive surgery, subcutaneously once daily at a dose of 10 mg/kg. The rats were also started on the specialized post-surgical diet at this time to familiarize them with an altered routine before surgery.

2.2.2: Surgical Procedure

Surgeries were performed in a sterile environment, with the animal draped and resting on a water-circulating blanket maintained at 37°C to avoid hypothermia. The surgeon wore a cap, mask, gloves and surgical scrubs, and all surgical tools were thoroughly cleaned and autoclaved before each surgery. The lab manager Erin Eriskine performed all SHAM and SCI surgeries to ensure study reliability. Dr. Malihe-

Sadat Poormasjedi-Meibod, a post-doctoral fellow in the West lab performed all outcome echocardiography and catheterization surgeries at the end of the 10-week study.

At the beginning of both the T3 transection and SHAM surgical procedures, anesthesia was induced in a perfusion chamber using 4% isoflurane and 2L/min of O_2, then maintained at a stable plane of anesthesia using 2% isoflurane via a nose-cone. Eyes were protected with an ocular ointment (Refresh, Lactri-Lube, Allergan) throughout the procedure. Following the induction of anesthesia, rats were weighed, and the incision site was shaved and disinfected thoroughly with alternating swabs of chlorhexidine (Hibitane) and 70% ethanol, for a total of three times each. Provodine iodine (Betadine) was then be applied for at least one minute to ensure sterilization from local bacteria, before being removed with 70% ethanol. Buprenorphine (Temgesic) was then administered at a dose of 10mg/kg via subcutaneous injection to provide an analgesic effect. Additionally, Enrofloxacin (Baytril) was administered subcutaneously at 10mg/kg as an antibiotic agent. Lastly, a local nerve block was performed using bupivacaine at 5mg/kg subcutaneously at the incision site, as per ACC suggestion, before the prep was finished with administration of 10ml/kg of warmed lactated Ringer's solution subcutaneously to ensure hydration.

2.2.3: T3 Transection

Once preparation was completed, the rat was secured with a 5mL syringe underneath the thorax, just caudal to the shoulder blades, to flatten the curvature of the spine and optimize the access to the T1-T4 vertebrae. An incision was then be made on the dorsal midline, opening the skin and muscle over the C8-T5 vertebrae. Musculature overlying the T2 vertebrae was dissected to access the T2-T3 vertebral region. In the resulting gap, the dura overlaying the T2-T3 segments was opened using micro-scissors and complete spinal transection performed by cutting the spinal cord with extra fine scissors (Fine Science Tools #14084-08). Completeness of injury was confirmed under the dissecting microscope, and sterile gel foam was placed between the two stumps. Once bleeding had been stopped at the site, the incision was

closed; muscle layers closed using continuous absorbable sutures (monocryl; 4-0), after which the skin was closed with interrupted non-absorbable sutures (Prolene; 4-0).

2.2.4: Dorsal Durotomy

This surgical procedure was performed with the exact same anesthetic, positioning and incisions, up until the spinal dura over segments T2-T3 had been opened. Instead of undergoing complete spinal transection at this point, bleeding was quelled and the incision closed using the same two measures as the previous section.

2.2.5: Acute Recovery

Immediately following surgery, isoflurane was turned off and the animal was placed in a temperature-controlled chamber to recover under close monitoring. A 5mL subcutaneous injection of warmed lactated Ringer's solution was administered below the level of injury for hydration.

2.3: Nine-Week Recovery

2.3.1: Post-Operative Animal Care

Survival time was nine weeks following surgery. During the first three days following surgery, animals received injections of two specific drugs. The opioid Buprenorphine was administered at a dose of 0.02mg/kg subcutaneously, once in the morning and once at night as an analgesic. Enrofloxacin was administered as the antibiotic of choice subcutaneously at a dose of 10mg/kg each morning.

Nutrition

As previously discussed, the rats received standard lab rat chow, but also had additional food spread throughout the cage to encourage innate foraging behaviours and general movement. This consisted of a variety of fruits, cereals and commercially available rat treats. In addition, the meal replacement shakes and nutritive gel used in the three days preceding surgery continued to ensure adequate micro and macronutrient intake for the first fourteen days following surgery. This timeline was

based on previous work by our lab[72,80–82], in which it was observed that rats were gaining 5-10g/day of body weight by this point, and no longer required the additional dietary support.

Bladder Care

For both SCI groups, urinary bladders were emptied by manual expression four times per day, at approximately 8:00 am, 12:00pm, 5:00pm and 10:00pm. This continued until return of reflexive micturition7-10 days following surgery, at which point manual checking was continued each day to ensure there were no urethral blockages or any other urinary concerns.

Monitoring

During the first week following surgery, all animals were monitored four times daily to ensure bladder health in the SCI animals, and full checks were performed twice daily (AM and PM) using our lab's standardized monitoring sheet. Monitoring was based on six categories of evaluation used previously by our lab; weight, physical appearance, behaviour/activity, clinical signs, lesions/wounds and tumors/cysts. Any score on this ranking that exceeded 20 indicated a humane endpoint and required immediate euthanasia. As during previous studies by our lab, the monitoring scores of SCI animals recovered to match those of the healthy SHAM animals by two weeks following surgery.

Special Caging

Rats with T3 SCI no longer had volitional control over hindlimbs, trunk or tail and therefore required specialized housing. As they were only capable of ambulating using their forelimbs, a rubber grid was placed under the woodchip bedding which the rats were able to grasp with their paws to move more readily around the cage and access food and water. Bedding was changed every 1-2 days to ensure that rats remain dry and clean. This set-up has been used previously by our lab with great success, allowing the rats to move around their cages freely by two days following SCI.

Humane Endpoint

While the experimental endpoint was at 9 weeks time following the initial spinal surgery, humane endpoints were determined during the daily monitoring sequences. If animals reached a score of 20 or greater on our monitoring protocol, or exhibit any of the following: unrepairable skin perforations due to biting/scratching, lack of sufficient motor capacity to obtain easily accessible food/water, loss of more than 20% of preoperative body mass or significant digital autotomy (beyond first digit of forepaw, or to metatarsals of hindpaw), euthanasia was performed immediately. Euthanasia was performed by urethane overdose and confirmed using cardiac exsanguination as a secondary measure. Animals were then transcardially perfused with first PBS, then 4% paraformaldehyde. The heart and brain were dissected and stored at -80°C for later tissue processing.

2.3.2: Daily Simulation of OH using Lower Body Negative Pressure

Rationale

Recent *in vivo* investigations into cardiac function after SCI have significantly advanced our understanding about the influence of SCI on cardiovascular function. Rodent models have been widely used for these studies, due to the relative ease to which one can care for and house these animals and the widespread availability of training for experimental handling[131,132]. However, as discussed in the literature review, our understanding of the effect of chronic OH on cardiac function is sorely lacking. The highly controlled experimental setting and invasive measurements available in rodent models presents an opportunity to resolve this lack of insight. However, as rodents are quadrupeds and not as susceptible to tilt-induced cardiovascular symptoms, a model to simulate OH in a quantifiable and reproducible manner is required. Lower Body Negative Pressure (LBNP) has been used to assess orthostatic tolerance clinically in both able bodied[49,56] individuals and those with SCI[30,133], and has also been used in rodent models to assess baroreflex function during anesthesia[134]. However, no studies have previously used LBNP to

provide a controlled, reproducible simulation of OH in a rodent model of SCI. With this rationale, we designed a custom rodent LBNP chamber to be used on both SHAM and SCI rats.

Design

Constructed based on our specifications by the Richmond Plastics Company, the LBNP chamber was a rectangular plexiglass box measuring roughly 10 ¼ ”x5 ¾”x4”.The chamber was equipped with a tightly-sealing lid, two release valves, a vacuum pump, a pressure manometer and an opening for the animal. Rats were secured in the opening with a custom-made rubber seal, creating a stable pressure barrier between the animal and the brim of the box.

Implementation of daily stress

During weeks 2-9 following the select surgical procedure, T3 OH group underwent simulated OH under isoflurane anesthesia for 10 minutes per day, every day until study termination. The LBNP chamber was placed on a water-circulating blanket at 37°C, the animal was anesthetized with isoflurane gas and secured with the lower limbs inside the LBNP box and the rubber seal secured at the base of the ribcage. Once the seals around both the lid and the rat were secured, the pressure release valve was opened, and finally the vacuum was turned on. The release valve was then slowly closed until the pressure inside the LBNP chamber reached the pre-determined pressure target (discussed in the following section). Pressure was maintained at this level for 1 minute, while the rat was monitored to ensure continued anesthesia. Following this 1 minute of LBNP, the release valve was fully opened to allow pressure inside the box to return to baseline atmospheric levels for the following 1 minute. This pattern of 1 minute of negative pressure and 1 minute of atmospheric pressure was repeated 5 times during each LBNP session. Following the last minute of LBNP, the release valve was fully opened and the vacuum turned off, before the seal around the lid of the chamber was broken. Finally, the rodent was removed from the chamber and allowed to recover in a temperature-controlled room under close monitoring. Once fully recovered, the rat was fed treats and returned to its cage. The rationale behind delivering five 1-minute bouts of LBNP each day

per animal was to allow for examination of the effect of multiple bouts of simulated OH each day (there is clinical evidence to suggest patients experience up to 28 episodes in a single day), while also keeping the study logistically feasible for the one investigator overseeing the daily OH simulation.

As rodents are known to be stressed by handling and the long-term effects of daily anesthesia with isoflurane are unknown, three animals from the T3 SCI group were used to control for these extra influences. Each day these three rats underwent the exact same anesthesia and placement in the box, but instead of turning the vacuum on they were simply secured in the LBNP chamber for 10 minutes under atmospheric pressure. They were then removed and allowed to recover in a temperature-controlled chamber under close monitoring, then fed treats and returned to their cage.

Setting the pressure dose for the T3 OH group: A pilot study

As discussed in the literature review, the clinical criteria for OH is characterized by a decrease of >20mmHg in systolic blood pressure or >10mHg in diastolic blood pressure[58]. The only previous study that implemented an LBNP chamber in a rodent model demonstrated that an LBNP magnitude of -10mmHg was sufficient to achieve this reduction in uninjured animals. However, this study involved rats of a different breed, older age and no SCI. As clinical studies have shown that SCI increases the sensitivity to LBNP, we conducted a small pilot study involving 3 animals with T3 SCI to determine the magnitude of LBNP required to consistently simulate OH in the T3 OH group during the daily bouts of simulated OH. It was determined that an LBNP magnitude of -5.5mmHg was adequate to simulate OH in animals with a complete T3 transection, based on both SBP and DBP criteria for OH diagnosis (see ***figure 2.2*** for sample

pilot data). Moreover, the change in box pressure and arterial pressure were very tightly coupled during both the onset and release of LBNP, demonstrating that monitoring box pressure during bouts of simulated OH would be adequate to ensure a consistent hemodynamic stimulus in all animals. Therefore, in the present study a negative pressure of -5.5mmHg for T3 OH was used to elicit changes in both SBP and DBP that mimicked the hemodynamic factors of OH. While we acknowledge that this method does not simulate all physiological effects of orthostatic stress, it does allow for the induction of hemodynamic stresses equivalent with those reported during OH in humans and will therefore be referred to as "simulated OH" for the remainder of this thesis.

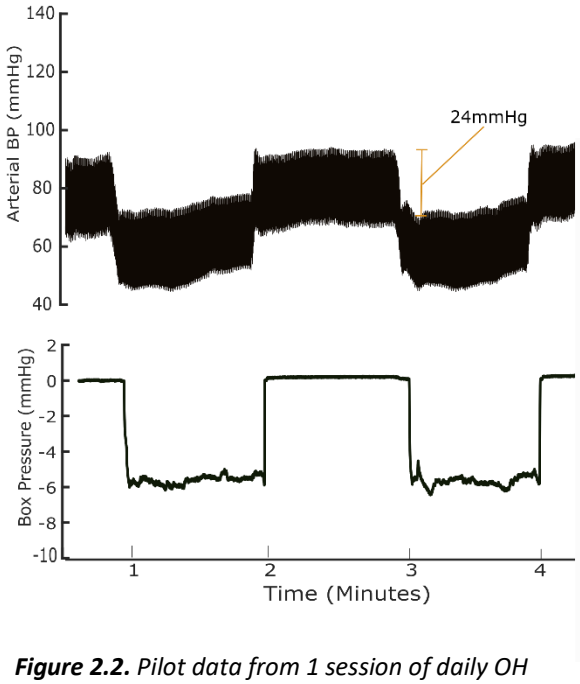

Figure 2.2. *Pilot data from 1 session of daily OH simulation in an animal with a complete T3 transection. The top panel is carotid blood pressure measured with an indwelling pressure catheter, while the lower panel is the pressure measured inside the LBNP chamber using a pressure transducer. Note that the hemodynamic criteria (decrease in SBP >20mmHg & in DBP >10mmHg) for OH are achieved during the LBNP bout of -5.5mmHg.*

2.3.3: Echocardiographic Assessment:

Two days before the end of the 9-week study, echocardiography was performed to provide direct measurements of LV dimensions and volumes. Imaging was performed using a Vevo 3100 imaging system equipped with an MX400 probe designed (Visualsonics, Canada). Rats were anesthetized with isoflurane (initially via chamber induction at 4% isoflurane with 2L/min oxygen), then maintained on a Bain's system at 1.5-2% isoflurane with 1.5-2L/min of oxygen. Once in a state of stable anesthesia, the rat was secured in dorsal recumbency to an adjustable rodent echo platform specially equipped with electrocardiogram transducers which allowed for continuous monitoring of heart and respiration rate. Body temperature

was maintained using a water-circulating heat blanket and monitored via rectal probe, while heart rate was maintained between 300-350 beats per minute (bpm). Lastly, ventilation was monitored with plethysmography. M-mode echocardiography was used to assess LV structure and dimensions from a parasternal short-axis view, while volumetric function was measured by tracing the boundaries of the LV in the parasternal long-axis view[80]. Early diastolic filling velocity was quantified using Pulse-wave Doppler from the apical four-chamber view. Lastly, pulse-wave doppler was used in the parasternal long-axis view to assess flow in the pulmonary outflow track as an estimation of aortic flow. This estimation was used in lieu of direct assessment of aortic flow due to anatomical restrictions, as the aortic outflow tract cannot be readily imaged in rats. These measurements were averaged over the course of ten cycles, with the peak of the P-wave being used to delineate each cardiac cycle.

2.4: Terminal Catheterization and Data Collection

Nine weeks after the SCI or SHAM surgeries, PV catheterization was performed to assess LV function *in vivo* and collect tissue for further histological analyses (***figure 2.3).***

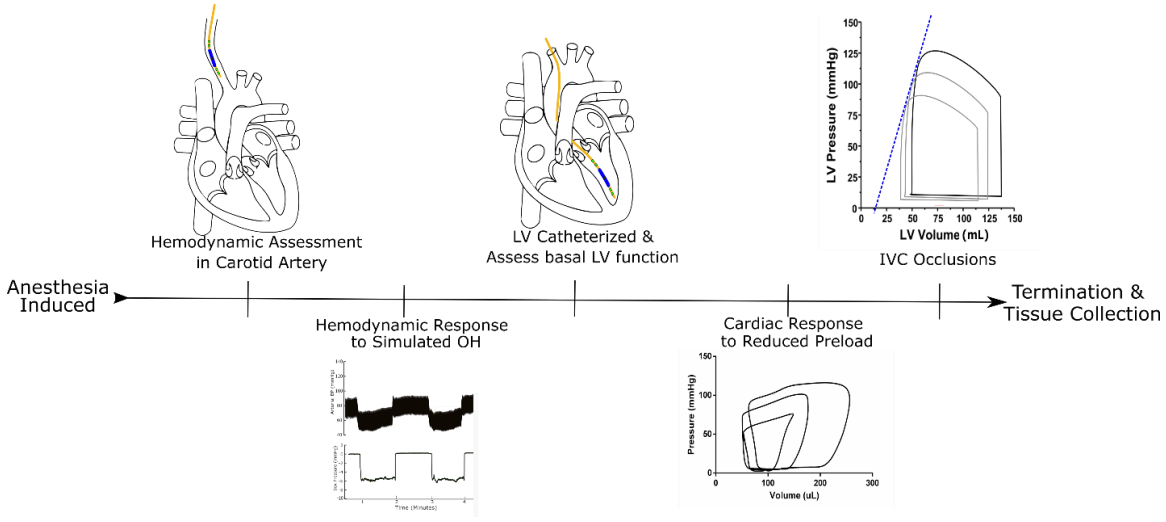

Figure 2.3 *Timeline of the catheterization surgery at study termination, during which all load-dependent and load-independent PV data was collected.*

2.4.1: Rationale for Pressure-Volume Catheterization

In the present study, an admittance catheter was inserted in the LV via a closed-chest approach to lie parallel to the long axis of the heart (see ***figure 2.3***). This type of catheter was selected because it allows for real-time measurement of both pressure and volume, while the closed-chest catheterization method was used due to its minimally-invasive nature. To ensure correct positioning of the catheter in the LV, the placement was confirmed visually using echocardiography. The catheterization protocol of this study was based on highly regarded publications in Nature Protocols[47].

Why an Admittance Catheter?

Our lab has recently performed a series of elegant investigations of LV function following SCI using a conductance catheter[72,81,82]. This technology has allowed us to provide the first direct evidence for decreased load-independent LV function following SCI, and has opened the door to many further investigations, such as the present study. Conductance catheters assess LV volume by creating an electrical field and assessing how this field's voltage changes as it passes through blood and myocardial tissue, resulting in a voltage signal that must be calibrated using either echocardiography or a three-step calibration process after collection is complete to obtain LV volume measurements. While effective, this conductance technology has two clear draw-backs: 1) it does not allow for the real-time analysis of LV volume, and 2) the mathematics behind the distinction of myocardial tissue conductance from blood conductance are based on assumptions which lead to overestimations of LV systolic volume and underestimations of LV diastolic volume. Recent advances in *in vivo* catheter technology have led to the emergence of a new type of catheter that instead operates on the theory of admittance. In addition to measuring the resistive capacity of the blood and myocardium, as in conductance theory, admittance catheters also assess the conductive capacity of the cardiac tissue. This conductive capacity causes the electrical signals that travel through the myocardial wall to undergo a change in phase angle. The magnitude of this change in phase angle varies throughout the cardiac cycle, becoming greater during

systole as the myocardial walls intrude further into the electrical field, and diminishing during diastole. This ability to assess the contribution of the myocardium to the voltage signal allows for two crucial advantages; 1) Volumetric measurements are more accurate, particularly at the extremes of the cardiac cycle, and 2) LV volume can be measured and viewed by the experimenter in real-time during catheterization. With these clear advantages in mind, an admittance catheter was used in this study for the first time in our lab to capitalize on this new technology and perform the most accurate volume assessment possible.

2.4.2: LV Catheterization and Hemodynamic Assessment

The rat was anesthetized with isoflurane (chamber introduction at 4%Iso/2L/min O_2), after which urethane was administered intraperitoneally to provided prolonged anesthesia. While Urethane does have an effect on chronotropic cardiac function and cause mild vasodilation, it was selected due to its minute impact on inotropic cardiac function and prolonged anesthetic stability compared to other conventional options[47,134,135]. The animal was placed supine on a water-circulated heating blanket at 37°C to prevent hypothermia, with three paws secured with ties, and the fourth paw left free to be used as an indicator of level of anesthesia. Lab-chart data collection was begun, the catheter was calibrated and surgery progressed in the following steps: 1) As the closed-chest approach was used to leave the thoracic cavity intact, the surgery began with an inverted T-shaped incision from the mandible to sternum. Through this opening the parotid gland was removed, superficial throat musculature was dissected, and the carotid artery was isolated from the Vagus nerve. 2) One suture was

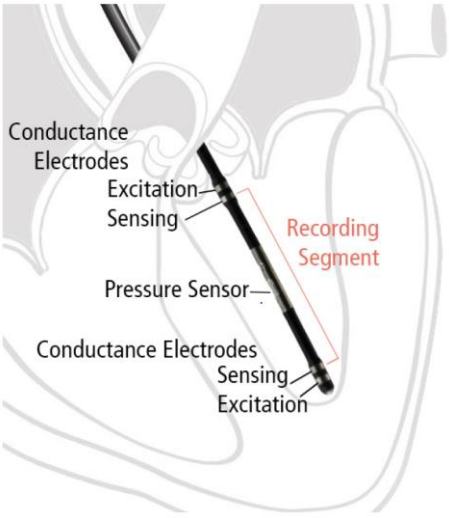

Figure 2.4. *An ideally placed rodent LV PV catheter. Note how all electrodes are inside the LV without touching the walls, allowing for the outer electrodes to generate a signal uninterrupted by valves. Retrieved from the Transonic handbook of Tools & Techniques for Pressure-Volume Hemodynamic Studies (©2017 Transonic systemics Inc)*

threaded underneath the carotid artery, with the ends secured to the table above the rat's head with tape. Two more sutures were then threaded underneath the carotid, with the middle suture being lightly knotted while the distal suture was taped to the skin distal to the incision. With the carotid now secured and pulled under mild tension, a saline solution was used to wet the area before an incision was begun at the proximal area of the carotid and extended distally with micro scissors. 3) Once this incision was made, slack was given to the artery and the tip of the pre-soaked (for 30 minutes in saline) catheter was inserted into the artery. 4) The distal suture was then released. At this point, the lower half of the rat was inserted carefully into the opening of the LBNP chamber and the seal secured. The rat was then allowed to rest undisturbed for 15 minutes to collect baseline hemodynamic data. Following this 15-minute period, a routine session of simulated OH (5x 1-minute bouts of LBNP interspersed with 1-minute rest periods) was performed to provide a direct measurement of the arterial response to -5.5mmHg of LBNP. Afterwards, the seal around the rat was removed and the catheter was advanced slowly to the heart. 5) Placement inside the LV was confirmed with long-axis echocardiographic imaging to ensure optimal transducer orientation.

2.4.3: Baseline Assessment

After correct placement of the LV catheter was confirmed with echocardiography, the instrumentation was left in place for 10-15 minutes to allow for pressure and volume measures to return to relative baseline. A minimum of 10 minutes of stable resting data were collected to ensure a sufficient quantity of baseline data was available for later analysis. During this time, investigators monitored both the condition of the animal and the quality of the pressure, volume, phase and magnitude signals. If the animal became unstable or the signals became unclear, necessary adjustments were made and more time provided to ensure true baseline measurements were collected.

2.4.4: Manipulations of cardiac loading using graded LBNP

Rationale

Preclinical studies of cardiac function following SCI have largely focused on assessing load-dependent function at rest. However, the acute cardiac response to periods of highly controlled unloading, such as those generated by bouts of LBNP, have never been assessed invasively. Such assessments would provide an index of how cardiac function is influenced by acute preload reductions, such as would occur during bouts of OH. We therefore propose to assess load-dependent cardiac function at rest and during two progressive stages of LBNP to investigate the cardiac response to acute preload reductions.

Protocol

Following the collection of adequate baseline data, the box was sealed, the pressure release valve completely opened, and the vacuum turned on. Once air flow had been established, the release valve was slowly closed until the pressure inside the box reached -5.5mmHg relative to atmospheric pressure. Pressure was maintained at this level for a minimum of 1 minute before advancing to a chamber pressure of -8.5mmHg below atmospheric pressure for an additional 1 minute. This second magnitude of LBNP was selected to provide a consistent stage of "severe" preload reduction to allow for the study of cardiac function across three loading conditions. Following this second stage of LBNP, the release valve was fully opened, and the vacuum turned off to allow chamber pressure to normalize to atmospheric pressure.

2.4.5: Inferior Vena Cava Occlusion

The rat was removed from the LBNP chamber and a laparotomy was performed to open the abdominal cavity and access the inferior vena cava (IVC) superior to the hepatic portal vein and inferior to the diaphragm. Once this section of the IVC had been isolated, a minimum rest-time of 2 minutes was allowed for indices to return to resting values before the IVC was occluded transiently with a cotton-tipped applicator, just superior to the insertion of the hepatic portal vein. Occlusions were repeated a minimum

of 3 times, or until the researcher judged that sufficient clean occlusion data had been obtained. A minimum of 120 seconds was left between occlusion trials to allow PV indices to return to resting values.

2.4.6: Euthanasia and tissue excision and processing

Upon completion of all IVC trials, the rats were overdosed with urethane and direct cardiac exsanguination performed to collect fresh blood samples and act as a secondary measure of euthanasia in accordance with UBC ACC guidelines. Perfusion was then conducted transaortically with phosphate buffered saline (PBS) followed by fixation with 4% formaldehyde in PBS. Whole hearts were then excised, the great vessels removed and the tissue sectioned and stored in paraformaldehyde for histological analyses. Heart cross sections were embedded in paraffin blocks (Wax-It Histology Services, UBC. Vancouver, Canada) and stored at room temperature for later histological and immunohistochemical analysis.

2.5: Analysis of *In Vivo* Data

Due to 4 of the 29 animals reaching their humane endpoint before the end of the 9 week study, complete echocardiographic (pre-injury and termination scans) and histological data was collected from 25 animals. The group-distribution for these animals was; T3 OH (n=8), T3 SCI (n=10) and SHAM (n=7). LV catheterization was successfully performed in 20 animals, which were distributed as follows: T3 OH (n=6), T3 SCI (n=8) and SHAM (n=6).

2.5.1: Echocardiographic Analysis

The group ID and individual ID of all animals were blinded by an independent researcher to remove analyst bias. A parasternal short-axis view was used to assess the following indices of LV dimensions: IVSd (interventricular septum thickness at end diastole), LVIDd (LV internal lumen diameter at end diastole), LVPWd (LV posterior wall thickness at end diastole) and estimated LV mass. The following indices of LV volume were then assessed from a parasternal long-axis view: LVEDV (end diastolic volume),

LVESV (end systolic volume), SV (stroke volume), EF (ejection fraction) and CO (cardiac output). All indices of LV dimension and volume were normalized to body mass, as performed by our lab in previous publications[82]. From an apical four chamber view, Doppler was then used to assess E (early mitral filling). Finally, pulse-wave doppler was used from a parasternal long-axis view to measure TTP (time-to-peak blood flow velocity) and V_{peak} (peak blood flow velocity) in the Pulmonary Outflow Tract, which together were used to calculate VSI (ventricular stiffness index)[136] of the right ventricle. The pulmonary outflow tract was imaged instead of the aortic outflow tract due to the thoracic anatomy of rats, which does not allow for accurate echo-assessment of the aortic outflow tract. However, similarly to the manner in which Swan-Ganz catheterization is used to estimate LV function in humans[137], we assume that a change in the RV VSI would also occur in the LV to a similar degree.

2.5.2: Basal hemodynamic function

Resting hemodynamic pressure data obtained from the carotid artery was analyzed to assess general hemodynamic function. Specifically, we assessed: systolic blood pressure (SBP), mean arterial pressure (MAP), diastolic blood pressure (DBP) and heart rate (HR).

2.5.3: Acute Hemodynamic Response to Simulated OH

Hemodynamic analyses were repeated for all groups during a -5.5mmHg bout of LBNP (the same bout used to simulate OH in the T3 OH group) ensure that this magnitude of LBNP was sufficient to simulate the hemodynamic stress of OH.

2.5.4: PV Analysis

Pressure and Volume data from the LV catheterization were also blinded and analyzed using Labchart by compiling the data into a series of pressure volume loops, each of which represent one cardiac cycle. The analysis process involved selecting relevant areas of data and isolating loops which represented cardiac cycles from one specific phase of ventilation to control for the confounding influence of

intrathoracic pressure changes throughout the respiratory cycle. In the present study, only loops from the expiratory phase were assessed.

2.5.5: Basal PV function

Resting data obtained from when the rat was placed inside the LBNP box with no vacuum applied was analyzed to evaluate load-dependent LV function. Volume signals were calibrated to echo-derived measures of EDV and ESV to ensure accuracy. Outcome measures to assess load-dependent systolic function were: Stroke Work (SW), Stroke Work Indexed to body mass (SWI) Cardiac Output (CO), Cardiac Output Indexed to body mass (CI), maximum pressure during systole (Pmax), range of developed pressure during the cardiac cycle (Pdev), and the maximal rate of contraction (dP/dT_{max}). Additionally, Effective Arterial Elastance (Ea) and Total Peripheral Resistance (TPR) were calculated from ventricular data to characterize the arterial pressure as it fluctuated beat-by-beat to represent ventricular afterload and the stiffness of the arterial system[2,138]. LV end systolic wall stress (σ) was also calculated to examine the direct effect of afterload on the myocardium in accordance with the Laplace law of the heart ($\sigma = (P*r)/h$, whereby P= LV Pmax, r = LV radius and h = LV wall thickness). Finally, the load-dependent indices of diastolic function were: The maximal rate of relaxation ($-dP/dT_{min}$), Pressure at the end of diastole (Ped) and an index of compliance (Tau).

2.5.6: Acute LV Response to LBNP

Indices of load-dependent systolic function were also assessed at two incremental stages of LBNP: -5.5mmHg and -8.5mmHg. Ten seconds of data were selected and analyzed from each bout as described in section 2.5.3. The outcome measures for combined LV pressure/volume function during systole were Stroke Work (SW) and Cardiac Output (CO). Stroke Volume (SV) was used to assess LV volume function, while Developed Pressure (Pdev) and Maximum Pressure in the LV (Pmax) were used to assess LV pressure function and Heart Rate (HR) to assess chronotropy.

2.5.7: Load-independent systolic function

As previously indicated, altering the preload on the heart will affect the pressure and volume generated inside the LV throughout the cardiac cycle. This changes the profile of the PV loops in a predictable manner and tracking this change can provide an index of load-independent function, as displayed in ***figure 2.4***. When studying contractility, the change to the top left-hand corner of the loop, called the end systolic pressure-volume point and representing the point at which the heart is at its maximal point of contraction and is therefore stiffest, is of particular interest. When preload to the heart is reduced within physiological ranges, this point shifts downwards and to the left in a relatively linear manner with each consecutive PV loop. A slope plotted for this linear relationship can be used as an index of the intrinsic contractility of the LV, also referred to as End Systolic Elastance (Ees)[2] ***(figure 2.4a)***.

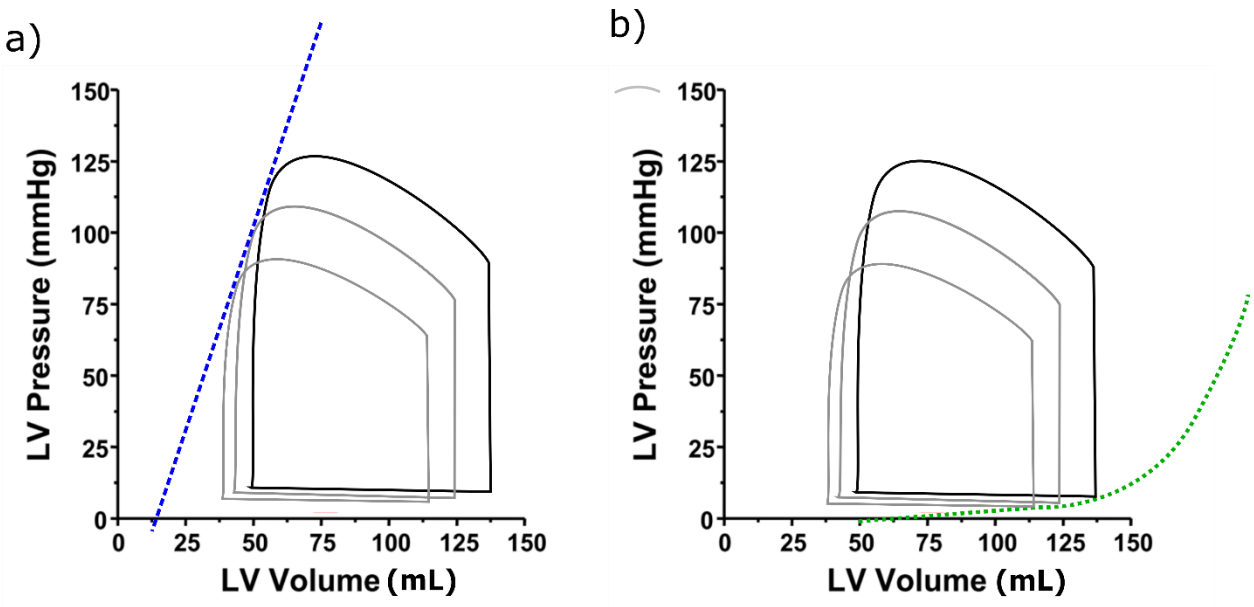

Figure 2.5. *Sample ESPVR slope and EDPVR curve traced onto PV loops generated by manipulation of cardiac preload. The solid black loop represents a PV loop at baseline and the two left loops represent the response to reduced preload.* ***a****) The blue line represents the ESPVR, which is an index of LV contractility.* ***b****) The green line represents the exponential EDPVR, which is an index of LV compliance.*

Data from the IVC occlusion trials will be used to assess the end systolic pressure-volume relationship (ESPVR), as described above and in previous works by our lab[72,81,82]. Additionally, the VSI will

be used to provide a further index of changes in right ventricular function, with the assumption that load-independent changes in RV function also take place in the LV. This is the first study to apply VSI to an SCI model of cardiac injury. Previous works have verified its accuracy in assessing end-systolic elastance has through comparisons of VSI measures to catheter-based PV data preclinically[139]. VSI was therefore used as a secondary measure of LV contractility to limit study error.

2.5.8: Load independent diastolic function

These predictable changes to PV loop dimensions in response to altered loading can also be analyzed to study the diastolic function of the LV, as displayed in ***figure 2.4(b)***. Plotting the changes to the pressure and volume inside the left ventricle at the end of diastole, when the heart is most relaxed, allows for the generation of a variable known as the End Diastolic Pressure-Volume Relationship (EDPVR). Unlike the ESPVR, the EDPVR is curvilinear in nature. This is because as the volume loaded into the LV changes, the way that the chamber relaxes and fills is altered in a curvilinear, but still predictable manner. The fact that this curvilinear trajectory is still predictable and can be traced mathematically across loading conditions makes this a load-independent index of cardiac function.

When the change in EDP and EDV are traced during changes in LV loading conditions, an exponential constant can be generated to characterize the curvilinear EDPVR, which itself is an index of LV compliance[2,140] Compliance can be defined as a "change in volume for a given change in pressure"[2], and it is often used as the gold standard to measure the intrinsic diastolic function of the LV.

For this study, we assessed the changes in end-diastolic pressure and volume during the same transient IVC occlusions discussed in the previous section to generate EDPVR curves and obtain an index of load-independent LV diastolic function. This same technique has been applied previously in our lab[72,81,82], but this is the first to do so using an admittance catheter which provides more reliable volume data.

2.5.9: Ventricular-Arterial Coupling (VAC)

To characterize the interaction between the LV and arterial system, the VAC ratio will be calculated by dividing effective arterial elastance (Ea) by end systolic elastance (Ees). The resulting ratio has previously been used to characterize the efficiency of ventricular-vascular interaction in humans, with a value of 1.0 allowing for maximization of SV, while a ratio of 0.5-0.7 represents an "optimally efficient" interaction between the heart and vasculature[51–53,90].

2.6: Histology

Two histological procedures were performed in this study; 1) Immunohistochemical staining to assess changes in cardiomyocyte dimensions and 2) Masson's Trichrome staining to quantify the deposition of interfibrillar collagen in the myocardium. In preparation for both staining procedures; the paraffin-embedded hearts were sectioned at 7µm, mounted on coated slides and baked for 120 minutes at 60 degrees Celsius. Deparaffinization was performed using two xylene baths, followed by rehydration in graded alcohol solutions (3 minutes each). Respective staining protocols were then immediately carried out.

2.6.1: Immunohistochemistry

To restore tertiary protein structure, antigen retrieval was performed by microwaving sections in 10mM sodium citrate dihydrate for 17 minutes, after which they were cooled in an ice bath to return to room temperature. A pap-pen was then used to draw a hydrophobic barrier around the sample, after which sections underwent 3x 5-minute washes in 0.1M PBS-Triton. To reduce staining noise, blocking solution (1% bovine serum albumin + 10% normal donkey serum) was applied for 2 hours. Sections were then incubated overnight in a primary antibody solution prepared in 0.1M PBS. The following day, sections underwent 3x 5-minute PBS-Triton washes, then were incubated in a secondary antibody solution prepared in 0.1M PBS for an additional 2 hours. Following this, sections were washed 3x in PBS-Triton,

then 3x in Hank's Balanced Salt Solution (HBSS) before being incubated overnight in Wheat-Germ Agglutenin solution prepared in HBSS. On the third and final day, sections were washed an additional 3 times with HBSS and incubated with Hoechst solution for 15 minutes. Finally, three more 5-minute PBS washes were conducted before sections were cover-slipped and stored in the dark at 4°C.

The following primary antibodies were used: rabbit anti-actinin (αA, 1:400, Abcam, EP2529Y) to stain the z-discs of cardiomyocytes, and goat anti-connexin 43/GJA1 (CX, 1:1000, Cedarlane, NBP1-51938) to stain connexin 43 in the myocardial endplate. The secondary antibodies used were: Alexa Fluor 647 Donkey Anti Goat (1:1000; Jackson ImmunoResearch; 705-606-147), Alexa Fluor 594 Donkey Anti Rabbit (1:1000; Jackson ImmunoResearch; 711-586-152). Additionally, Alexa Fluor 488 Wheat Germ Agglutinin (1:2000; Thermo Fisher Scientific; 1853992) was used to stain cell membranes and Hoechst 33342 Reagent (1:10000, Thermo Fischer Scientific; 1874027) to stain cell nuclei.

Imaging was performed using a confocal microscope (Zeiss Axio Observer, equipped with a Yokogawa Spinning Disc) to image 10 distinct regions of the myocardial free-wall for longitudinal analysis, as well as 5 distinct sections of the epicardium for cross-sectional analysis of each section.

Image Analysis

Using ImageJ to analyze longitudinal images, cardiomyocyte length was quantified by averaging the distance between z-discs along a continuous myocyte, z-disc width was quantified by averaging the width of αA labels and sarcomere length was quantified by averaging the distance between αA labels. In each image, 10 measurements were made to accurately assess both cardiomyocyte length and z-disc width, while 20 measurements of were taken for sarcomere length. This resulted in 40 measurements per image, and 400 per animal.

Cross-sectional images were also analyzed using ImageJ. Cardiomyocytes which were transected to display nuclei, and therefore their point of greatest diameter, were identified and tagged. The WGA channel was isolated to eliminate signal noise and examine solely the cell membranes, and the image was

transformed to 8-bit format. The tagged cardiomyocytes were then selected and the area of the cell measured using the built in "area'" function of ImageJ. A minimum of 15 cardiomyocytes were measured per cross-sectional image, leading to a minimum of 75 measurements per animal.

All measurements were corrected to body mass to ensure that observed trends reflected the true changes in myocardial dimensions relative to each animal, as opposed to reflecting differences in blood volume and body mass.

2.6.2: Collagen Deposition: Masson's Trichrome Stain

Following deparaffinization, slides were incubated in preheated Bouin's solution for 60 minutes at 56-64 degrees Celsius. Sections were then rinsed in warm tap water until clear before beginning the following standardized Masson's Trichrome procedure; Weigert's Hematoxylin (5 minutes), distilled water (2 minutes), Beibrich Scarlet/Acid Fuchsin (15 minutes), distilled water (2 minutes), Phosphomolybic/Phosphotungstic Acid solution (15 minutes), Analine Blue (5 minutes), distilled water rinse, 1% Acetic Acid (5 minutes), and dehydrate in graded ethanol and xylene solutions. Finally, sections were cover-slipped using a synthetic mounting solution and stored at 4 degrees Celsius until imaging. Imaging was performed using an Aperio CS2 slide scanner (Leica, Concord, ON) at 40x magnification to produce high-quality scans of the entire stained cardiac section.

Image Analysis

For each section, Aperio ImageScope version 12.3.3.5048 (Aperior Technologies Inc., Vista, CA) was used to image 10 distinct regions of the LV myocardial freewall at 40x magnification, each measuring 1000x1000 pixels. The Positive Pixel Count v9 algorithm applied using standard parameter settings (hue value = 0.66; hue width = 0.55) as used previously in the study of cardiac fibrosis[141].

2.7: Statistical Analyses

Both histological and basal/load independent pressure-volume data from the three groups were analyzed using a one-way ANOVA for to determine whether a difference exists between any of the groups based on different functional indices. A Tukey's Test was used post-hoc to identify between which groups differences existed. This specific post-hoc test was selected due to its conservative nature which allows for comparisons of groups with unequal numbers of participants. Echocardiographic and Acute LBNP response indices were analyzed using a two-way repeated measure ANOVA, with a Tukey's Test conducted post hoc to assess main effects and pairwise comparisons performed to identify where interaction effects were present. Additionally, linear regression analysis was performed on indices of acute cardiac response to LBNP for each group, the slopes of which were compared using one-way ANOVA with a Tukey's test post-hoc. An alpha of 0.05 was used for all statistical tests, while outlier tests were also run on all datasets to omit values that fell outside of a 99% confidence interval.

Chapter 3 – Results

3.1: Animal Details:

Comparison of descriptive group characteristics of the 29 animals with complete echocardiographic and histological data revealed that body mass was significantly higher at study termination in SHAM compared to both SCI groups. There was no difference in femur length or age.

Table 3.1: Group Statistics

	SHAM	T3 SCI	T3 OH
Age at surgery (weeks)	9	10	10
Age at termination (weeks)	18	19	19
Body Mass at termination (g)	481 ± 33	407 ± 33[a]	392 ± 33[a]
Femur Length (cm)	4.02 ± 0.11	4.07 ± 0.05	4.01 ± 0.09

Values are means ± SD. [a]P<0.05 compared to SHAM, [b]P<0.05 compared to SHAM LBNP, [c]P<0.05 compared to T3 SCI, [d]P<0.05 compared to T3 LBNP.

3.2: Acute Response to Simulated OH

3.2.1: Hemodynamic Response

At the experimental endpoint it was noted that an LBNP magnitude of -5.5mmHg was sufficient to meet all criteria for simulating OH in SCI animals, but not in SHAM animals (**Table 3.2**).

Table 3.2: Acute Hemodynamic Response to simulated OH

		SHAM	T3 SCI	T3 OH
Absolute Hemodynamic Response				
SBP (mmHg)	*Resting*	113 ± 9	98 ± 6[a]	99 ± 9[a]
	-5.5mmHg	97 ± 10	72 ± 2[a]	78 ± 6[a]
DBP (mmHg)	*Resting*	65 ± 10	60 ± 8	69 ± 5
	-5.5mmHg	52 ± 9	37 ± 6	49 ± 5
MAP (mmHg)	*Resting*	84 ± 11	75 ± 7[a]	82 ± 7
	-5.5mmHg	68 ± 10	48 ± 4[a]	60 ± 4
ΔSBP (mmHg)	*-5.5mmHg*	16 ± 4	26 ± 7*	21 ± 6*
ΔDBP (mmHg)	*-5.5mmHg*	13 ± 3*	23 ± 7*	20 ± 7*
ΔMAP (mmHg)	*-5.5mmHg*	16 ± 3	27 ± 7	22 ± 7

*Hemodynamic responses were assessed at rest and during an LBNP stress of -5.5mmHg. Values are means ± SD. [a]P<0.05 compared to SHAM, [b]P<0.05 compared to T3 SCI. *Denotes a change in BP adequate to match the physiological criteria of OH.*

3.2.2: Cardiac Response

There was a main effect for 'group' across all LBNP conditions for SW and CO ***figure 3.1 (a&b),*** as well as HR ($p < 0.05$). Posthoc testing revealed that SW, CO and HR were significantly reduced in the T3 SCI and T3 OH groups compared to SHAM ($p < 0.01$). As expected, there was a significant main effect for LBNP condition (***figure 3.1 (a-d))***, implying that LBNP significantly reduced both pressure and volume in a dose-dependent manner in all groups ($p = 0.0064$).

There was a significant interaction for both SW and CO (**Table 3.3**). Pairwise comparisons revealed that SW was reduced at rest in both T3 SCI and T3 OH groups compared to SHAM ($p < 0.001$), but this difference disappeared during both bouts of LBNP. Additionally, CO was further reduced in T3 OH compared to T3 SCI at rest ($p = 0.014$), but this difference disappeared during LBNP. However, the linear slope of the change in SW and CO was significantly greater in the SHAM group than T3 OH ($p < 0.015$), and there was a strong trend for the same compared to T3 SCI ($p < 0.0801$).

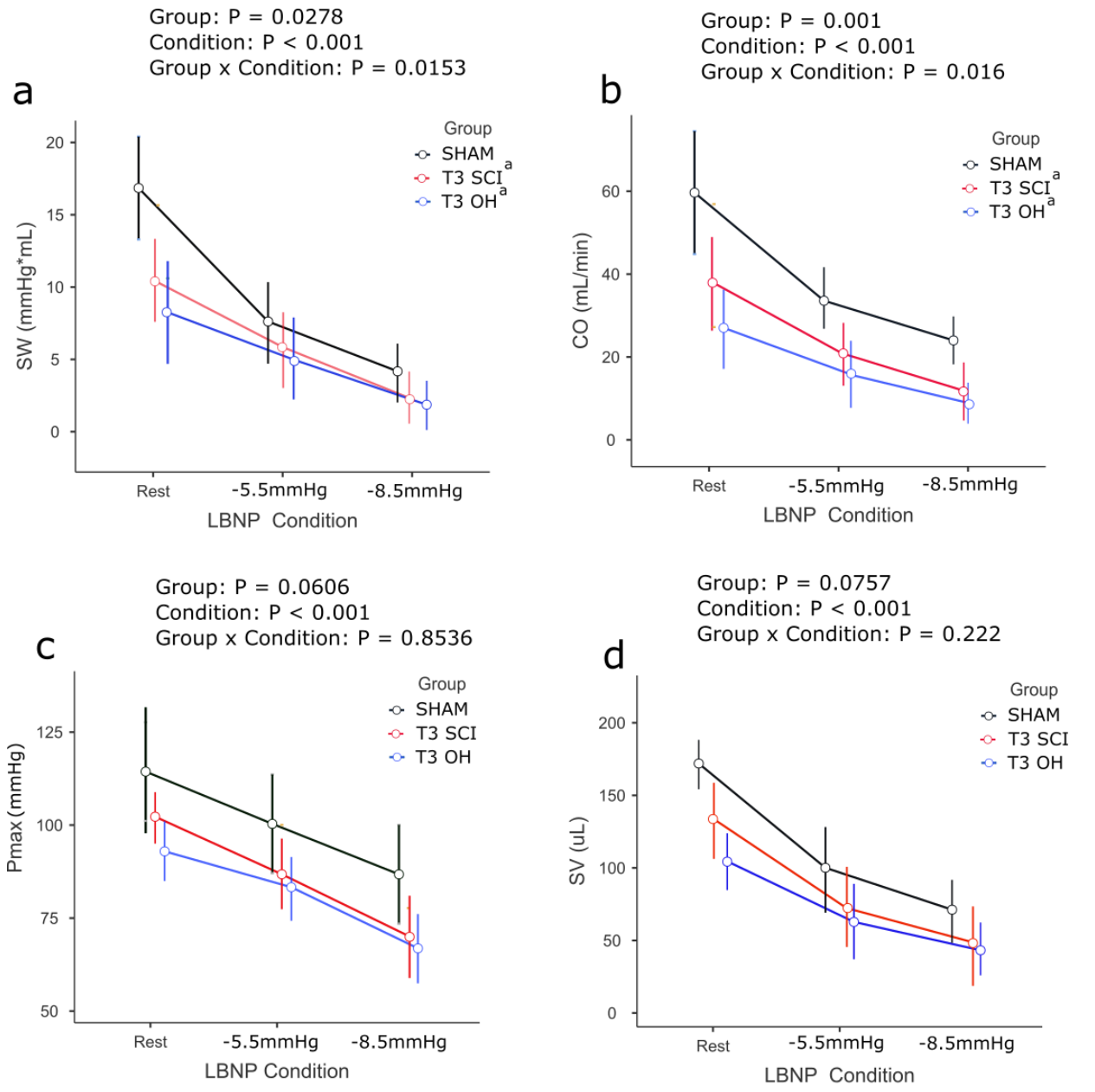

Figure 3.1. ***Acute cardiac response to graded LBNP. a)*** *Stroke Work (SW), b****)*** *Cardiac Output (CO),* ***c)*** *Maximum LV Pressure (Pmax) and* ***d)*** *Stroke Volume (SV). Values are group means ± SD. Group effects are represented by; [a]P < 0.05 compared to SHAM and [b]P < 0.05 compared to T3 SCI*

Table 3.3: Acute Cardiac Response to simulated OH

		SHAM	T3 SCI	T3 OH
Cardiac Function				
SW (mmHg/mL)	*Basal*	16.4 ± 3.7	10.7 ± 3.4†	8.49 ± 3.3†
	-5.5mmHg	7.84 ± 2.9	5.47 ± 2.7	5.38 ± 2.7
	-8.5mmHg	4.02 ± 1.8	2.69 ± 1.5	2.69 ± 1.46
CO (mL/min)	*Basal*	60 ± 4	39 ± 10†	30 ± 8†‡
	-5.5mmHg	36 ± 9	24 ± 8†	21 ± 9†
	-8.5mmHg	27 ± 8	17 ± 9†	14 ± 5†
SV (µL)	*Basal*	171 ± 18	134 ± 39	110 ± 26
	-5.5mmHg	106 ± 29	86 ± 36	76 ± 30
	-8.5mmHg	77 ± 22	62 ± 37	51 ± 17
Pmax (mmHg)	*Basal*	118 ± 19	102 ± 6	96 ± 12
	-5.5mmHg	103 ± 14	88 ± 10	84 ± 11
	-8.5mmHg	84 ± 16	70 ± 13	70 ± 11
Pdev (mmHg)	*Basal*	115 ± 16	100 ± 3	95 ± 13
	-5.5mmHg	100 ± 12	86 ± 4	85 ± 14
	-8.5mmHg	82 ± 13	69 ± 9	70 ± 15
HR (BPM)	*Basal*	353 ± 30	291 ± 28	274 ± 68
	-5.5mmHg	343 ± 30	290 ± 26	281 ± 66
	-8.5mmHg	346 ± 31	290 ± 26	280 ± 66

Cardiac function was assessed at rest, -5.5mmHg and -8.5mmHg for all groups. Values are means ± SD. Pairwise tests were performed on variables were interaction effects were discovered, where-in $^{\dagger}P<0.05$ compared to SHAM and $^{\ddagger}P<0.05$ compared to T3 SCI. Abbreviations are: Stroke Work (SW), Cardiac Output (CO), Stroke Volume (SV), Developed Pressure (Pdev), Maximum Pressure (Pmax) and Heart Rate (HR).

3.3 : Indices of Chronic Cardiovascular Function

3.3.1: Basal Hemodynamic Function

There was a significant reduction in both resting SBP and MAP in T3 SCI and T3 OH compared to SHAM ($p < 0.0015$) (***figure 3.2a&b***). Resting DBP was significantly decreased in T3 SCI groups compared to SHAM ($p < 0.023$). HR was reduced in the T3 SCI group alone compared to SHAM alone ($p < 0.007$) ***(figure 3.2c)***.

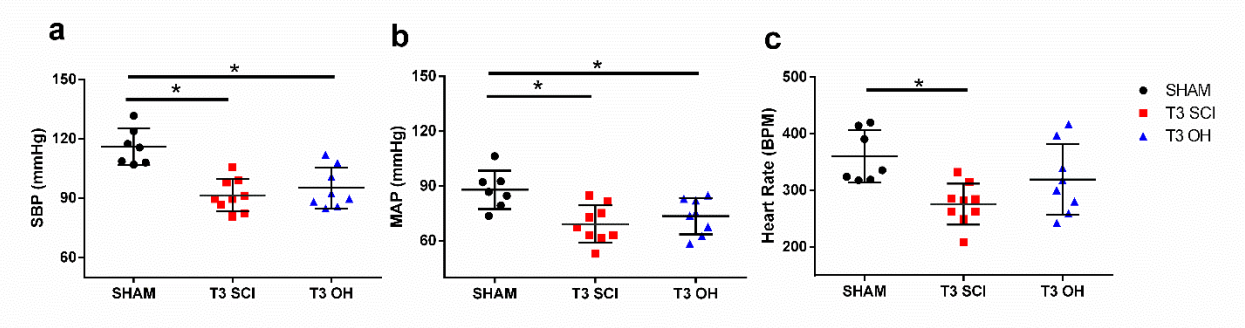

Figure 3.2. ***Resting hemodynamic data.*** *Markers represent individual animals organized into the three study groups, and bars represent the 95% confidence interval.* ***a)*** *Systolic Blood Pressure (SBP),* ***b)*** *Mean Arterial Pressure (MAP) and* ***c)*** *Heart Rate (HR) *P<0.05.*

3.3.2: LV Dimensions

Echocardiographic analysis was performed pre-injury, at which point there were no differences in cardiac dimensions or mass. When echocardiography was repeated at study termination (**Table 3.4)**, both T3 SCI and T3 OH had significantly reduced LV mass, septal and posterior wall thickness, as well as LV lumen diameter compared to SHAM ($p < 0.033$)***(figure 3.3d)***.. There was no significant impact of simulated OH on LV mass and dimensions.

3.3.3: Load Dependent LV Function

Using echocardiography to assess LV volumes and PV catheterization to assess LV pressure and volume relationships, we observed a decline in load-dependent systolic function following SCI (**Table 3.4**). Specifically, SW, CO, SV, EDV, Pmax, Pdev and $dPdT_{max}$ were significantly reduced in both T3 SCI and T3 OH vs. SHAM ($p < 0.018$)***(figure 3.3b,c,d)***. A visual of this change in basal LV function is provided in ***figure 3.3a,*** which depicts one group-averaged pressure-volume loop for each group. There was, however, no significant change in diastolic LV function in any group comparison based on echocardiography or PV analysis. The only impact of simulated OH on load-dependent LV function was a significant increase in both Ea and TPR in T3 OH compared to SHAM, which was not present in comparisons of T3 SCI and SHAM ($p < 0.011$) ***(figure 3.3e, Table 3.4)***.

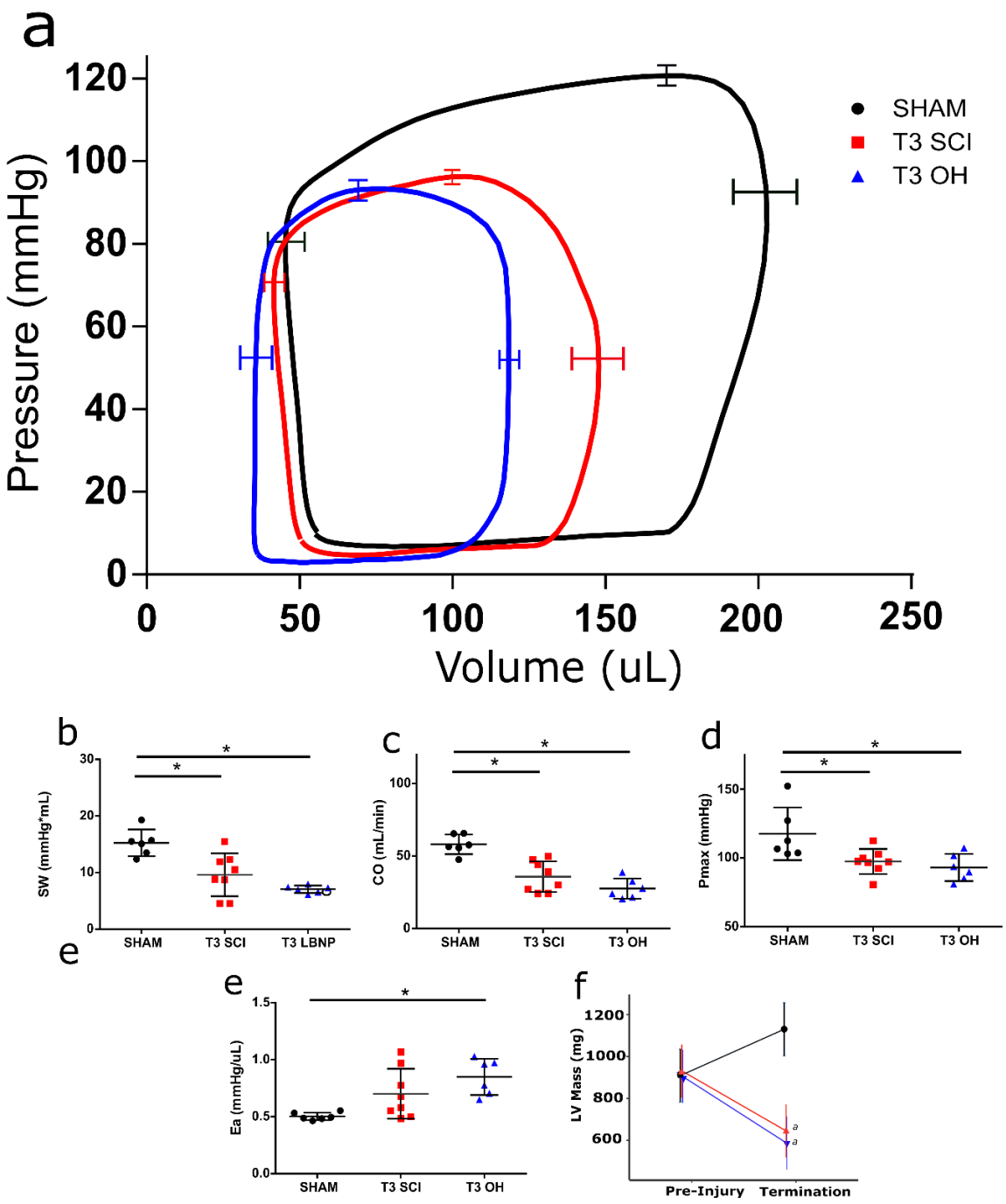

Figure 3.3. Basal LV function and dimensions. ***a)*** *PV loops created from averaged data for each of the three groups, with bars representing SEM* ***b)*** *Stroke Work (SW),* ***c)*** *Cardiac Output (CO),* ***d)*** *Maximum LV Pressure (Pmax),* ***e)*** *Arterial Elastance (Ea) and* ***f)*** *Estimated left ventricular mass (LV Mass). *P < 0.05, [a]P < 0.05 compared to SHAM, [b]P < 0.05 compared to T3 SCI. Markers are individual means values for individual animals and bars represent the 95% confidence interval.*

3.3.4: Load Independent LV Function

Load-independent LV systolic function was significantly reduced in both T3 SCI and T3 OH vs SHAM (**Table 3.4)**. ESPVR was significantly reduced in both the T3 SCI and T3 OH ($p < 0.04$), while there was also a trend for a further reduction of ESPVR in the T3 OH group compared to T3 SCI ($p=0.187$) ***(figure 3.3b-e)***. Additionally, the echo-derived VSI was significantly reduced only in the T3 OH group compared to SHAM ($p < 0.0296$). Load-independent diastolic function, however, was not significantly different across any group comparison.

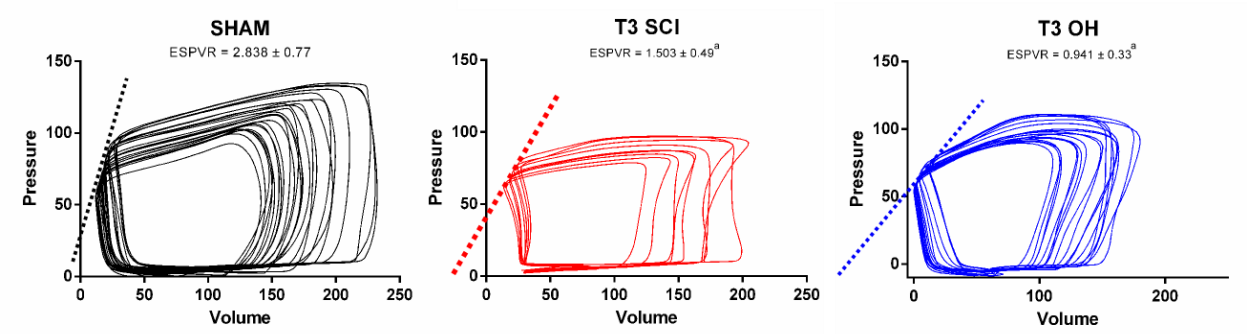

Figure 3.4. *Representative Inferior Vena Cava Occlusions from animals in each of the three groups. The dotted line is the End Systolic Pressure-Volume Relationship (ESPVR) representing the End Systolic Elastance (Ees), while the numerical values provided are the group means mean ± SD. [a]P < 0.05 compared to SHAM.*

3.3.5: Ventricular-Arterial Coupling

The VAC ratio was significantly increased in the T3 OH group compared to all both T3 SCI and SHAM ($p > 0.004$), and is visualized in ***figure 3.5.***

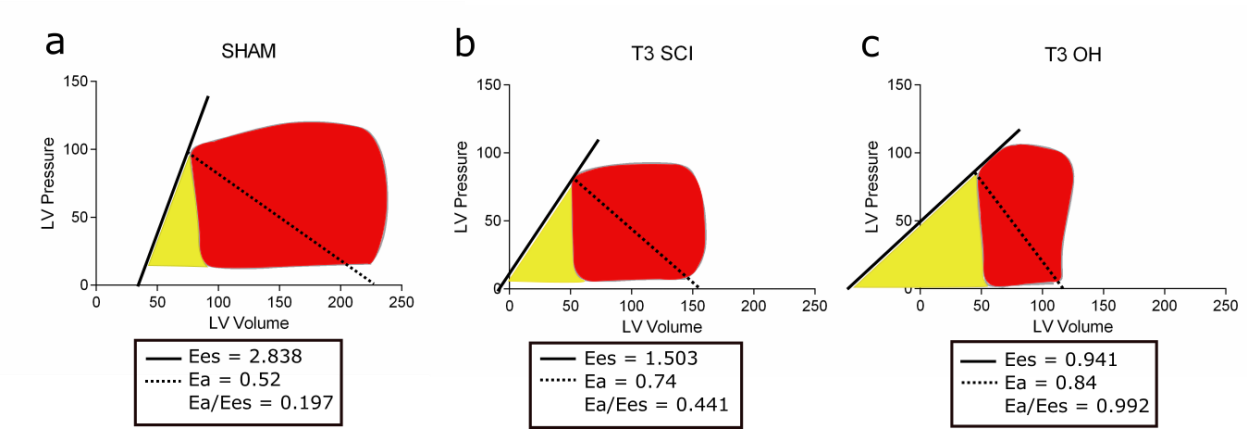

Figure 3.5*. Illustration of the relation between ventricular end-systolic elastance (Ees) and arterial elastance (Ea), which together allow for the characterization of the ventricular-arterial interaction (Ea/Ees). By overlaying the Ees and Ea onto basal representative PV loops for each group, we provide a visualization of the decreased ventricular-arterial efficiency caused by 9 weeks of daily simulation of OH in rats with complete T3 transection. The yellow shading represents potential ventricular energy, and the red shaded region represents the mechanical work performed by the heart.*

Table 3.4: Hemodynamics & LV structure and function

	SHAM	T3 SCI	T3 OH
Hemodynamic Data			
SBP (mmHg)	116 ± 9	91 ± 8[a]	95 ± 10[a]
DBP (mmHg)	69 ± 11	54 ± 11[a]	59 ± 9
MAP (mmHg)	87 ± 10	68 ± 11[a]	73 ± 9[a]
HR (BPM)	360 ± 46	275 ± 36[a]	319 ± 65
Echocardiographic Data			
Dimensions and Volumes			
LV Mass (mg)	930.3 ± 168.4	677.0 ± 108[a]	664.7 ± 151[a]
IVSd (mm)	2.02 ± 0.27	1.42 ± 1.2[a]	1.52 ± 0.34[a]
LVIDd (mm)	6.29 ± 0.98	4.95 ± 0.77[a]	4.78 ± 0.98[a]
LVPWd (mm)	2.15 ± 0.27	1.51 ± 0.17[a]	1.30 ± 0.23[a]
LVPWs (mm)	3.20 ± 0.19	2.56 ± 0.51[a]	2.31 ± 0.52[a]
EDV (µL)	477 ± 77	346 ± 103[a]	299 ± 50[a]
ESV (µL)	117 ± 33	106 ± 56	94 ± 33
Systolic Function			
SV (µL)	359 ± 58	236 ± 67[a]	205 ± 46[a]
EF (%)	68 ± 9	76 ± 8	75 ± 4
CO (mL/min)	126 ± 20	74 ± 16[a]	67 ± 20[a]
VSI ($m*s^2$)	35.4 ± 10.9	25.0 ± 3.9	20.5 ± 3.9[a]
VSI ($m*s^2$/HRR)	0.09 ± 0.02	0.07 ± 0.02	0.06 ± 0.01[a]
Diastolic Function			
E (mm/s)	781.5 ± 136.4	710.5 ± 119	739.8 ± 126

Table 3.4 (cont): Hemodynamics & LV structure and function

	SHAM	T3 SCI	T3 OH
Pressure Volume Data			
Systolic Function			
SW (mmHg*µL)	16360 ± 3700	9440 ± 4000[a]	7160 ± 520[a]
SWI (mmHg*µL/100g)	3180 ± 500	2414 ± 930	1840 ± 200[a]
Pmax (mmHg)	117 ± 19	97.4 ± 9.1[a]	93.1 ± 9.9[a]
Pdev (mmHg)	114 ± 16	94.6 ± 8.4[a]	92.23 ± 9.7[a]
dP/dT_{max} (mmHg/sec)	8078 ± 1188	5575 ± 810[a]	6073 ± 1914[a]
TPR (mmHg/mL)	1.41 ± 0.09	2.11 ± 0.85	2.786 ± 0.66[a]
End systolic wall stress (σ) ($kdyne/cm^2$)	39.4 ± 13.9	40.4 ± 21.4	50.6 ± 39.6
Ea (mmHg/µL)	0.52 ± 0.04	0.74 ± 0.29	0.84 ± 0.15[a]
Ees (mmHg/µL)	2.84 ± 0.77	1.58 ± 0.50[a]	0.94 ± 0.33[a]
Ea/Ees	0.197 ± 0.06	0.442 ± 0.21	0.992 ± 0.5[a,b]
Diastolic Function			
$-dP/dt_{min}$ (mmHg/sec)	-4022 ± 330	-3268 ± 520	-4097 ± 1721
Ped (mmHg)	5 ± 6	5 ± 7	4 ± 5
Tau (msec)	10.59 ± 4.28	13.05 ± 7.30	10.58 ± 3.0
EDPVR (mmHg/µL)	0.034 ± 0.03	0.037 ± 0.06	0.031 ± 0.04

Values are means ± SD. [a]P<0.05 compared to SHAM, [b]P<0.05 compared to T3 SCI. Note that the VSI correction was made to the Heart Rate Ratio (HRR) to control for differences in heart rate during assessment. Abbreviations are: Systolic blood Pressure (SBP), Diastolic Blood Pressure (DBP), Mean Arterial Pressure (MAP) and Heart Rate (HR), Stroke Work (SW), Stroke Work Index (SWI), Cardiac Output (CO), Cardiac Output indexed to HR (CI), (Stroke Volume (SV), Maximum LV Pressure (Pmax), Developed Pressure (Pdev), Ejection Fraction (EF), Maximal Rate of Pressure Increase (dP/dT_{max}), Arterial Elastance (Ea), End Systolic Elastance (Ees), Preload Recruitable Stroke Work (PRSW), Maximal positive pressure derivative normalized to EDV ($dPdt_{max}$ vs EDV), Ventricular Vascular Coupling Ratio (Ea/Ees), Maximal rate of pressure decay ($-dP/dt_{min}$), Pressure at the end of Diastole (Ped), Volume at the end of Diastole (Ved), Time Constant of Relaxation (Tau) and the End Diastolic Pressure-Volume Relationship (EDPVR).

3.4: LV Myocardial Histology

Myocyte dimensions are reported as both raw values and values corrected to body weight in **Table 3.5**. Significant decreases in corrected cardiomyocyte length and width (***figure 3.6(g-j))*** were identified in the T3 SCI and T3 OH groups compared to the SHAM group ($p < 0.041$). Furthermore, length:width ratio was increased while corrected cross-sectional area was significantly reduced in the T3 SCI group compared to SHAM ($p < 0.028$). Sarcomere width was significantly reduced in the T3 OH group

compared to SHAM ($p < 0.027$). There was no difference in collagen deposition between the T3 SCI and SHAM groups, however the T3 OH group exhibited a significant increase in collagen compared to SHAM ($p = 0.004$), and a strong trend for increase compared to T3 SCI ($p = 0.073$) (**Table 3.5** & ***figure 3.7 (a-d)***).

Table 3.5: Cardiomyocyte Dimensions and Collagen Quantification

	SHAM	**T3 SCI**	**T3 OH**
Myocyte Dimensions			
Uncorrected			
Myocyte Length (µm)	99.0 ± 10.7	101.4 ± 5.6	97.4 ± 5.06
Alpha-Actinin width (µm)	15.89 ± 1.9	13.19 ± 1.6[a]	12.97 ± 1.4[a]
Length/Width Ratio	6.32 ± 1.2	7.81 ± 1.1[a]	7.59 ± 0.9
Sarcomere Length (µm)	0.98 ± 0.13	0.99 ± 0.11	0.97 ± 0.09
Myocyte Cross-Sectional Area (μm^2)	383.5 ± 59.6	317.8 ± 50.1	364.3 ± 102
Corrected			
Myocyte Length (µm)	91.9 ± 6.97	80.2 ± 8.95[a]	74.0 ± 8.36[a]
Alpha-Actinin width (µm)	14.85 ± 2.2	10.46 ± 1.9[a]	9.856 ± 1.5[a]
Length/Width Ratio	6.32 ± 1.18	7.81 ± 1.12[a]	7.59 ± 0.91
Sarcomere Length (µm)	0.89 ± 0.08	0.79 ± 0.14	0.73 ± 0.08[a]
Myocyte Cross-Sectional Area (μm^2)	356.3 ± 50.3	268.8 ± 68.1[a]	293.0 ± 44.5
Myocardial Fibrosis			
Proportion of Collagen : Myocardial tissue	0.013 ± 0.006	0.017 ± 0.002	0.025 ± 0.008[a]

Values are means ± SD. [a]P<0.05 compared to SHAM, [b]P<0.05 compared to T3 SCI.

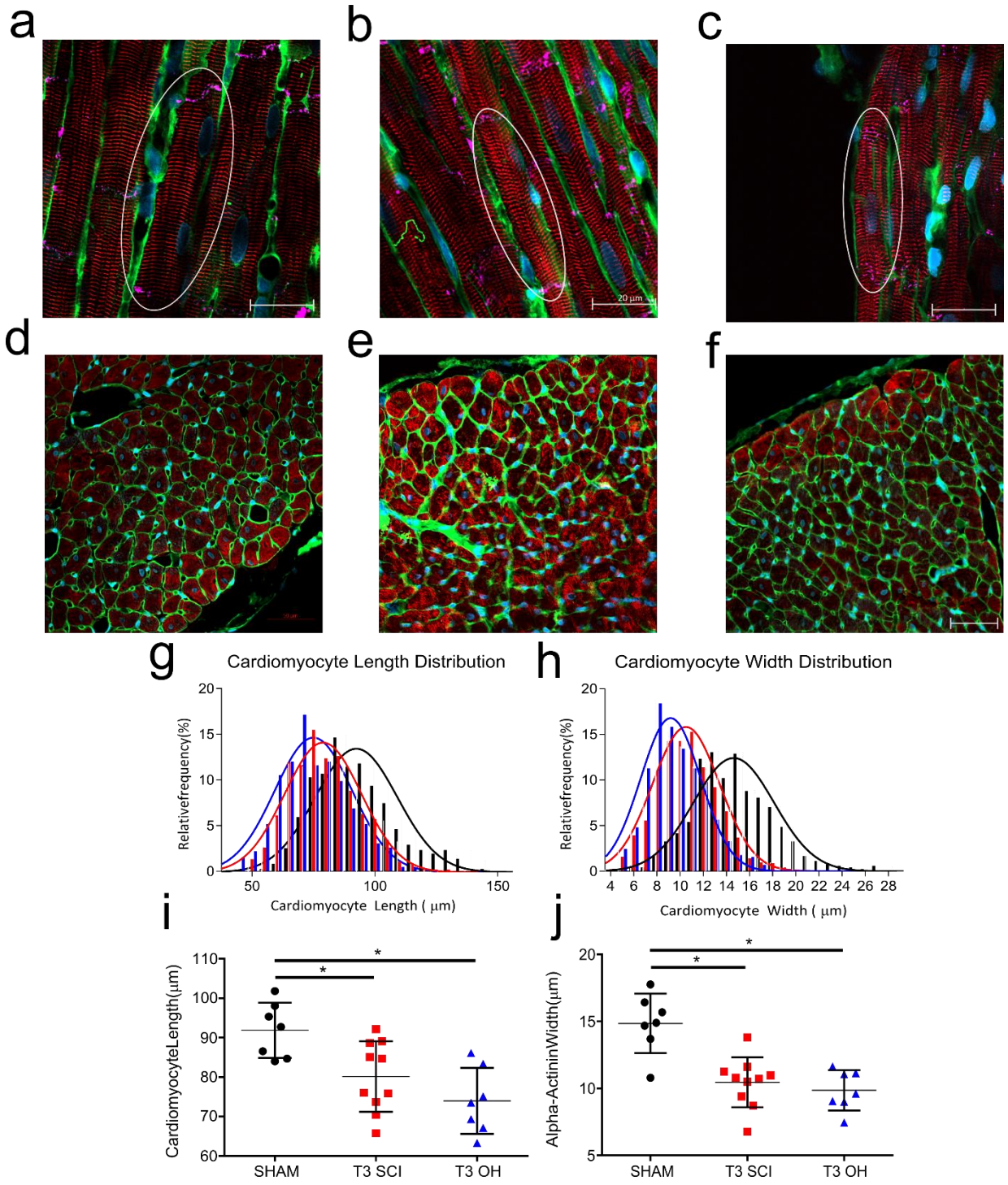

Figure 3.6. ***Myocyte Dimensions***. *Representative Images for **a)** Longitudinal view of SHAM cardiomyocyte and **b)** Longitudinal view of T3 SCI cardiomyocyte, **c)** Longitudinal view of T3 OH myocyte **d)** Cross-sectional view of epicardium of SHAM animal, **e)** Cross-sectional view of epicardium of T3 SCI animal. **f)** cross-sectional view of epicardium of T3 OH animal. Colours represent: alpha actinin (red), connexin (pink), Wheat Germ Agglutinin in the cell membrane (green) and nuclei (blue). Longitudinal images were taken at 63x magnification, cross-sectional images were taken at 20x magnification. Frequency distributions for **g)** cardiomyocyte length and **h)** cardiomyocyte width. Individual animal length and width measurements are quantified in **(i)** and **(j)** using means and 95% confidence intervals. *P < 0.05. Scale bars are 20µm (panels **a-c**) or 50µm (panels **d-f**).*

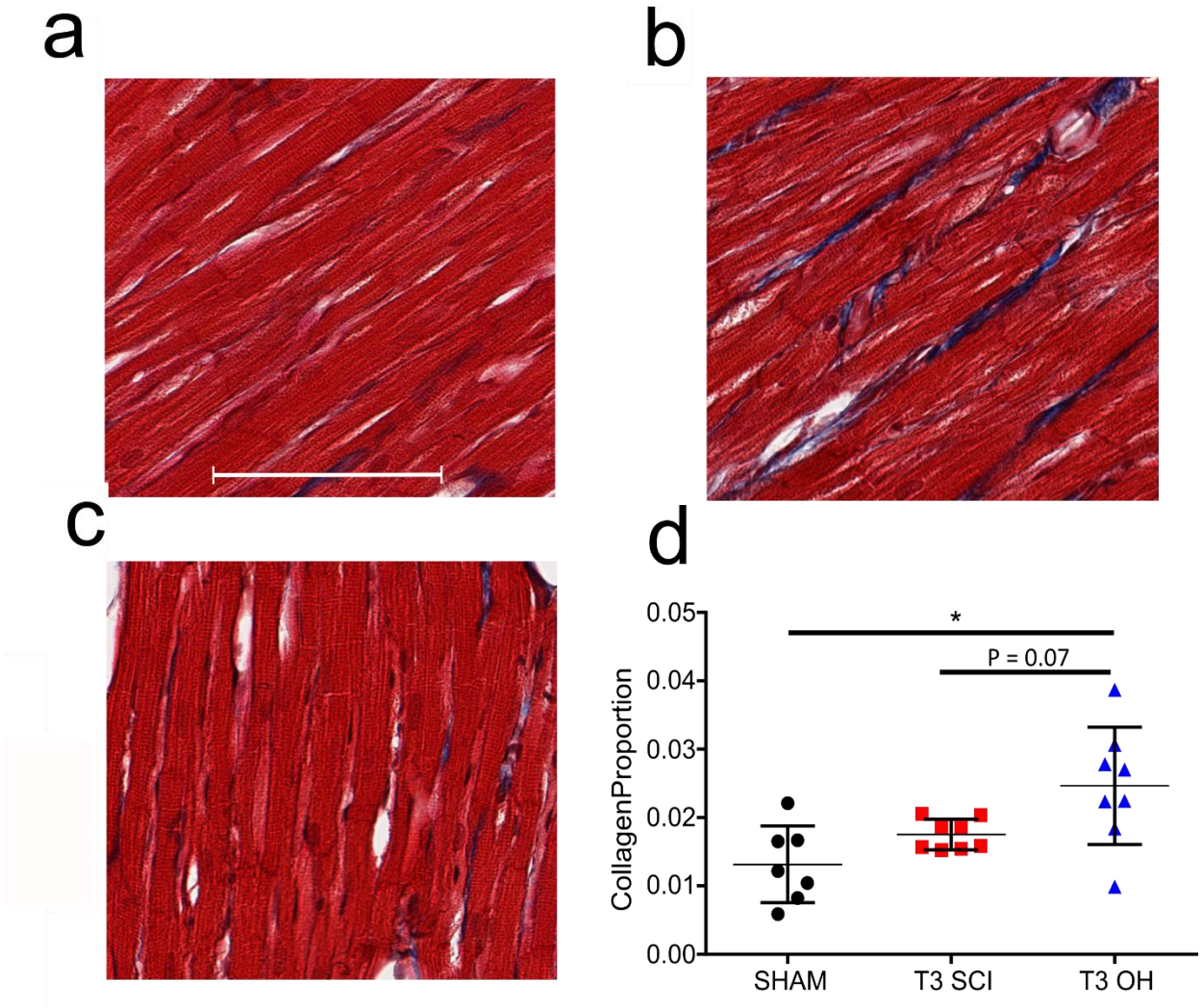

Figure 3.7. Myocardial Collagen Content. *Representative images of Masson's Trichrome Stained myocardium from the LV freewall in* ***a)*** *SHAM,* ***b)*** *T3 OH and* ***c)*** *T3 SCI. Scale bar is 50µm.* ***d)*** *Individual animal data for proportion of collagen: myocardial tissue represented by means and 95% confidence intervals . *P < 0.05.*

Chapter 4 – Discussion

In the present study we provide the first insight into the physiological impact of chronically simulated OH on cardiac function following high thoracic SCI. We validated our model of OH simulation for animals with SCI and performed the first robust preclinical analysis of cardiac function following SCI during varied loading conditions. Furthermore, we provide the first preclinical demonstration that LBNP causes acute reductions in load-dependent cardiac indices of both SCI and SHAM animals in a dose-dependent manner. In addition to confirming previously observed chronic changes in LV dimensions and function following T3 SCI, we identified a trend for further decrement of ventricular contractility and an increase in arterial afterload in our T3 OH group. Together these changes manifested as a clear uncoupling of the ventricular-vascular interaction in the T3 OH group alone compared to both other groups, which was largely driven by the diminished LV contractility. In addition, we found evidence to suggest that while T3 SCI causes significant myocardial atrophy, both T3 SCI and daily simulated OH together were required to increase myocardial collagen deposition compared to SHAM animals. Together, the findings of this thesis imply that the frequent occurrence of OH following high thoracic SCI may impair the both the intrinsic function and efficiency of the LV, as well as promote the development of myocardial fibrosis.

4.1: Validation of OH Simulation Model

This is the first preclinical study to combine an OH simulation model using LBNP with a robust analysis of both hemodynamic and cardiac function following SCI. We demonstrated that a bout of -5.5mmHg of LBNP was sufficient to simulate all hemodynamic criteria for OH diagnosis in animals with high thoracic SCI but not a SHAM injury. This is in line with clinical work comparing the orthostatic tolerance of able-bodied individuals and those with chronic SCI[58,142], and more specifically is also in agreement with reports of decreased LBNP tolerance following chronic high level SCI[133]. While it was noted that DBP of the SHAM group was reduced sufficiently to diagnose OH during the -5.5mmHg bout of

LBNP, the lack of adequate change in SBP indicates that tissue perfusion may have been maintained in the SHAM group. Therefore, in the present study it was determined that OH was successfully simulated when the LBNP stress met all hemodynamic criteria for OH (changes in both SBP and DBP). These data, therefore, suggest that our method of OH simulation at a pressure of -5.5mmHg is a valid tool for use in preclinical investigations of repetitive OH in the setting of SCI.

4.2: Effect of SCI and OH on cardiac function during LBNP

We conducted two degrees of LBNP (-5.5mmHg and -8.5mmHg) with the catheter placed in the LV to provide the first ever assessment of the changes to load-dependent cardiac function during graded preload reductions. A dose dependent response was observed in both the pressure and volume indices of LV function, as demonstrated in ***figure 3.1***, clearly demonstrating the connection between cardiac preload and load-dependent cardiac function. This ability to assess the cardiac response to highly stable, controlled and reproducible preload manipulations opens the door for future analyses of cardiac function both within and outside of SCI.

Analysis of the load-dependent LV response to preload manipulation in the present study revealed two interaction effects: one in which the SW of the SHAM group was significantly different than both SCI groups at rest but not during LBNP, the other in which the CO of the T3 OH group was significantly less than T3 SCI at rest but not during LBNP. These observations could be interpreted as differences in the sensitivity to LBNP, however this seems unlikely due to the plethora of data showing that high thoracic SCI increases sensitivity to orthostatic stress[30,57,58]. A more likely explanation is that these differences were caused by a "bottoming out" of SV, a variable which has a major influence on both SW and CO. There is evidence to suggest that when SV is pushed to physiological extremes by altered loading (either unloading or overloading), further extreme loading alterations no longer have a significant effect on SV. This concept can be alluded to the relationship between a balloon (the heart) inflated with air (blood), whereby

changes in air pressure at the extremes of inflation/deflation cause little change in the volume of the balloon. The use of this analogy is further complimented our linear regression data, which demonstrated that the slope of change in SW and CO for SHAM was significantly greater than T3 OH and was strongly trending to be greater than T3 SCI as well. The present data, therefore, demonstrates that there may be a limit to how low LBNP can reduce SV despite further reductions in cardiac preload.

4.3: Reduction in LV Dimensions and Systolic Function

The next major finding of this study was that both the T3 OH and T3 SCI groups exhibited a significant decrease in LV mass, dimensions and systolic function compared to SHAM. The T3 OH group additionally exhibited an increase in arterial elastance compared to SHAM that was not seen in the T3 SCI vs SHAM comparison.

4.3.1: SCI-induced reduction in LV dimension and volumetric indices

The reduction in LV mass, dimensions and volumetric function following SCI mirror previous findings from both preclinical and clinical investigations, which attributed these changes to the chronic unloading of the heart and reduced skeletal muscle pump activity following SCI[61,63,66,72,75,80–82,87,92,143]. Support for the concept of chronic unloading as a major stimulus for reduced LV dimensions also exists in studies of cardiac unloading outside of SCI such as prolonged bedrest, spaceflight and even the loss of significant body mass[103,105,144,145]. The chronic cardiac unloading in the present study is likely attributed to the removal of descending sympathetic control over the systemic vasculature, as well as a lack of skeletal muscle pump function in the lower body. This is based on evidence that sympathetic decentralization reduces cardiac preload by promoting venous blood pooling in the splanchnic region and lower limbs, and reduces resting cardiac afterload by impairing vascular tone in the arterial system[57,61,75]. Furthermore, past works have shown that when skeletal muscle pump activity is even partially restored with passive leg exercise, the increased venous return can prevent post-SCI declines in cardiac dimensions[82,146,147]. It is

unlikely that there was any restoration of muscle pump function or central sympathetic control in the present study, as no exercise interventions were conducted and our model of complete T3 transection ensures that absence of axonal sparing through the injury site[72,80,148].

This relationship between chronic cardiac loading and LV volume also explains why the daily simulation of OH in the present study did not induce significant alterations in LV dimensions. Outside of 5 minutes of acute reduced loading each day, the aforementioned key factors regulating cardiac preload (vascular tone, exercise level, blood volume, skeletal muscle pumps, etc.) would be unaltered in the T3 OH group compared to T3 SCI. Additionally, there were no significant differences in measures of afterload between the T3 SCI and T3 OH group either.

4.3.2: Reductions in pressure-derived indices of systolic function and arterial afterload

SCI Impaired LV Systolic Function

The observation that SCI impaired the load-dependent pressure function of the LV, as demonstrated by reductions in Pmax, Pdev and $dPdt_{max}$ aligns with previous studies that attributed these effects to the loss of descending sympathetic control over the heart. Two different experiments used infusions of dobutamine, a β1/2 & α1 agonist, to simulate an increase in sympathetic activity on the heart itself, and in doing so increased the pressure-function of the LV of rats with chronic T2 SCI back to levels observed in SHAM animals[81,114]. There is, however, no direct evidence that chronic unloading of the heart played a role in the long-term decrease in LV pressure function. When passive hind-limb training was used to increase preload in rats with T3 SCI, no change was observed in LV pressure function, despite the restoration of volume function discussed in the previous section[82].

Simulated OH Increased Arterial Elastance and Total Peripheral Resistance in Animals with SCI

The finding that simulated OH exerted a deleterious influence on only arterial afterload (Ea and TPR) in T3 OH animals compared to SHAM, with no further influence on load-dependent LV pressure

function, can be rationalized by examining the physiology of the simulated bouts of OH. As simulated OH would have little-to-no effect on descending sympathetic input at rest, which we previously described as the primary determinant of LV pressure function, the unaltered LV pressure function in T3 OH compared to T3 SCI makes sense. However, this indication of increased afterload in T3 OH compared to SHAM from Ea and TPR is at direct odds with both the suggestion of decreased afterload from reduced MAP following in both SCI groups compared to SHAM, and the lack of change in LV wall stress. We postulate that this discrepancy between Ea, TPR and MAP is likely due to Ea and TPR being calculated from a combination of hemodynamic and ventricular data, directly relating SV and blood pressure to provide an index of afterload that is *relative* to ventricular function. MAP, meanwhile, was directly measured by a pressure transducer in the carotid artery and is generally regarded as an index of absolute afterload. The utility of Ea as a measure of arterial afterload relative to cardiac function has been demonstrated in clinical studies outside of SCI, in which arterial elastance calculated from SV and Pes was shown to be an independent predictor of exercise capacity in individuals with cardiorespiratory dysfunction[149]. As for the discrepancy between Ea, TPR and wall-stress, there is evidence to suggest that LV morphology adapts in response to changes in absolute arterial afterload to maintain constant LV wall stress[150,151]. In light of this, the lack of significant change in LV wall stress in the present study is likely due to the decrease of both MAP and LVPWs (LV posterior wall thickness at end systole) in T3 SCI and T3 OH compared to the SHAM.

The increase in arterial afterload suggested by Ea and TPR is likely related to an increase in central arterial stiffness, which has been attributed to elevated resting RAAS activity in both preclinical and clinical cases of SCI[72,76] and would be further aggravated by the additional increase in RAAS activity caused by daily OH in SCI animals[70,126,152,153]. In particular, prolonged elevations in plasma concentration of the mineralocorticoid aldosterone, a direct end-product of RAAS activity, causes chronic impairment of vascular function in a manner independent from blood pressure[32,34,154]. This would explain both the trend for increased afterload seen in T3 SCI compared to SHAM, and the significant increase in afterload seen

in T3 OH animals compared to SHAM. Taken together, these data suggest that SCI and simulated OH together did not alter LV wall stress at rest but did cause an increase in arterial afterload relative to LV function, which may decrease tolerance to cardiorespiratory stress. While elevated RAAS activity may be to blame for this dysfunction, direct investigation into the effect of simulated OH and SCI on plasma concentrations of RAAS by products is necessary to establish a clear causal relationship.

In summary, the load-dependent outcomes indicate that the ability of the LV to eject blood into systemic circulation at rest is grossly restricted following complete T3 transection. The reduction in both volume and pressure function due to reduced cardiac preload and removal of central sympathetic control, respectively, is summarized in the group-averaged PV loops in ***figure 3.3a***. Together these findings illustrate a bleak scenario in which SCI reduces cardiac reserve and increases the resistance to blood being ejected from the LV into systemic circulation relative to LV function. The finding that daily simulation of OH increases arterial afterload following SCI suggests that chronic blood pressure instability may reduce the functional arterial reserve, and therefore further limit the adaptability of the cardiovascular system to stress. However, as we have already elucidated, the variables discussed up until this point are dependent not only on cardiac function, but also on the loading conditions placed on the heart by the rest of the cardiovascular system. Therefore, to truly understand the influence of our model of T3 transection and simulated OH on cardiac function specifically, measures of function which are *independent* of cardiac loading must also be discussed.

4.3.3: SCI decreased LV contractility, with implications for further decline following simulated OH

In addition to impairing resting cardiac function, SCI also hampered the load-independent function of the LV. Our lab has previously demonstrated this using LV conductance catheters[72,73,82], but this is the first study to do so using novel admittance technology. This is noteworthy, as conductance catheters tend to overestimate end systolic volume but accurately assess end systolic pressure, bringing

into question the accuracy of conductance-derived LV pressure-volume relationships. Therefore, the present study's use of an admittance catheter to further demonstrate that SCI impairs LV contractility validates this previous body of conductance-based work. SCI-induced LV contractile dysfunction has previously been attributed to a loss of direct descending sympathetic control of the heart. This is based on the previously-discussed administration of dobutamine to simulate cardiac sympathetic excitation in rats with a complete high thoracic SCI, which resulted in an increase in LV contractility that was comparable to SHAM-injured animals[81,112].

We also provide the first evidence that daily simulated OH may further impair LV contractility following high level SCI. This is implied by the trend for a further decrease in the ESPVR of the T3 OH group compared to T3 SCI, as well as the decreased VSI in the T3 OH group alone compared to the SHAM group. However, there is presently no clear physiological explanation of this impairment. Daily simulation of OH is unlikely to have further altered descending sympathetic control, as our model of T3 transection ensures no difference in injury level or sparing between animals. While we cannot identify the exact mechanism behind these changes with our present data, we postulate two potential physiological causes.

The first possible physiological explanation for simulated OH further impairing LV contractility following SCI is the impact of elevated RAAS activity on cardiac function. As discussed in section 4.3.2, high level SCI causes elevated plasma-renin concentrations at rest and an exaggerated RAAS response to physiological stress[30,125,126,142,155,156]. By-products of the RAAS system, namely the mineralocorticoid aldosterone, are known to amplify pre-existing ventricular dysfunction and shift the myocardium towards a pro-inflammatory phenotype[154]. This combination of an inflammatory phenotype and increased arterial afterload would decrease the functional reserve of the cardiovascular system, thus hindering the ability of animals in the T3 OH group to respond to noxious stimuli such as autonomic dysreflexia (AD). AD has been found to occur spontaneously up to 39 times each day in similar rodent models of SCI[148], and the incidence of AD has been correlated with decreased systolic function in both clinical and preclinical

settings[85]. While elevated RAAS activity is likely also responsible for the increased myocardial collagen in the T3 OH group, no research presently exists to draw a direct link between such collagen deposition and myocardial contractility. We therefore propose that augmented RAAS activity in the T3 OH group increased the risk of myocardial injury during episodes of abnormal cardiovascular function, such as AD.

The second possible physiological explanation for simulated OH impairing LV contractility following SCI is the negative impact of repeated bouts of acute cardiac ischemia, and consequent decreased myocardial perfusion, on the metabolic profile of the myocardium. Previous work on coronary occlusions demonstrated that when coronary perfusion pressure (arterial EDP – LV EDP) dropped below 40mmHg, subendocardial perfusion became restricted in a dose-dependent manner[157]. Based on these criteria, we suggest that during bouts of LBNP the animals in the T3 OH group experienced repeated periods of limited subendocardial perfusion. Such episodes are reported to cause no structural damage when lasting less than 15 minutes, but do cause a suppression of myocardial function that lasts for 2-3 hours following reperfusion[157]. This concept that has been coined "myocardial stunning"[157], and preclinical evidence has suggested that the repeated occurrence of myocardial stunning (as would be caused by daily simulated OH in the T3 OH animals) can drive myocardial remodelling that prevents functional stunning at the cost of reduced LV contractile capacity[157–159]. This myocardial remodelling is characterized by an increase in cardiomyocyte width that leads to a decrease in the length:width ratio. While this is at odds with our histological findings of cardiomyocyte atrophy and increased length:width ratio, the differences in chronic loading and other neurohumoral factors in the present study of SCI from previous works on acute myocardial ischemia provide too many confounding factors to distinguish chance from causal relationships. Further work is needed to confirm the presence of this acute subendocardial perfusion and determine what effects it may have on myocardial structure following SCI. We therefore postulate that the repeated bouts of OH could have reduced LV contractility by causing episodes of reduced subendocardial perfusion which could drive a shift in the metabolic profile of the myocardium.

In summary, both proposed physiological mechanisms have the potential to explain how simulating OH following T3 SCI can further decrease LV contractility. However, further work is needed to better understand the direct impact of increased RAAS activity and repeated acute ischemia on myocardial function when both atrophy and reduced loading are present following SCI. We are therefore able to provide further evidence for intrinsic LV contractile dysfunction following SCI, as well as the first evidence that the occurrence of OH in individuals with SCI may further the progression of this impairment.

4.3.4: No evidence of diastolic dysfunction following high thoracic SCI and/or daily simulation of OH

The finding that diastolic function was unchanged by SCI and/or simulated OH is largely in agreement with previous literature on preclinical investigations of SCI. Studies on both clinical and preclinical SCI have traditionally reported trends for decreased diastolic function that rarely reach significance[66,79–82]. In the present study, the findings that both Tau and -dP/$_{dtmin}$ were unchanged following SCI corroborates previous works from our lab, confirming that intrinsically-measured LV diastolic pressure function is not significantly changed by SCI. However, a meta-analysis recently published by our lab reported a significant reduction in mitral flow and early-diastolic relaxation in patients with chronic SCI, a finding which implies a pathological shift in LV diastolic function despite no specific outcome measures exceeding the able-bodied cut-off for diastolic dysfunction[87]. This discrepancy between these clinical and preclinical data may, in part, be attributed to the drastically higher heart rate of rodents compared to humans. In addition, the level of SCI was not consistent across preclinical and clinical studies, as the preclinical investigations involved complete transection of either the T2 or T3 spinal segments but the clinical investigations involved a range of high thoracic and cervical injuries. However, the clinically-reported changes in diastolic function have largely been attributed to chronic unloading of the heart due to similar changes being found in models of chronic unloading outside of the field of SCI[87]. For example, echocardiographic assessment of astronauts immediately upon return from space identified reductions in both early mitral filling and isovolumic relaxation time[105]. However, as the majority of literature on

diastolic function focuses on more prevalent cases of chronic overload, such as hypertension and congestive heart failure[160–163], the physiology underlying the changes in diastolic function during chronic unloading is not well understood. In looking beyond the load-dependent data, the present finding of no reduction in load-independent diastolic function supports previous preclinical work[81], with the use of a more reliable admittance catheter reinforcing the legitimacy of this conclusion.

The lack of change in diastolic function in the T3 OH group compared to T3 SCI is, similarly to section 4.3.1, likely due to simulated OH having little-to-no effect on chronic cardiac loading. As discussed in the previous section, chronic loading is known to be a major contributing factor to resting diastolic function[103,105,164], and aside from the five minutes of daily simulated OH chronic cardiac loading would be unchanged in the both OH groups compared to their injury-matched controls. As there is also no evidence to suggest that daily simulation of OH influences chronic cardiac loading at rest, there is presently no clear physiological stimulus to drive a decrease in diastolic function. However, this lack of diastolic dysfunction in the T3 OH group is surprising when contrasted with the significant increase in collagen deposition in the myocardium of animals in the T3 OH group. This is interesting to note, as collagen deposition is a marker of cardiac fibrosis, and has long be considered a structural marker for myocardial stiffening and decreased diastolic function[17,101]. This peculiarity may be evidence that decrements in diastolic function are preceded by structural changes in the present model, and a longer study timeline could have resulted in the emergence of diastolic dysfunction in the animals with increased cardiac fibrosis.

4.4: Frequent simulation of OH following SCI leads to uncoupling of the LV and arterial system

In the third major finding of this study, we demonstrate for the first time that daily simulated OH is detrimental to the mechanical efficiency of the ventricular-arterial interaction following high thoracic SCI, but not following a SHAM injury. This change signifies an “uncoupling” of the cooperative action of the LV and arterial system, the likes of which have previously been reported to decrease cardiovascular

efficiency and increase the risk of cardiac disease[54,55,89,90]. The present findings of significant uncoupling in the T3 OH group, but not the T3 SCI group, is in contrast with previous evidence that high thoracic SCI causes ventricular-arterial uncoupling[82]. However, this previous study used a conductance catheter to assess LV pressure-volume function, and therefore had an increased risk of errors in the assessment of LV volumes. In addition, in the present study the mean VAC ratio of T3 SCI did still double compared to the SHAM, but the variability of the measures meant that no changes were statistically significant. ***Figure 3.5*** provides a visual representation of the change in efficiency across the three groups, with the yellow-shaded area representing an estimate of the potential energy invested by the LV to overcome afterload and begin ejecting blood, and the red-shaded area depicting the mechanical work done by the LV to eject blood. Together, the yellow and red regions represent the energy required to deliver sufficient blood to systemic circulation despite resistance from arterial afterload. The combination of greater potential energy (yellow) and less mechanical work (red) in the T3 OH group (***figure 2.5, panel c***) indicates that more energy is required to be invested in order to eject an adequate amount of blood into systemic circulation, which can be interpreted as a decrease in cardiac efficiency.

This drastic increase in VAC ratio in the T3 OH group was driven by the decrease in LV contractility (trend compared to T3 SCI, and significance compared to SHAM), but also to a lesser extent by an increased arterial afterload compared to SHAM animals. This dual contribution of ventricular and arterial dysfunction is key, as it implies a severe decrease in the functional reserve of the cardiovascular system. Previous clinical studies of VAC have reported that a change in VAC driven by only altered afterload can be compensated for by changes to LV contractility, forcing the heart to work harder to maintain adequate perfusion of both systemic and coronary circulation. The same can be said for compensations in arterial load to offset LV dysfunction[51,54,55]. However, when both ventricular and vascular dysfunction are present, the cardiovascular system becomes highly limited in its compensatory abilities. This lack of functional flexibility has been reported to cause further decreases in the cardiac contractile reserve and sensitizes

LV performance to alterations in either pressure or volume loading[54,55]. The implications of these findings are alarming for patients with high-level SCI who regularly experience both OH and AD and are already limited in their ability to compensate for altered blood flow distribution due to the removal of descending sympathetic control. Furthermore, this decreased tolerance of orthostatic stress holds the potential to take on a positive feedback nature, wherein the decreased ability to tolerate orthostatic stress causes further arterial and ventricular dysfunction.

Therefore, this increased VAC ratio in the T3 OH group implies that individuals with high level SCI who regularly experience OH may experience more drastic cardiovascular dysfunction and have further decreases in cardiac reserve than individuals of the same injury level who do not regularly experience OH. This is in line with a combination of previous works that identify cardiovascular disease risk as being three times greater in the SCI population[127], cardiovascular dysfunction (such as OH) as increasing in severity with higher level injuries and OH being correlated with CAD and stroke in able-bodied populations[63,87,120,121]. The only previous study to examine VAC in SCI demonstrated that passive lower-limb exercise can be used as a treatment to improve/maintain healthy coupling following experimental high thoracic SCI[82]. This suggests that further studies are needed to examine this phenomenon in a clinical setting with the goal of identifying 1) whether OH has a similar effect on VAC in humans, and 2) if so, whether exercise is a valid treatment.

4.5: SCI-induced Atrophy and OH-induced Cardiac Fibrosis

The final major finding of this study was that SCI induced significant cardiomyocyte atrophy, while the daily simulation of OH appeared to accelerate the deposition of interfibrillar collagen in the myocardium following SCI.

4.5.1: SCI caused cardiomyocyte atrophy, but chronically simulated OH had no additive effect

Significant decreases in both cardiomyocyte length and width, as observed in this study, are widely reported in the literature following experimental high level SCI[72,73,81,165,166]. While this reflects a decrease in sarcomeres aligned both in parallel and in series, in the present study these changes may not have occurred in a balanced manner. Additional increase in length:width ratio following SCI suggests that reductions in width may have exceeded the reductions in length. This is the first study, to our knowledge, reporting an increased myocyte length:width ratio following SCI. Similar changes in length:width ratio have been demonstrated in cases of dilated cardiomyopathy, however these changes were driven by increases in myocyte length as opposed to reductions in width[167]. It is not clear what underlying stimulus drove the change in ratio in the present study, but previous works have observed alterations in length:width ratio in response to a variety of stimuli from mechanical stress to changes in the cardiac metabolic environment[157,167]. In the only study to investigate the cellular mechanisms of cardiomyocyte atrophy after SCI, our lab has previously associated cardiomyocyte atrophy following SCI with increases in both UPS and autophagy pathways at both the mRNA and protein levels, as well as chronic increases in atrophy-linked AngII type I receptor[72,168]. Outside of SCI, ablation of sympathetic nerves has been shown to induced cardiac atrophy with no change in body mass[113], while unloading select regions of the myocardium by severing chordae tendinae has led to a rapid decrease in myocyte cell volume and cross sectional area[169]. This suggests that the cardiomyocyte atrophy in the present study could be multifactorial, involving a disruption in the balance of proteolytic pathways due to one or more of the altered neurohumoral rhythm and cardiac loading. Regardless of what drove the change in cardiomyocyte structure or in which direction the ratio changed, these morphological changes have been consistently reported to cause decreases in the contractile function of the myocytes themselves[157,167,170]. Therefore, it is very likely that this reduced myocyte length and width, as well as the increased length:width ratio, contributed to the previously-discussed impairment in contractile function following SCI.

The lack of significant impact of simulated OH on cardiomyocyte dimensions was surprising, as animals in the T3 OH group likely experienced drastically elevated RAAS activity, which have been associated with cardiomyocyte atrophy following SCI[72]. However, the magnitude of the influence of RAAS activity on myocyte atrophy following SCI has not been compared to other stimuli, such as chronic unloading, reduced circulating catecholamines and frequent bouts of AD, which were likely exerting influence on myocyte size in the present study. Outside of SCI, studies of both chronic unloading[171] and overloading[172] have provided evidence that the loading conditions placed on the heart exert a much stronger remodelling stimulus than RAAS activity. Furthermore, while connections have been drawn between specific Ang II receptors and atrophy[168], increased RAAS activity has also been widely reported to drive hypertrophy in a load-independent manner[32,33,160,173]. Additional work is therefore needed to provide a clear understanding of the relationship between RAAS activity, cardiac remodelling and SCI, to provide further context to the interaction of OH and cardiac structure.

4.5.2: Myocardial fibrosis following chronic simulation of OH and exacerbated by SCI

In contrast with the lack of change in collagen deposition in the T3 SCI compared to SHAM, the significant increase in collagen deposition of T3 OH compared SHAM and strong trend compared to T3 SCI indicates that SCI alone may not exert a strong pro-fibrotic effect on the LV myocardium, but SCI and daily simulated OH together does. This is the first study to examine the relationship between cardiac fibrosis and the occurrence of simulated OH in an SCI model. We postulate that this shift to a pro-fibrotic cardiac phenotype was driven by the promotion of RAAS during the daily bouts of simulated OH. Increased plasma renin concentrations, the marker of the beginning of RAAS activation, have been noted in able-bodied individuals in response to orthostatic stress despite the existence of a functional baroreflex[56]. However, this RAAS response is exaggerated in those with high level SCI, leading to greater release and prolonged action of aldosterone in this population. This is important, as in addition to the previously discussed influence of aldosterone on vascular structure and function, increased mineralocorticoid presence is

known to cause cardiac fibrosis in a load-independent manner[33,174]. However, while this may provide evidence for structural changes to the myocardium following simulated OH, with or without SCI, this did not translate to functional impairment, as no decrease in diastolic function was identified in the present study.

The lack of cardiac fibrosis following SCI alone reinforces the uncertainty about the influence of high level SCI on interfibrillar collagen deposition. The majority of previous preclinical investigations of SCI and myocardial fibrosis have reported an increase in collagen deposition[80,114,165], however there are also studies of both high thoracic SCI and cardiac denervation which have found evidence to the contrary[73,113]. Those that did report an increase in myocardial fibrosis attributed the development to a combination of chronically elevated RAAS activity and the frequent bouts of extreme pressure caused by spontaneous AD. While both elevated RAAS and AD have been shown to occur in similar preclinical models of SCI[72,148], neither were directly measured in the same studies which reported cardiac fibrosis, so the direct relationship remains unclear. This lack of consensus in the literature is also due in part to the variety of analytical methods applied to quantify collagen deposition in the myocardium. These previous works used either semi-quantitative[80] or software-based[73,111,114] assessments, the latter of which were not conducted using the same programs or threshold cut-offs during analysis (sometimes not even reporting the program used). In the present study, we therefore elected used the software Aperio ImageScope version 12.3.3.5048 (Aperio Technologies Inc., Vista, CA), which has highly intuitive and manipulatable algorithms that have recently been used to detect changes in cardiac fibrosis in multiple independent studies[141,175]. In applying algorithms and thresholds that are known to be valid in detecting changes in interfibrillar collagen, and reporting them in detail in our methods, we hope to contribute to future endeavours to clarify the relationship between SCI and collagen deposition.

Chapter 5 – Conclusion

In this thesis I provide a comprehensive review of our present understanding of the influence SCI on LV function, as well as the prevalence and implications of OH following SCI. While the literature clearly indicates that high thoracic and cervical SCI are detrimental to LV structure and function, little-to-no work has investigated the physiological impact of the frequent bouts of OH on the heart. Our lab, therefore, designed a preclinical model of OH simulation in rats with high thoracic SCI, and conducted a 9-week preclinical investigation using novel admittance PV technology and echocardiography to assess how daily simulated OH and/or high thoracic SCI impact LV function. These *in vivo* measures were then followed-up with standardized histological assays to assess complimentary structural changes.

5.1. Main Findings

This study resulted in two main findings: 1) The daily simulation of OH following T3 transection caused an uncoupling of ventricular-arterial function by further amplifying the LV contractile dysfunction caused by SCI and increasing the arterial afterload compared to uninjured controls. 2) SCI induced cardiomyocyte atrophy and increased length:width ratio, while daily simulated OH caused significant interfibrillar collagen deposition in SCI animals compared to SHAM animals.

5.2: Implications and future direction

These findings shed new light onto the effect of SCI on cardiovascular health and function, providing the first implication that the frequent occurrence of OH following high level SCI may further exacerbate the cardiac dysfunction caused by SCI alone. While previous works had loosely correlated OH with coronary artery disease, hypertension and stroke[120,176] and demonstrated a direct tie between the occurrence of OH and accelerated cerebrovascular disease and cognitive dysfunction[119,123], this is the first

study to provide direct evidence that the repetitive hemodynamic stress of OH can impair cardiac function itself.

We suggest, therefore, that more direct investigations into the connection between OH and cardiac dysfunction are needed in both preclinical and clinical models of SCI to explore whether this deleterious effect of OH is also present in humans, and if so, how it can be treated moving forward. The previous preclinical demonstration from our lab that passive lower-limb exercise can prevent the uncoupling of the ventricular-arterial interaction when began soon after injury does provide a likely treatment candidate. However, whether this translates to a larger animal or clinical model has yet to be explored, as well as whether passive lower-limb exercise can be used to reverse chronically uncoupled cardiovascular systems when initiated during the chronic phase of recovery. We also suggest that future preclinical investigations explore how different injury models and severities affect the relationship between OH and cardiac dysfunction, to identify whether the occurrence of OH alone following SCI is enough to assume associated dysfunction, or whether those with less complete injuries retain the capacity to adapt to OH. Lastly, we recommend that future investigations of OH and SCI assess RAAS activity in order to provide more concrete evidence for the changes observed in the present study.

5.3 Study strengths and limitations

In the present study we provide a direct*, in vivo* assessment of LV function using gold-standard PV catheterization techniques, complimented by non-invasive echocardiography and *ex vivo* tissue analysis. Additionally, this is the first study of its kind to use an admittance catheter as opposed to an older conductance catheter, as the admittance technology allows for real-time assessment of volumetric function and provides more accurate measurements of LV dimensions at the extremes of the cardiac cycle (end systole and diastole). Furthermore, our model of OH simulation allowed us to induce highly controlled, consistent and repeatable bouts of OH on a daily basis in animals with high thoracic SCI.

While this study provided very clear data on cardiac function, the use of a preclinical rodent model of complete T3 transection does limit the direct translation of these findings into a clinical setting. It is our hope, however, that these findings can be used to inform future clinical investigations that will provide a "bedside" perspective on the present research questions and assist in developing a complete understanding of the interaction between SCI, OH and cardiac function. We also recognize that our assessment of VAC in the present study was based upon PV analysis alone, which allows us to examine how both Ees and Ea are changing to influence the VAC ratio but does not provide insight into the mechanism by which Ees and Ea are changes. We therefore recommend that future works in this field assess factors such as aortic stiffness and pulsatility, as well as myocardial strain and deformation, to identify how they contribute to the progression of altered ventricular-arterial uncoupling and better inform the development of future treatments.

Bibliography

1. Tortora, G. J. & Derrickson, B. *Principles of anatomy and physiology*. (John Wiley & Sons, 2010).
2. Burkhoff, D. Mechanical Properties of the Heart and its Interaction with the Vascular System. *Card. Physiol.* 1–28 (2011).
3. Iaizzo, P. A. *Handbook of Cardiac Anatomy , Physiology , . Journal of Cardiac Surgery* **21,** (2006).
4. Ovalle, W. K., Nahirney, P. C. & Netter, F. H. (Frank H. *Netter's essential histology*. (Saunders/Elsevier, 2008).
5. Gupta, P., Ibrahim, A. & Butany, J. in *Cellular and Molecular Pathobiology of Cardiovascular Disease* 297–314 (2014).
6. Johnson, L. R. *et al.* in *Essential Medical Physiology* **i,** 155–258 (Elsevier Academic Press, 2009).
7. Conti, C. R. (Charles R. *The Netter Collection of medical illustrations. Volume 8, Cardiovascular system*. (Saunders, 2014).
8. Gartner, L. P. & Hiatt, J. L. *Color textbook of histology*. (Saunders/Elsevier, 2007).
9. Lockhart, M., Wirrig, E., Phelps, A. & Wessels, A. Extracellular matrix and heart development. *Birth Defects Res. A. Clin. Mol. Teratol.* **91,** 535–50 (2011).
10. Willis, M. S., Homeister, J. W. & Stone, J. R. *Cellular and Molecular Pathobiology of Cardiovascular Disease*. *Elsevier* 1-22 (2014)
11. Robb, J. S. R. R. C. The Normal Heart. *Am. Heart J.* 455–467 (1941).
12. Sengupta, P. P. *et al.* Left Ventricular Structure and Function. Basic Science for Cardiac Imaging. *J. Am. Coll. Cardiol.* **48,** 1988–2001 (2006).
13. Stöhr, E. J., Shave, R. E., Baggish, A. L. & Weiner, R. B. Left ventricular twist mechanics in the context of normal physiology and cardiovascular disease: a review of studies using speckle tracking echocardiography. *Am. J. Physiol. - Hear. Circ. Physiol.* **311,** H633–H644 (2016).
14. Rohmer, D., Sitek, A. & Gullberg, G. T. Reconstruction and Visualization of Fiber and Laminar Structure in the Normal Human Heart from Ex Vivo DTMRI Data. *Invest. Radiol.* **42,** 777–789 (2007).
15. Asp, M. L., Martindale, J. J., Heinis, F. I., Wang, W. & Metzger, J. M. Calcium mishandling in diastolic dysfunction: Mechanisms and potential therapies. *Biochim. Biophys. Acta - Mol. Cell Res.* **1833,** 895–900 (2013).
16. Thum, T. Noncoding RNAs and myocardial fibrosis. *Nat. Publ. Gr.* **11,** (2014).
17. Daniels, A., Van Bilsen, M., Goldschmeding, R., Van Der Vusse, G. J. & Van Nieuwenhoven, F. A. Connective tissue growth factor and cardiac fibrosis. *Acta Physiol.* **195,** 321–338 (2009).
18. Jänig, W. *Anatomy of central autonomic systems*. *The integrative action of the autonomic nervous system: neurobiology of homeostasis* (2006).
19. Weidner, N., Rudiger, R. & Tansey, K. E. *Neurological Aspects of Spinal Cord Injury*. (Springer

International Publishing, 2017).

20. Jänig, W. Functional anatomy of the peripheral sympathetic and parasympathetic system. *Integr. Action Auton. Nerv. Syst.* 13–34 (2006).

21. Raven, P. B. Neural control of the circulation: exercise. *Exp. Physiol.* **97,** 10–13 (2012).

22. Battipaglia, I., Lanza, G. A., Battipaglia, I. & Lanza, G. A. The Autonomic Nervous System of the Heart. *Auton. Inn. Hear.* (2015).

23. Schwartz, P. J. *Cardiac sympathetic denervation to prevent life-threatening arrhythmias*. *Nature Reviews Cardiology* **11,** 346–353 (2014).

24. McArdle, W., Katch, F. & Katch, V. *Exercise physiology: nutrition, energy, and human performance*. (2010).

25. Stansfield, W. E. *et al.* in *Cellular and Molecular Pathobiology of Cardiovascular Disease* 51–78 (Elsevier, 2014).

26. Gilbey, M. P. *Entrainment of Sympathetic Rhythms*. *Primer on the Autonomic Nervous System* (2012).

27. White, D. W. & Raven, P. B. Autonomic neural control of heart rate during dynamic exercise: revisited. *J. Physiol.* **592,** 2491–2500 (2014).

28. Lundvall, J. & Järhult, J. Beta Adrenergic Dilator Component of the Sympathetic Vascular Response in Skeletal Muscle Influence on the micro-circulation and on transcapillary exchange. *Acta Physiol. Scand.* **96,** 180–192 (1976).

29. Braunwald, B. E. & Ross, J. Applicability of Starling ' s Law of the Heart to Man. 169–178 (1964).

30. Phillips, A. A., Krassioukov, A. V., Ainslie, P. N. & Warburton, D. E. R. Baroreflex Function after Spinal Cord Injury. *J. Neurotrauma* **29,** 2431–2445 (2012).

31. Lanfranchi, P. A. & Somers, V. K. Arterial baroreflex function and cardiovascular variability: interactions and implications. *Am. J. Physiol.* **283,** 815–826 (2002).

32. Briet, M. & Schiffrin, E. L. Vascular actions of aldosterone. *J. Vasc. Res.* **50,** 89–99 (2013).

33. White, P. C. Aldosterone: Direct effects on and production by the heart. *J. Clin. Endocrinol. Metab.* **88,** 2376–2383 (2003).

34. McCurley, A. & Jaffe, I. Z. Mineralocorticoid receptors in vascular function and disease. *Mol. Cell. Endocrinol.* **350,** 256–265 (2012).

35. Pandey, A. *et al.* Effect of mineralocorticoid receptor antagonists on cardiac structure and function in patients with diastolic impairment and preserved ejection fraction: A meta-analysis. *J. Card. Fail.* **20,** S41–S42 (2014).

36. Vanhoutte, P. M., Shimokawa, H., Feletou, M. & Tang, E. H. C. Endothelial dysfunction and vascular disease – a 30th anniversary update. *Acta Physiol.* **219,** 22–96 (2017).

37. Anderson, R. J., Berl, T., McDonald, K. M. & Schrier, R. W. Prostaglandins : Effects on blood pressure , renal blood flow , sodium and water excretion. *Kidney Int.* **10,** 205–215 (1976).

38. Norel, X., Walch, L., Gascard, J. P., De Montpreville, V. & Brink, C. Prostacyclin release and receptor activation: Differential control of human pulmonary venous and arterial tone. *Br. J. Pharmacol.* **142,** 788–796 (2004).

39. Busse, R. *et al.* EDHF : bringing the concepts together. *Trends Pharmacol. Sci.* **23,** 374–380 (2002).

40. Garland, C. J., Hiley, C. R. & Dora, K. A. EDHF : spreading the influence of the endothelium. (2011). doi:10.1111/j.1476-5381.2010.01148.x

41. Marasciulo, F. L., Montagnani, M. & Potenza, M. A. Endothelin-1: the yin and yang on vascular function. *Curr. Med. Chem.* **13,** 1655–65 (2006).

42. Vane, B. J. R., Sc, D. & D, J. C. M. M. Possible Contributions of Endogenous Prostaglandins to the Control of Blood Pressure. *Suppl. to Circ. Res.* **36,** 68–75 (1975).

43. Frank, O. On the Dynamics OF Cardiac Muscle. *Am. Heart J.* **58,** 282–316 (1969).

44. Starling, E. The Linacre Lecture on the Law of the Heart. (1915).

45. Suga, H. Time Course of Left Ventricular Pressure-Volume Relationship under Various End Diastolic Volumes. *Jpn Hear. J.* **10,** 509–515 (1969).

46. Suga, H. Ventricular Energetics. **70,** (1990).

47. Pacher, P., Nagayama, T., Mukhopadhyay, P., Bátkai, S. & Kass, D. A. Measurement of cardiac function using pressure–volume conductance catheter technique in mice and rats. *Nat. Protoc.* **3,** 1422–1434 (2008).

48. Carrick-Ranson, G., Hastings, J. L., Bhella, P. S., Shibata, S. & Levine, B. D. The effect of exercise training on left ventricular relaxation and diastolic suction at rest and during orthostatic stress after bed rest. *Exp. Physiol.* **98,** 501–513 (2013).

49. Fu, Q. *et al.* Hemodynamics of orthostatic intolerance : implications for gender differences Hemodynamics of orthostatic intolerance : implications for gender differences. *Am. J. Physiol. - Hear. Circ. Physiol.* **75231,** 449–457 (2003).

50. Fujimoto, N. *et al.* Effect of ageing on left ventricular compliance and distensibility in healthy sedentary humans. *J. Physiol.* **590,** 1871–80 (2012).

51. Kass, D. A. Age-related changes in venticular-arterial coupling: Pathophysiologic implications. *Heart Fail. Rev.* **7,** 51–62 (2002).

52. Starling, M. R. Left ventricular-arterial coupling relations in the normal human heart. *Am. Heart J.* **125,** 1659–1666 (1993).

53. Borlaug, B. A. & Kass, D. A. Ventricular-Vascular Interaction in Heart Failure. *Cardiol. Clin.* **29,** 447–459 (2011).

54. Ikonomidis, I. *et al.* The role of ventricular–arterial coupling in cardiac disease and heart failure: assessment, clinical implications and therapeutic interventions. A consensus document of the European Society of Cardiology Working Group on Aorta & Peripheral Vascular Diseas. *Eur. J. Heart Fail.* 402–424 (2019).

55. Chirinos, J. A. & Sweitzer, N. Ventricular-Arterial Coupling in Chronic Heart Failure. *Pathophysiology* **3,** 86–96 (2017).

56. Blomqvist, C. G. & Stone, H. L. Cardiovascular Adjustments to Gravitational Stress. *Handb. Physiol. Cardiovasc. Syst.* **3,** 50–87 (1991).

57. Phillips, A. A. & Krassioukov, A. V. Contemporary Cardiovascular Concerns after Spinal Cord Injury: Mechanisms, Maladaptations & Management. *J. Neurotrauma* **16,** 150512042022004 (2015).

58. Krassioukov, A. V. & Claydon, V. E. The clinical problems in cardiovascular control following spinal cord injury: an overview. *Prog. Brain Res.* **152,** 223–9 (2006).

59. Noonan, V. K. *et al.* Incidence and Prevalence of Spinal Cord Injury in Canada: A National Perspective. *Neuroepidemiology* **38,** 219–226 (2012).

60. Lee, B. B., Cripps, R. A., Fitzharris, M. & Wing, P. C. The global map for traumatic spinal cord injury epidemiology: update 2011, global incidence rate. *Spinal Cord* **52,** 110–6 (2014).

61. Teasell, R. W., Arnold, J. M., Krassioukov, A. V. & Delaney, G. A. Cardiovascular consequences of loss of supraspinal control of the sympathetic nervous system after spinal cord injury. *Arch. Phys. Med. Rehabil.* **81,** 506–16 (2000).

62. Anderson, K. D. Targeting Recovery: Priorities of the Spinal Cord-Injured Population. *J. Neurotrauma* **21,** 1371–1383 (2004).

63. West, C. R., Mills, P. & Krassioukov, A. V. Influence of the neurological level of spinal cord injury on cardiovascular outcomes in humans: a meta-analysis. *Spinal Cord* **50,** 484–492 (2012).

64. Krassioukov, A. V. Autonomic function following cervical spinal cord injury. *Respir. Physiol. Neurobiol.* **169,** 157–164 (2009).

65. Garshick, E. *et al.* A prospective assessment of mortality in chronic spinal cord injury. *Spinal Cord* **43,** 408–16 (2005).

66. Kessler, K. M. *et al.* Cardiovascular findings in quadriplegic and paraplegic patients and in normal subjects. *Am. J. Cardiol.* **58,** 525–30 (1986).

67. Phillips, W. T. *et al.* Effect of spinal cord injury on the heart and cardiovascular fitness. *Curr. Probl. Cardiol.* **23,** 641–716 (1998).

68. Boot, C. R. L., Groothuis, J. T., van Langen, H. & Hopman, M. T. E. Shear stress levels in paralyzed legs of spinal cord-injured individuals with and without nerve degeneration. *J. Appl. Physiol.* **92,** (2002).

69. Faber, M. J. *et al.* Right and left ventricular function after chronic pulmonary artery banding in rats assessed with biventricular pressure-volume loops. *Am J Physiol Hear. Circ Physiol* **291,** 1580–1586 (2006).

70. Kooner, J. S., Frankel, H. L., Mirando, N., Peart, W. S. & Mathias, C. J. Haemodynamic, hormonal and urinary responses to postural change in tetraplegic and paraplegic man. *Paraplegia* **26,** 233–7 (1988).

71. Lujan, H. L. & DiCarlo, S. E. Increasing venous return as a strategy to prevent or reverse cardiac dysfunction following spinal cord injury. *J. Physiol.* **592,** 1727–1728 (2014).

72. Poormasjedi-Meibod, M.-S. *et al.* Experimental Spinal Cord Injury Causes Left-Ventricular Atrophy

and Is Associated with an Upregulation of Proteolytic Pathways. *J. Neurotrauma* **36,** 950–961 (2018).

73. Squair, J. W., Liu, J., Tetzlaff, W., Krassioukov, A. V. & West, C. R. Spinal cord injury-induced cardiomyocyte atrophy and impaired cardiac function are severity dependent. *Exp. Physiol.* **103,** 179–189 (2018).

74. Squair, J. W. *et al.* High Thoracic Contusion Model for the Investigation of Cardiovascular Function after Spinal Cord Injury. *Am Journal of Physiology & Heart, **34**, 671-684 (2017)*.

75. West, C. R., Alyahya, A., Laher, I. & Krassioukov, A. V. Peripheral vascular function in spinal cord injury: a systematic review. *Spinal Cord* **51,** 10–9 (2013).

76. Lee, A. H. X., Phillips, A. A. & Krassioukov, A. V. Increased Central Arterial Stiffness after Spinal Cord Injury: Contributing Factors, Implications, and Possible Interventions. *J. Neurotrauma* **34,** 1129–1140 (2016).

77. Phillips, A. A., Cote, A. T., Bredin, S. S. D., Krassioukov, A. V. & Warburton, D. E. R. Aortic stiffness increased in spinal cord injury when matched for physical activity. *Med. Sci. Sports Exerc.* **44,** 2065–2070 (2012).

78. Cile, C., Boot, R. L., Groothuis, J. T., Langen, H. Van & Hopman, M. T. E. Shear stress levels in paralyzed legs of spinal cord- injured individuals with and without nerve degeneration. *Journal of Applied Physiology,* **92,** 2334-2340 (2002)

79. Eysmann, S. B., Douglas, P. S., Katz, S. E., Sarkarati, M. & Wei, J. Y. Left ventricular mass and diastolic filling patterns in quadriplegia and implications for effects of normal aging on the heart. *Am. J. Cardiol.* **75,** 201–3 (1995).

80. West, C. R. *et al.* Passive hind-limb cycling improves cardiac function and reduces cardiovascular disease risk in experimental spinal cord injury. *J. Physiol.* **592,** 1771–83 (2014).

81. Squair, J. W. *et al.* Spinal Cord Injury Causes Systolic Dysfunction and Cardiomyocyte Atrophy. *J. Neurotrauma* neu.2017.4984 (2017).

82. DeVeau, K. M. *et al.* A comparison of passive hindlimb cycling and active upper-limb exercise provides new insights into systolic dysfunction after spinal cord injury. *Am. J. Physiol. Circ. Physiol.* **313,** H861–H870 (2017).

83. De Groot, P. C. E., Bleeker, M. W. P. & Hopman, M. T. E. Magnitude and time course of arterial vascular adaptations to inactivity in humans. *Exerc. Sport Sci. Rev.* **34,** 65–71 (2006).

84. West, C. R., Campbell, I. G., Shave, R. E. & Romer, L. M. Resting cardiopulmonary function in paralympic athletes with cervical spinal cord injury. *Med. Sci. Sports Exerc.* **44,** 323–329 (2012).

85. West, C. R. *et al.* Cardiac consequences of autonomic dysreflexia in spinal cord injury. *Hypertension* **68,** 1281–1289 (2016).

86. Groah, S. L., Weitzenkamp, D., Sett, P., Soni, B. & Savic, G. The relationship between neurological level of injury and symptomatic cardiovascular disease risk in the aging spinal injured. *Spinal Cord* **39,** 310–317 (2001).

87. Williams, A. M., Gee, C. M., Voss, C. & West, C. R. Cardiac consequences of spinal cord injury: Systematic review and meta-analysis. *Heart* **105,** 217–225 (2019).

88. Suga, H. Total mechanical energy of a ventricle model and cardiac oxygen consumption. *Heart Energetics* H498-H505 (1979).

89. Ky, B. *et al.* Ventricular-arterial coupling, remodeling, and prognosis in chronic heart failure. *J. Am. Coll. Cardiol.* **62,** 1165–1172 (2013).

90. Chirinos, J. A. Ventricular-arterial coupling: Invasive and non-invasive assessment. *Artery Res.* **7,** 2–14 (2013).

91. Kawaguchi, M., Hay, I., Fetics, B. & Kass, D. A. Combined ventricular systolic and arterial stiffening in patients with heart failure and preserved ejection fraction: Implications for systolic and diastolic reserve limitations. *Circulation* **107,** 714–720 (2003).

92. Eysmann, S. B., Douglas, P. S., Katz, S. E., Sarkarati, M. & Wei, J. Y. Left ventricular mass and diastolic filling patterns in quadriplegia and implications for effects of normal aging on the heart. *Am. J. Cardiol.* **75,** 201–203 (1995).

93. Schreiber, R. *et al.* Matrix metalloproteinases and left ventricular function and structure in spinal cord injured subjects. *Clin. Chim. Acta* **437,** 136–140 (2014).

94. Matos-Souza, J. R. *et al.* Altered left ventricular diastolic function in subjects with spinal cord injury. *Spinal Cord* **49,** 65–69 (2011).

95. Lester, S. J. *et al.* Unlocking the Mysteries of Diastolic Function. Deciphering the Rosetta Stone 10 Years Later. *J. Am. Coll. Cardiol.* **51,** 679–689 (2008).

96. Goswami, N., Loeppky, J. A. & Hinghofer-Szalkay, H. LBNP: Past protocols and technical considerations for experimental design. *Aviat. Sp. Environ. Med.* **79,** 459–471 (2008).

97. Arbab-Zadeh, A. *et al.* Effect of aging and physical activity on left ventricular compliance. *Circulation* **110,** 1799–1805 (2004).

98. Carrick-Ranson, G. *et al.* Effect of healthy aging on left ventricular relaxation and diastolic suction. *AJP Hear. Circ. Physiol.* **303,** H315–H322 (2012).

99. Hitzig, S. L., Eng, J. J., Miller, W. C. & Sakakibara, B. M. An evidence-based review of aging of the body systems following spinal cord injury. *Spinal Cord* **49,** 684–701 (2011).

100. Hansson, J. *et al.* Biomarkers of Extracellular Matrix Metabolism (MMP-9 and TIMP-1) and Risk of Stroke, Myocardial Infarction, and Cause-Specific Mortality: Cohort Study. *Plos One* **6** (2011)

101. Rienks, M., Papageorgiou, A. P., Frangogiannis, N. G. & Heymans, S. Myocardial extracellular matrix: An ever-changing and diverse entity. *Circ. Res.* **114,** 872–888 (2014).

102. Hill, J. A. & Olson, E. N. Mechanisms of Disease Cardiac Plasticity. *J.A.H., E.N.O* **13,** (2008).

103. Perhonen, M. A. *et al.* Cardiac atrophy after bed rest and spaceflight. *J. Appl. Physiol.* **91,** 645–653 (2001).

104. De Groot, P. C., Van Dijk, A., Dijk, E. & Hopman, M. T. Preserved Cardiac Function After Chronic Spinal Cord Injury. *Arch. Phys. Med. Rehabil.* **87,** 1195–2000 (2006).

105. Summers, R., Coleman, T., Steven, P. & Martin, D. Systems analysis of the mechanisms of cardiac diastolic function changes after microgravity exposure. *Acta Astronaut.* **63,** 722–726 (2008).

106. Atrophy, C., Bed, A. & Deconditioning, R. Cardiac Atrophy After Bed - Rest Deconditioning. **0,** 1–26 (2017).

107. Martin, D. S., South, D. A., Wood, M. L., Bungo, M. W. & Meck, J. V. Comparison of echocardiographic changes after short- and long-duration spaceflight. *Aviat. Space. Environ. Med.* **73,** 532–6 (2002).

108. Gatica, D., Chiong, M., Lavandero, S. & Klionsky, D. J. Molecular mechanisms of autophagy in the cardiovascular system. *Circ. Res.* **116,** 456–467 (2015).

109. Gupta, S. K., Bang, C. & Thum, T. Circulating MicroRNAs as biomarkers and potential paracrine mediators of cardiovascular disease. *Circ. Cardiovasc. Genet.* **3,** 484–488 (2010).

110. Harvey, P. A. & Leinwand, L. A. in *Cellular and Molecular Pathobiology of Cardiovascular Disease* 37–50 (2014).

111. Lujan, H. L., Janbaih, H. & DiCarlo, S. E. Structural remodeling of the heart and its premotor cardioinhibitory vagal neurons following T 5 spinal cord transection . *J. Appl. Physiol.* **116,** 1148–1155 (2014).

112. DeVeau, K. M. *et al.* Challenging cardiac function post-spinal cord injury with dobutamine. *Auton. Neurosci. Basic Clin.* **209,** 19–24 (2018).

113. Zaglia, T. *et al.* Cardiac sympathetic neurons provide trophic signal to the heart via β2-adrenoceptor-dependent regulation of proteolysis. *Cardiovasc. Res.* **97,** 240–250 (2013).

114. DeVeau, K. M. *et al.* Challenging cardiac function post-spinal cord injury with dobutamine. *Auton. Neurosci.* (2016).

115. smund Røe, Å. T. *et al.* Increased passive stiffness promotes diastolic dysfunction despite improved Ca 21 handling during left ventricular concentric hypertrophy. *Cardiovascular Research* **113** (2017)

116. Gattoni, S. *et al.* Compensatory and decompensatory alterations in cardiomyocyte Ca2+dynamics in hearts with diastolic dysfunction following aortic banding. *J. Physiol.* **595,** 3867–3889 (2017).

117. Claydon, V. E. & Krassioukov, A. V. Orthostatic Hypotension and Autonomic Pathways after Spinal Cord Injury. *J. Neurotrauma* **23,** (2006).

118. Hubli, M., Gee, C. M. & Krassioukov, A. V. Refined assessment of blood pressure instability after spinal cord injury. *Am. J. Hypertens.* **28,** 173–181 (2015).

119. Phillips, A. A., Krassioukov, A. V., Ainslie, P. N. & Warburton, D. E. R. Perturbed and spontaneous regional cerebral blood flow responses to changes in blood pressure after high-level spinal cord injury: the effect of midodrine. *J. Appl. Physiol.* **116,** 645–653 (2014).

120. Eigenbrodt, M. L. *et al.* Orthostatic Hypotension as a Risk Factor for Stroke : The Atherosclerosis Risk in Communities (ARIC) Study, 1987-1996. *Stroke* **31,** 2307–2313 (2000).

121. Rose, K. M. *et al.* Orthostatic hypotension and the incidence of coronary heart disease: The Atherosclerosis Risk in Communities study. *Am. J. Hypertens.* **13,** 571–578 (2000).

122. Rose, K. M. *et al.* Orthostatic hypotension predicts mortality in middle-aged adults: The Atherosclerosis Risk in Communities (ARIC) Study. *Circulation* **114,** 630–636 (2006).

123. Phillips, A. A., Ainslie, P. N., Krassioukov, A. V. & Warburton, D. E. R. Regulation of Cerebral Blood Flow after Spinal Cord Injury. *J. Neurotrauma* **30,** 1551–1563 (2013).

124. Johnson, R. H. & Park, D. M. Effect of change of posture on blood pressure and plasma renin concentration in men with spinal transections. *Clin. Sci.* **44,** 539–46 (1973).

125. Mathias, C. J. *et al.* Plasma catecholamines, plasma renin activity and plasma aldosterone in tetraplegic man, horizontal and tilted. *Clin. Sci. Mol. Med.* **49,** 291–9 (1975).

126. Mathias, C. J., Christensen, N. J., Frankel, H. L. & Peart, W. S. Renin release during head-up tilt occurs independently of sympathetic nervous activity in tetraplegic man. *Clin. Sci. (Lond).* **59,** 251–6 (1980).

127. Cragg, J. J., Noonan, V. K., Krassioukov, A. V. & Borisoff, J. Cardiovascular disease and spinal cord injury: Results from a national population health survey. *Neurology* **81,** 723–728 (2013).

128. Squair, J. W. *et al.* High Thoracic Contusion Model for the Investigation of Cardiovascular Function after Spinal Cord Injury. *J. Neurotrauma* **34,** 671–684 (2017).

129. Krassioukov, A. V & Weaver, L. C. MORPHOLOGICAL CHANGES IN SYMPATHETIC PREGANGLIONIC NEURONS AFTER SPINAL CORD INJURY IN RATS. *Neuroscience* **70,** (1996).

130. Lujan, H. L. & DiCarlo, S. E. T5 spinal cord transection increases susceptibility to reperfusion-induced ventricular tachycardia by enhancing sympathetic activity in conscious rats. *Am. J. Physiol. Heart Circ. Physiol.* **293,** H3333-9 (2007).

131. Ramsey, J. B. G. *et al.* Care of rats with complete high-thoracic spinal cord injury. *J. Neurotrauma* **27,** 1709–22 (2010).

132. Inskip, J., Ramer, L., Ramer, M. & Krassioukov, A. V. Autonomic assessment of animals with spinal cord injury: tools, techniques and translation. *Spinal Cord* **47,** (2009).

133. Wecht, J. M. & Bauman, W. A. Implication of altered autonomic control for orthostatic tolerance in SCI. *Auton. Neurosci. Basic Clin.* **209,** 51–58 (2018).

134. Usselman, C. W., Mattar, L., Twynstra, J., Welch, I. & Shoemaker, J. K. Rodent cardiovascular responses to baroreceptor unloading: Effect of plane of anaesthesia. *Appl. Physiol. Nutr. Metab.* **36,** 376–381 (2011).

135. Altura, B. M. & Weinberg, J. Urethane and contraction of vascular smooth muscle. *Br. J. Pharmacol.* **67,** 255–63 (1979).

136. Her, A. Y. *et al.* Value of Ventricular Stiffness Index and Ventriculoarterial Interaction in Patients With Nonischemic Dilated Cardiomyopathy. *Circ. J.* **73,** 1683–1690 (2009).

137. Chatterjee, K. The Swan-Ganz catheters: Past, present, and future: A viewpoint. *Circulation* **119,** 147–152 (2009).

138. Sunagawa, K., Sagawa, K. & Maughan, W. L. in *Ventricular/Vascular Coupling: Clinical, Physiological, and Engineering Aspects* (ed. Yin, F. C. P.) 210–239 (Springer New York, 1987).

139. Bauer, F. *et al.* Left ventricular outflow tract mean systolic acceleration as a surrogate for the slope of the left ventricular end-systolic pressure-volume relationship. *J. Am. Coll. Cardiol.* **40,** 1320–1327 (2002).

140. Burkhoff, D. Pressure-Volume Loops in Clinical Research* A Contemporary View. *J. Am. Coll. Cardiol.* **62,** 1173–1176 (2013).

141. Mota, R. *et al.* Increasing Cardiomyocyte Atrogin-1 Reduces Aging-Associated Fibrosis and Regulates Remodeling in Vivo. *Am. J. Pathol.* **188,** 1676–1692 (2018).

142. Claydon, V. E., Steeves, J. D. & Krassioukov, A. V. Orthostatic hypotension following spinal cord injury: Understanding clinical pathophysiology. *Spinal Cord* **44,** 341–351 (2006).

143. Phillips, W. T. *et al.* Effect of spinal cord injury on the heart and cardiovascular fitness. *Curr. Probl. Cardiol.* **23,** 641–716 (1998).

144. Levine, B. D., Zuckerman, J. H. & Pawelczyk, J. A. Cardiac atrophy after bed-rest deconditioning: a nonneural mechanism for orthostatic intolerance. *Circulation* **96,** 517–25 (1997).

145. Hellerstein, H. K. & Santiago-Stevenson, D. Atrophy of the Heart: A Correlative Study of Eighty-Five Proved Cases. *Circulation* **93–126,** 93–126 (1950).

146. Taylor, J. A., Picard, G. & Widrick, J. J. Aerobic Capacity With Hybrid FES Rowing in Spinal Cord Injury: Comparison With Arms-Only Exercise and Preliminary Findings With Regular Training. *PMRJ* **3,** 817–824 (2011).

147. Cash, M. S. *et al.* Evaluation of a Training Program for Persons With SCI Paraplegia Using the Parastep®l Ambulation System: Part 5. Lower Extremity Blood Flow and Hyperemic Responses to Occlusion Are Augmented by Ambulation Training.*Arch Phys Med Rabilitation* **78** (1987*)*

148. West, C. R., Popok, D., Crawford, M. A. & Krassioukov, A. V. Characterizing the Temporal Development of Cardiovascular Dysfunction in Response to Spinal Cord Injury. (2015).

149. Argulian, E., Agarwal, V., Makani, H., Herzog, E. & Chaudhry, F. A. Association of exercise tolerance with effective arterial elastance obtained noninvasively in patients with exertional dyspnea. *J. Am. Soc. Echocardiogr.* **27,** 675–679 (2014).

150. Grossman, W., Jones, D. & McLaurin, L. P. Wall stress and patterns of hypertrophy in the human left ventricle. *J. Clin. Invest.* **56,** 56–64 (1975).

151. Zhong, L., Ghista, D. N. & Tan, R. S. Left ventricular wall stress compendium. *Comput. Methods Biomech. Biomed. Engin.* **15,** 1015–1041 (2012).

152. Mathias, C. J., Matthews, W. B. & Spalding, J. M. K. Postural changes in plasma renin activity and responses to vasoactive drugs in a case of Shy Drager syndrome. *J. Neurol. Neurosurg. Psychiatry* **40,** 138–143 (1977).

153. Johnson, R. H., Park, D. M. & Frankel, H. L. Orthostatic hypotension and the renin-angiotensin system in paraplegia. *Paraplegia* **9,** 146–152 (1971).

154. Li, X. *et al.* Impact of mineralocorticoid receptor antagonists on changes in cardiac structure and function of left ventricular dysfunction a meta-analysis of randomized controlled trials. *Circ. Hear. Fail.* **6,** 156–165 (2013).

155. Schmid, A. *et al.* Free plasma catecholamines in spinal cord injured persons with different injury levels at rest and during exercise. *J. Auton. Nerv. Syst.* **68,** 96–100 (1998).

156. Ondrusova, K. *et al.* Impaired Baroreflex Function during Orthostatic Challenge in Patients after

Spinal Cord Injury. *J. Neurotrauma* **34,** 3381–3387 (2017).

157. Canty, J. M. & Suzuki, G. Myocardial perfusion and contraction in acute ischemia and chronic ischemic heart disease. *J. Mol. Cell. Cardiol.* **52,** 822–831 (2012).

158. Canty, J. M. J. & Fallavollita, J. A. Hibernating myocardium. *J. or Nucl. Cardiol.* **12,** 104–119 (2005).

159. Kim, S.-J. *et al.* Persistent Stunning Induces Myocardial Hibernation and Protection. *Circ. Res.* **92,** 1233–1239 (2003).

160. Aziz. Diastolic Heart Failure: A Concise Review. *J. Clin. Med. Res.* **5,** 327–334 (2013).

161. Zile, M. R., Baicu, C. F. & Gaasch, W. H. Diastolic Heart Failure — Abnormalities in Active Relaxation and Passive Stiffness of the Left Ventricle. *n engl j med* **35019350,** 1953–9 (2004).

162. Zile, M. R. & Brutsaert, D. L. New concepts in diastolic dysfunction and diastolic heart failure: Part II: causal mechanisms and treatment. *Circulation* **105,** 1503–8 (2002).

163. Stansfield, W. E. *et al.* in *Cellular and Molecular Pathobiology of Cardiovascular Disease* 51–78 (2014).

164. Sharif, H., Wainman, L., O'Leary, D. & Ditor, D. The effect of blood volume and volume loading on left ventricular diastolic function in individuals with spinal cord injury. *Spinal Cord* **55,** 753–758 (2017).

165. Lujan, H. L., Palani, G. & DiCarlo, S. E. Structural neuroplasticity following T5 spinal cord transection: increased cardiac sympathetic innervation density and SPN arborization. *Am. J. Physiol. Regul. Integr. Comp. Physiol.* **299,** R985-95 (2010).

166. Bigford, G. E., Bracchi-Ricard, V. C., Keane, R. W., Nash, M. S. & Bethea, J. R. Neuroendocrine and Cardiac Metabolic Dysfunction and NLRP3 Inflammasome Activation in Adipose Tissue and Pancreas following Chronic Spinal Cord Injury in the Mouse. *ASN Neuro* **5,** AN20130021 (2013).

167. Gerdes, A. M. & Capasso, J. M. Structural remodeling and mechanical dysfunction of cardiac myocytes in heart failure. *J. Mol. Cell. Cardiol.* **27,** 849–856 (1995).

168. Porrello, E. R. *et al.* Angiotensin II type 2 receptor antagonizes angiotensin ii type 1 receptor-mediated cardiomyocyte autophagy. *Hypertension* **53,** 1032–1040 (2009).

169. Thompson, E. W., Marino, T. A., Uboh, C. E., Kent, R. L. & Cooper IV, G. Atrophy reversal and cardiocyte redifferentiation in reloaded cat myocardium. *Circ. Res.* **54,** 367–377 (1984).

170. Kuo, P. L. *et al.* Myocyte shape regulates lateral registry of sarcomeres and contractility. *Am. J. Pathol.* **181,** 2030–2037 (2012).

171. Lisy, O. *et al.* Mechanical unloading versus neurohumoral stimulation on myocardial structure and endocrine function in vivo. *Circulation* **102,** 338–343 (2000).

172. Zierhut, W., Zimmer, H. G. & Gerdes, A. M. Effect of angiotensin converting enzyme inhibition on pressure-induced left ventricular hypertrophy in rats. *Circ. Res.* **69,** 609–617 (1991).

173. Zucker, I. H., Xiao, L. & Haack, K. K. V. The central renin-angiotensin system and sympathetic nerve activity in chronic heart failure. *Clin. Sci. (Lond).* **126,** 695–706 (2014).

174. You, J. *et al.* Differential cardiac hypertrophy and signaling pathways in pressure versus volume

overload. *Am. J. Physiol. Circ. Physiol.* ajpheart.00212. (2017).

175. Pascual, F., Schisler, J. C., Grevengoed, T. J., Willis, M. S. & Coleman, R. A. Modeling the transition from decompensated to pathological hypertrophy. *J. Am. Heart Assoc.* **7,** (2018).

176. Rose, K. M. *et al.* Association between the blood pressure response to a change in posture and the 6-year incidence of hypertension: Prospective findings from the ARIC study. *J. Hum. Hypertens.* **16,** 771–777 (2002).